

Exhaust Plume Characterization of a
Mini-PPT Using a Time-of-Flight/Grided Energy Analyzer

Travis A. Burton

A thesis submitted in partial fulfillment of the requirements for the degree of

Master of Science

University of Washington

2002

Program Authorized to Offer Degree: Aeronautics and Astronautics

DISTRIBUTION STATEMENT A
Approved for Public Release
Distribution Unlimited

20020829 057

University of Washington
Graduate School

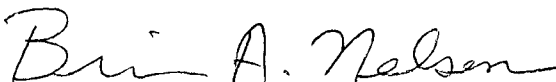
This is to certify that I have examined this copy of a master's thesis by

Travis A. Burton

and have found that it is complete and satisfactory in all respects,
and that any and all revisions required by the final
examining committee have been made.


Committee Members:


Uri Shumlak


Brian Nelson

Date: 21 Mar 02

In presenting this thesis in partial fulfillment of the requirements for a Master's degree at the University of Washington, I agree that the Library shall make its copies freely available for inspection. I further agree that extensive copying of this thesis is allowable only for scholarly purposes, consistent with "fair use" as prescribed in the U.S. Copyright Law. Any other reproduction for any purposes or by any means shall not be allowed without my written permission.

Signature 

Date 21 March 2002

TABLE OF CONTENTS

	Page
List of Figures	iii
List of Tables	v
Chapter 1: Introduction	1
1.1 PPT Flight Heritage	2
1.2 PPT Theory of Operation	4
1.3 Previous PPT Exhaust Plume Investigations	7
1.3.1 Electrostatic Probes	7
1.3.2 Magnetic Probes	9
1.3.3 Spectroscopy	10
1.3.4 Interferometry	11
1.3.5 Mass Flux Measurements	12
1.3.6 Witness Plates	12
1.3.7 Mass Spectrometry	13
1.3.8 Other Methods	14
1.4 Motivation Behind Time-of-Flight/Gridded Energy Analyzer Research	14
Chapter 2: Experimental Setup	17
2.1 Dawgstar PPT	17
2.2 Vacuum Facilities	20
2.3 Data Acquisition	23
Chapter 3: Time-of-flight/Gridded Energy Analyzer Design	24
3.1 Theory of Operation	25
3.1.1 Time-of-Flight Mass Spectrometry	26
3.1.2 Gridded Energy Analyzer	27
3.2 Design Principles	30
3.3 Practical Design Considerations	33
3.4 Description of Apparatus	38
Chapter 4: Data Analysis	47

4.1 Measurements on a Dawgstar PPT	49
4.2 Discussion of Results	52
Chapter 5: Conclusions	63
Chapter 6: Future Work	64
Bibliography	68
Appendix: Mechanical Drawings	74

List of Figures

	Page
Figure 1: Schematic Overview of the Pulsed Plasma Thruster.....	5
Figure 2: Typical PPT Current Pulse	6
Figure 3: Dawgstar Pulsed Plasma Thruster Module	18
Figure 4: Vacuum Facility	21
Figure 5: Schematic of Vacuum Facility	21
Figure 6: Plot of Potential of Gridded Energy Analyzer Elements	28
Figure 7: Ideal TOF Spectra	31
Figure 8: TOF Spectra With Two Ion Creation Times	32
Figure 9: TOF Spectra With No Gating.....	33
Figure 10: TOF Spectra With Gating.....	33
Figure 11: TOF/GEA Instrument.....	39
Figure 12: Schematic of TOF/GEA Instrument.....	40
Figure 13: PPT and First Section of Drift Tube.....	41
Figure 14: Gridded Energy Analyzer Components	42
Figure 15: The Gridded Energy Analyzer	43
Figure 16: GEA Instrumentation Line Set-up.....	45
Figure 17: First Survey Max. Collector Current vs. Ion Repelling Grid Potential.....	50
Figure 18: Second Survey Max. Collector Current vs. Ion Repelling Grid Potential	51
Figure 19: Technique Used to Determine Time of Initial Collector Current Increase	53
Figure 20: Collector Current For Ion Repeller At 150 V, PPT Pulse 1	54
Figure 21: Collector Current For Ion Repeller At 150 V, PPT Pulse 2	55
Figure 22: Collector Current For Ion Repeller At 150 V, PPT Pulse 3	56
Figure 23: Collector Current For Ion Repeller At 150 V, PPT Pulse 4.....	57
Figure 24: Collector Current For Ion Repeller At 150 V, PPT Pulse 5	58
Figure 25: $dI(V)/dV$ Data For Maximum Collector Current In First Survey	60
Figure 26: $dI(V)/dV$ Data For Avg. Maximum Collector Current In Second Survey.....	61
Figure 27: Log Plot of $I(V)$ For Both Surveys.....	62

Figure 28: Schematic of the 45° Electrostatic Energy Analyzer	65
---	----

List of Tables

	Page
Table 1: Early Flight PPT Specifications.....	3
Table 2: LES-6 PPT Species Velocities From Spectroscopy	10
Table 3: Dawgstar PPT Specifications	19
Table 4: GEA Grid Specifications	44
Table 5: Mass-to-Charge Ratio of Ionic Elements of Teflon	59

Acknowledgements

This work would not of been possible were it not for the help and assistance of a good number of people. The biggest thanks goes to my advisor, Prof. Uri Shumlak, for his guidance and support throughout the development of the instrument and its implementation. Another big thanks must be given to the ZaP project members who let me regularly take their attention, time, and even money, over the course of this research. In particular, without the help and advice of Ray Golingo, Stuart Jackson, and Brian Nelson this thesis might of just been about the repair of a diffusion pump. Chris Rayburn was a huge help in getting the PPT set up and working in the tank, so many thanks to him also.

My research partner, Krystal Parker, shared much of the grunt work in getting the instrument made and working, and hopefully she will begin to start to see some bigger rewards from that work as she continues the work with the TOF/GEA. Robert Gordon and Dennis Peterson are as responsible for the actual fabrication of the TOF/GEA as I am, and without their help the instrument would undoubtedly still be on the lathe being machined. Thanks also to David Okada for applying some of his machining expertise to a few parts of the GEA.

Lastly, many, many thanks for the support of my friends and family over the past eighteen months. Thanks to them there has always been something to look forward to in life outside of the lab.

Chapter 1: Introduction

Despite first seeing operational use aboard spacecraft nearly forty years ago, electric propulsion (EP) systems have only gained widespread acceptance over the past decade. Long recognized for the higher specific impulse and lower system mass fraction they offer over chemical propulsion systems; EP systems stayed largely unproven during the early days of the space age because the spacecraft power systems they require had not yet been developed. The maturation of the EP field in recent years has been due to both the gradual development of adequate spacecraft power systems and the increased focus on high performance, low weight spacecraft components by the spacecraft engineering community. Today a variety of EP devices are employed across nearly the entire spectrum of spacecraft missions.

Widespread acceptance is a mixed blessing for any propulsion system, as it directs research away from improving performance and towards understanding how the system will interact with an actual spacecraft. This is especially true for spacecraft propulsion systems, whose primary byproduct is an exhaust plume that can be a large contamination threat to the spacecraft or any other spacecraft in close proximity. Specifically, exhaust plume contamination can lead to degradation of solar cells, optics, and thermal control surfaces. This is of primary concern to the spacecraft designer, and is why an increase in experimental investigations into and modeling of the exhaust plume of EP devices has been an integral part of EP's maturation.

Of the three classes of EP systems (electrothermal, electrostatic, and electromagnetic), the exhaust plumes of electrostatic and electromagnetic devices have proven the most difficult to characterize. Unlike the exhaust plume of an electrothermal device, which is primarily hot neutral particles, the exhaust plumes of electrostatic and electromagnetic devices contain charged particles. The complex physics involved in the formation and

acceleration of these charged particles also varies from one type of thruster to another. The severity of this variation has led to separate experimental and modeling efforts for each electrostatic and electromagnetic device exhaust plume.

Not every EP device exhaust plume has yet received the same amount of inquiry, and as a result, some EP systems' exhaust plumes are better characterized than others. Among the devices whose exhaust plumes are still not completely understood is that of the pulsed plasma thruster (PPT). One of the first EP concepts to see operational use in space, the PPT was first utilized because of its relative simplicity and high specific impulse. After its initial development the PPT fell by the wayside somewhat as EP systems with higher thrust efficiency were investigated. In recent years however, the PPT's low required input power and ability to deliver small impulse bits have revived its popularity.

This chapter provides a brief summary of PPTs built to fly aboard spacecraft, a basic description of PPT operating theory, a history of experimental investigations into the PPT exhaust plume, and the motivation behind this particular study.

1.1 PPT Flight Heritage: Past, Present, and Future

The early flight history of the PPT is well outlined in the *Journal of Propulsion and Power* paper by Burton and Turchi.¹ The Soviet Union was the first to develop the PPT as an EP concept, launching the Zond 2 spacecraft to Mars in 1964 with several PPTs onboard to provide three-axis attitude control. Unfortunately, contact (and control of the PPTs) was lost with the spacecraft after a few months. The LES-6 satellite carried the first U.S. PPT into space in 1968. Operating on orbit for 10 years, the LES-6 PPT design set the precedent for later U.S. PPT designs that eventually flew on the Synchronous Meteorological Satellite (SMS) in 1974 and the Navy's three NOVA satellites starting in 1981. A PPT was also developed and flight qualified by 1975 for the two LES-8/9 spacecraft, but was replaced by a cold gas system in the final spacecraft design. Outside

of the U.S. and U.S.S.R., the Chinese and Japanese both flew separate PPT designs on separate missions in 1981^{2,3}. Further specifications for each of these early flight PPTs can be found in Table 1.

Table 1: Early Flight PPT Specifications

PPT	Pulse Rate (Hz)	Isp (s)	Thrust (μN)	Purpose
Zond 2	1	410	2000	Attitude Control
LES-6	1	312	26	Attitude Control
SMS	1	450	133	Spin Axis Precession Control
LES-8/9	1	1000	297	Attitude Control, Station Keeping/Changing
TIP-II (NOVA)	1	850	375	Drag Compensation
MDT-2A (Chinese)	1	280	64	Suborbital Test
ETS-IV (Japanese)	1	300	29	Spin Rate Control

Following the end of the NOVA mission, a number of years would pass before another PPT saw use in space. During this time many experimental efforts continued to refine and improve upon the PPT concept,¹ but none of the PPTs developed reached flight status. This trend finally ended in the late 1990's with the development of a PPT for pitch attitude control aboard NASA's Earth Orbiter 1 (EO-1). The EO-1 PPT has a scalable impulse bit (90-860 μ N-s) and specific impulse (650-1400 s),⁴ and was flight validated on orbit in 2001.

The development of the EO-1 PPT has been accompanied by the development of a few other flight PPTs for missions in the near future. A MicroPPT is currently being readied for deployment as a technology demonstrator aboard the USAF's TechSat 21 cluster of three microsatellites.⁵ The MicroPPT offers precision impulse bits in the 10 μ N-s range.⁶ The Japanese are also developing a flight PPT for NASDA's μ -Lab Sat II, which should be launched sometime in the next year.⁷ Finally, a PPT has also been developed for two

spacecraft in the ION-F nanosatellite cluster. As this was the PPT used in the reported research, a detailed description of it can be found in the next chapter.

The PPT's flight heritage, in addition to its ability to offer a small, precise impulse bit in pulsed operation, has led to its strong consideration by many groups doing conceptual planning for missions in the far future. In particular, several trade studies have found the PPT to be the best propulsion system currently available for certain future formation flying spacecraft.⁸⁻¹⁰ This being the case, extensive PPT research continues today in the U.S., Japan, Russia, China, France, and Argentina.^{2,5,7,11-15}

1.2 PPT Theory of Operation

Every PPT operates on the same simple electromagnetic and gas dynamic principles, but how those principles are implemented varies somewhat from one thruster design to the next. This variation is most severe when the propellant or the electrode/propellant orientation is changed. While such changes have often been made in experimental PPT designs, every flight PPT system listed in the previous section used the same propellant and (with the exception of the USAF's MicroPPT) orientation. This type of PPT is known as the "rectangular" type, and consists of a propellant bar fed in between two parallel electrodes by a constant force spring, as seen in Figure 1. It operates by first using a spark from an igniter plug in the cathode to ablate and ionize a small amount of the fuel surface. This provides a conduction path between the electrodes, which have been charged by a capacitor. Once enough electrons are liberated from the ablated material, a current arc forms between the electrodes and across the fuel surface. The heat of the arc causes more fuel to be ablated and ionized. Thrust is produced when this ablated material is accelerated out the PPT exhaust channel by Lorentz and pressure forces.

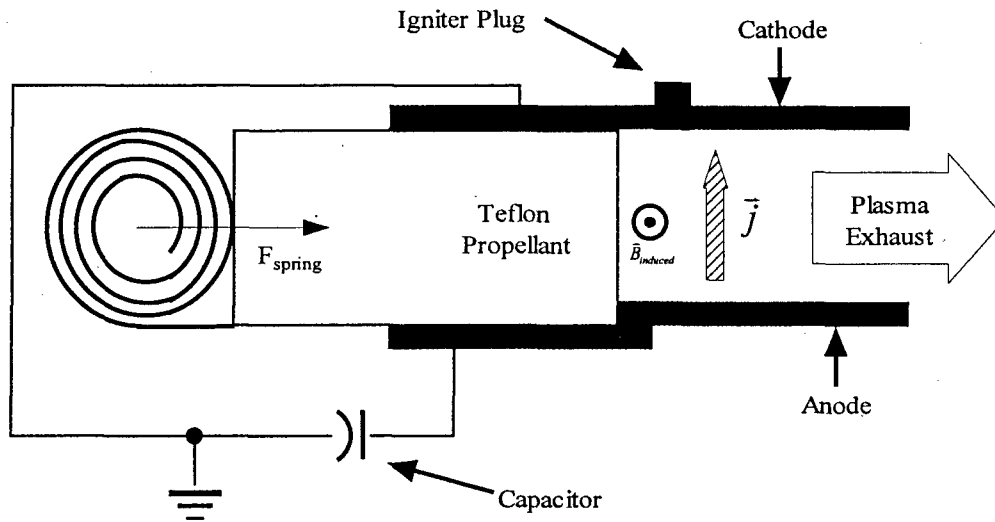


Figure 1: Schematic of the Rectangular Pulsed Plasma Thruster

The USAF MicroPPT varies from the other designs in that its electrodes and propellant are arranged in a coaxial configuration. In this design the propellant lies in a ring between a central, cylindrical cathode and a downstream anode ring. Again, thrust is produced in this design from the Lorentz and pressure forces that arise from the current arcing between the anode and cathode.

In both PPT types the pressure force is a result of the creation of what is essentially a high-pressure plasma from the ablated material, while the Lorentz force is generated by the current arc crossed with its self-induced magnetic field ($\vec{j} \times \vec{B}_{induced}$). While the high exhaust velocities of the Lorentz force accelerated particles are what gives the PPT a high specific impulse, the bulk of the ablated material is accelerated by the pressure force and travels at a much slower velocity. The exact proportion of the thrust that comes from either of these forces is different for each PPT.

The plasma dynamics of the PPT exhaust are dictated to a large degree by the oscillatory nature of its current waveform, which approximates a damped sine wave. The reason for this behavior lies with the fact that the external circuit impedance (which is basically an

LRC circuit) can exceed the arc discharge impedance.¹ A typical PPT current pulse is presented in Figure 2.

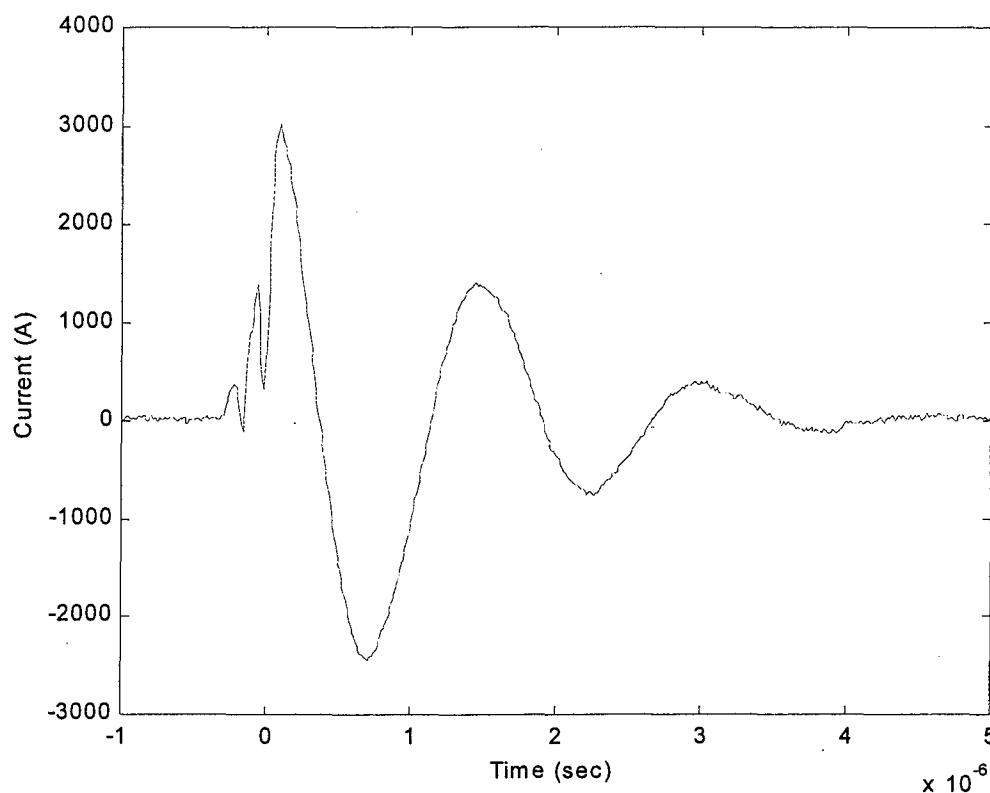


Figure 2: Typical PPT Current Pulse

For coaxial or rectangular PPTs operating on solid propellant, Teflon is the almost exclusive propellant choice. Unlike with many other dielectrics or possible propellants, current arcing across the face of Teflon does not leave a carbon track. Other propellants with lower ionization potentials have been tried,¹ but none of them were found to be as resistant to carbonization as Teflon. Known chemically as polytetrafluoroethylene, Teflon's monomer is C_2F_4 . Gaseous decomposition of Teflon at $783.15^\circ K$ in vacuum generates a gas that is 94% C_2F_4 , 0.86% CF_4 , 2.6% C_3F_6 , and 0.73% C_4F_8 .¹⁶

Once the Teflon in a PPT has been ablated and ionized into a plasma, complexities in its structure quickly emerge because of the low particle densities and high flow speeds allowed by the downstream vacuum.¹ This leads to non-equilibrium and non-uniform conditions in the exhaust plume, which makes experimentally characterizing and modeling the plume difficult.

1.3 Previous PPT Exhaust Plume Investigations

For any model of a PPT exhaust plume to be considered accurate, it must first be validated by an experimental characterization of the plume. Many efforts have been made to experimentally characterize different PPT plumes over the years, but none of them can be considered definitive. Rather, each study has simply added another element to our overall knowledge of the PPT exhaust plume. What follows is a sampling of those exhaust plume studies whose focus was upon Teflon fed rectangular and coaxial PPTs, for reasons that will be discussed the next section.

1.3.1 Electrostatic Probes

Electrostatic probes that have been used in the PPT exhaust plume include single, double, triple, and quadrupole Langmuir probes, and the Faraday cup. The basic theory behind each device has been well documented.¹⁷ A single Langmuir probe allows the electron temperature, plasma potential, and ion or electron density to be determined. A double Langmuir probe allows the same measurements to be made, but without disturbing the plasma. Triple Langmuir probes yield both electron temperature and density continuously, while quadrupole Langmuir probes go one step further and also give ion mach number (ion velocity divided by ion thermal speed). Faraday cups allow the ion velocity distribution to be measured by shielding out the electrons in the plasma and recording the current incident on a collector plate. Additionally, either kind of

electrostatic probe can be used to find the time of flight from the PPT or another electrostatic probe.

Single Langmuir probes have been used on the LES 8/9 PPT,^{18,19} the Russian MIPD-3 PPT,²⁰ and the ETS-IV PPT.²¹ The MIPD-3 PPT is a rectangular laboratory PPT whose fuel is fed from the side, and it gives a 1130 s specific impulse and 2250 $\mu\text{N}\cdot\text{s}$ impulse bit when operated at 100 J.¹ LES 8/9 PPT measurements by Myers et al., showed an ion density of around $6\times 10^{18} \text{ m}^{-3}$ at a location 24 cm from the thruster, and an ion velocity along the centerline of 42 km/s. Later LES 8/9 PPT measurements by Gatsonis et al., found two waves of ions, one traveling at 60 km/s and the other at 30 km/s. MIPD-3 PPT measurements yielded an electron density of $2\times 10^{22} \text{ m}^{-3}$ in the arc at a temperature of 1.8-2.6 eV. Two ion populations were also found to be generated by the MIPD-3 PPT; one moving at 30-35 km/s, and another at 14-16 km/s. Two single Langmuir probes spaced 0.95 m apart were used strictly to determine the ETS-IV PPT exhaust plume velocity, which was found to be 34 km/s.

The only application of a double Langmuir probe to a PPT was that done on the USAF's laboratory Millipound Thruster.²² The Millipound Thruster is another rectangular PPT whose fuel bar is fed from the side, and it operates with a 1210 s specific impulse and a 22.3 mN-s impulse bit at 750 J.¹ Along the PPT centerline, the maximum electron density was found to go from $3.35\times 10^{20} \text{ m}^{-3}$ at 71 cm from the PPT to $5.65\times 10^{19} \text{ m}^{-3}$ at 142 cm, while the electron temperature was around 2.1 eV. The speed of the plasma front was found to be around 24-24.9 km/s.

Triple Langmuir probes have been used to investigate laboratory versions of the LES 8/9 PPT¹⁹ and the EO-1 PPT.²³ When operated at 5, 10, and 40 J, the LES 8/9 PPT had a time averaged electron temperature of 1-3 eV and an electron density that varied from 10^{19} - 10^{21} m^{-3} . When operated at 5, 20, and 40 J, the EO-1 PPT had a maximum electron temperature of 5 eV and an electron density that varied from 10^{18} - $6\times 10^{21} \text{ m}^{-3}$. Both

studies looked at the exhaust plume across the perpendicular and parallel planes at distances of 2-20 cm from the PPT propellant surface.

A quadrupole Langmuir probe has been used on the PPT-4,²⁴ a coaxial laboratory PPT operating on 9 J to yield a 745 s specific impulse and 261 $\mu\text{N}\cdot\text{s}$ impulse bit. The peak electron density was found to be around $4.2 \times 10^{19} \text{ m}^{-3}$ and the initial electron temperature was near 2 eV. The ion Mach number was roughly 3.0, and the ion velocity was determined to be 34 km/s.

Faraday cups have been used on the Millipound Thruster,^{25,26} and the LES-6 PPT.²⁷⁻²⁹ Dawbarn et al. found the Millipound Thruster centerline ion velocity to be roughly 40 km/s. Rudolph and Jones used a Faraday cup in the backflow region of the Millipound Thruster exhaust plume and found it to be primarily electrically neutral particles. Studies of the LES-6 PPT by Vondra et al. and Thomassen and Vondra found a centerline plasma velocity of 40 km/s, and they also found that the charge on the Faraday cup varied inversely with the square of the cup's distance from the PPT (confirming the assumption that the exhaust plume approximates a drifting Maxwellian distribution). Further LES-6 PPT studies by Thomassen and Tong found 40% of the exhaust plume is ionized at 3.5 mm from the Teflon surface, but that this percentage decreases to 18% by 16 mm.

1.3.2 Magnetic Probes

Magnetic probes investigations of PPTs thus far have consisted of mapping out the magnetic field structure using magnetic coils. The theory behind magnetic probes is well documented,¹⁷ and in addition to measuring the magnetic field they can also be used to determine current density, electric fields, and magnetic pressure.

A magnetic probe survey of PPT-4 displayed a radial plume asymmetry corresponding to the Lorentz force component of the thrust, even though it is only responsible for 3.5% of

the total thrust.²⁴ A similar survey in different positions around the Millipound Thruster exhaust plume showed the peak magnetic field to be 0.85 Tesla at the throat of the PPT.³⁰

Magnetic field measurements of XPPT-1³¹ (a laboratory PPT similar to the LES-8/9 PPT) displayed a propagating current sheath during the first current half-cycle, indicating electromagnetic acceleration. During the second half-cycle the magnetic field was found to diffuse into the plasma, which was interpreted to mean that during this time the current is resistively heating the plasma. Similar current activity was found in the MIPD-3 PPT from magnetic field measurements,²⁰ with the current sheath in the first half-cycle found to be moving in the flow direction at 20-25 km/s. Another Russian study of new laboratory PPT designs with magnetic probes verified this current behavior once again.³²

1.3.3 Spectroscopy

Examining the optical emission spectra of the PPT exhaust plume with spectroscopy can yield the identity of the species in the plume as well as their velocities. Spectroscopic measurements of the LES-6 PPT yielded the species identification and velocity information found in Table 2.²⁸ The velocity was determined to be the average of the velocity ranges found for each species using Doppler shift and time of flight methods.

Table 2: LES-6 PPT Species Velocities From Spectroscopy

Species	Velocity (km/s)
C	10 ± 5
C ⁺	25 ± 5
C ⁺⁺	35 ± 5
C ⁺⁺⁺	
F	10 ± 5
F ⁺	20 ± 5
F ⁺⁺	30 ± 5
F ⁺⁺⁺	

A spectroscopic analysis of the MIPD-3 found C, F, C^+ , and F^+ , in the exhaust plume; with the ions and neutrals moving at 35 km/s and 15 km/s, respectively.²⁰ An extensive spectroscopic survey of the Millipound Thruster positively identified C, C^+ , C^{++} , C^{+++} , F, and F^+ in the exhaust plume; velocities were also found using the Doppler shift for F (2-15 km/s), F^+ (12-13 km/s), and C^+ (11-25 km/s).^{25,30} When used on the XPPT-1, spectroscopy identified F, F^+ , C^+ , C^{++} , and C_2 in the exhaust plume, and estimated the velocity of the ionized species to be 14-16 km/s following the first half-cycle of the current discharge.³³ This particular study also found that the relative spectra line ratios in the exhaust plume do not change with the discharge energy of the PPT, which suggests the bulk thermodynamic properties of the plume are the same regardless of capacitor energy. Determining the absolute intensity of the exhaust plume of a laboratory PPT at Ohio State University was the focus of another spectroscopic study, and C^+ and C^{++} were identified.³⁴

1.3.4 Interferometry

Interferometric measurements determine a plasma's refractive index, which can in turn be used calculate the plasma's particle density and velocity. The refractive index is obtained by comparing the two halves of a split laser beam, one side of which is passed through the plasma while the other side is not. Using interferometry Vondra et al. found the LES-6 PPT electron density in the current arc to be around $1-3 \times 10^{22} \text{ m}^{-3}$, while 0.2 m downstream it was reduced to 10^{18} m^{-3} .²⁷ Later interferometric measurements on the same PPT by Thomassen and Tong found the thermal and drift velocities of the plasma to be 9.3 km/s and 27.9 km/s, respectively.²⁹ The MIPD-3 has also been examined using an interferometer, and its electron density close to the electrodes was found to vary from $3.4 \times 10^{22} \text{ m}^{-3}$ near the cathode to $1.9 \times 10^{22} \text{ m}^{-3}$ near the anode.²⁰ The same study also found two distinct plasma blobs traveling out of the PPT, one at 25-35 km/s and the other at 13-15 km/s. Interferometric studies of other Russian laboratory PPTs (APPTs)

displayed a similar difference in electron density from the cathode to the anode, but also found that the density some 12 cm away from the electrodes is around $2 \times 10^{21} \text{ m}^{-3}$.³²

Interferometry was used to show that the neutral and electron density of the XPPT-1 scales linearly with its discharge energy.³⁵ The measured neutral density was around $2 \times 10^{22} \text{ m}^{-3}$, while the electron density was approximately one-fifth of this value. A neutral density was also observed to be maintained in the PPT exhaust channel after the end of the current pulse. Interferometry has been used in the exhaust plume of the USAF MicroPPT⁶ too, measuring a peak electron density of $4 \pm 2 \times 10^{21} \text{ m}^{-3}$ just outside the annular electrode.

1.3.5 Mass Flux Measurements

Four separate mass flux measurements of the Millipound Thruster exhaust plume have been made using collimated quartz crystal microbalances (QCMs).^{22,26,30,36} Rudolph, Pless, and Harstad found the plume to be axisymmetric, with 90% of the mass flux contained within the $\pm 40^\circ$ cone angle at a point 76 cm downstream from the exhaust nozzle. Using a specially designed vacuum tank cooled to limit wall backscatter, this study, as well one earlier by Rudolph and Jones, found the mass flux in the backflow region (87° off centerline) to be minimal. Guman and Begun also found the plume to be contained within the $\pm 30^\circ$ to the $\pm 40^\circ$ cone angle around the PPT centerline. Dawbarn et al. made QCM measurements with a chopper wheel and found that the bulk of the material in the plume was moving at 40 km/s.

1.3.6 Witness Plates

Many different kinds of witness plates and material samples have been placed in PPT exhaust plumes as part of several different research aims. Some of these studies examined the exhaust plume deposits left on witness plates in hopes of learning more

about the identity and structure of the particles in the plume. One such study on the XPPT-1 determined that 40 ± 3 % of the total propellant mass leaving the PPT is in particulate form, which points to a large propellant inefficiency.³⁷ A study on the Millipound Thruster used witness plates and a collimated QCM to conclude that up to 25% of the exhaust plume remains a polymer and travels at velocities near that of the largest plasmoid (40 km/s).³⁰ Another study on the same thruster identified four principle contaminants on witness plates exposed to the plume: C_2F_4 , Teflon sublimate, carbon flakes from carbon buildup on the electrodes, and an intermittent sputtering of carbon, electrode material, and Teflon.²⁵

Separate studies of the LES 8/9 PPT¹⁸ and a laboratory version of the EO-1 PPT³⁸ have examined the optical transmittance of collimated quartz witness plates placed in the plume and found the effect of the plume to be negligible. Both studies also placed the witness plates at angles of 50° and greater off the exhaust centerline; the former study found no contamination, but the latter did on the cathode side of the plume. Solar cell samples have also been exposed to the exhaust plume of the Millipound Thruster, and there appeared to be no degradation in their performance after the testing.²²

1.3.7 Mass Spectrometry

While no mass spectrometers have yet been successfully used directly in a PPT exhaust plume, a few quadrupole mass spectrometers (QMA's) have been used to determine the species composition of the residual gas left by the PPT exhaust. This residual gas is composed of the equilibrium products of the plume and often products from wall recombination, rather than the exact products that compose the plume just as it leaves the PPT. Residual gas analysis of the LES 8/9 PPT¹⁹ and the ETS-IV PPT²¹ found C, F, CF, CF_2 , and CF_3 , in both cases. The same analysis on the Millipound Thruster was either inconclusive or dominated by products of wall recombination.^{25,30}

1.3.8 Other Methods

A few other diagnostic devices have been used in the PPT exhaust plume, though to a lesser degree than those previously mentioned. Calorimeters have been used in the Millipound Thruster exhaust plume to determine that energy accommodation coefficient between the plasma and a surface is 95%,²⁵ and to find that the peak energy content of the plume is a few degrees off the exhaust centerline.²²

Image converter photographs of the PPT exhaust plume have also given some interesting results. Images of the LES-6 PPT during the first current half-cycle show an initial velocity of 11 km/s, while images from the second half-cycle indicate a velocity increase to 32 km/s.²⁷ A photographic study of the Millipound Thruster displayed a centerline velocity of 23 ± 5.5 km/s, a plume expansion angle of 40° , and a velocity along that outer angle of 26 ± 5 km/s.²⁶ Broadband emission of the XPPT-1 was studied using an image converter, and evidence of late time particulate emission from the Teflon surface was found.³⁷

1.4 Motivation Behind Time-of-Flight/Gridded Energy Analyzer Research

With so many experimental investigations into the PPT exhaust plume to date, it is astonishing that the exact composition and energy distribution of the plume is still not well known. This is especially surprising in light of how big a role the composition and energy distribution plays in determining the plume's contamination threat, as well as in validating models of the plume.

The contamination threat posed by a spacecraft propulsion system is something that must always be assessed, and this is especially true for the PPT. The ionized portion of the PPT plume is a particular threat because it can sputter or recombine with spacecraft

surfaces. The ionized carbon of the plume is certainly a threat in this sense, but the ionized fluorine is even worse, as fluorine is the most electronegative of all the elements. Additionally, the neutral portion of the plume can leave thick deposits on spacecraft surfaces, changing the surface's optical or thermal properties.

Examination of solar array degradation on spacecraft using PPTs has shown the thruster not to be responsible for additional degradation,^{1,21,22} but this does not necessarily mean that the PPT is not a contamination threat to other spacecraft surfaces. Also, in the past the PPT exhaust plume has only be considered as a backflow contamination threat to the spacecraft to which it is mounted. For it to remain a candidate for propulsion aboard formation flying satellites, the forward flow threat to other spacecraft in the vicinity must be assessed. The only methods used so far to examine the PPT plume contamination threat in an experimental setting are measurements of the mass and charged particle flux, and exposure of sample spacecraft surfaces (to include optics and solar panels) to the plume. These methods have yielded some important information about the PPT exhaust, but they could only determine the contamination threat to the specific surface being considered by the study. Knowledge of the composition and energy distribution of the plume allows its contamination threat to any spacecraft surface to be determined without repeated empirical study.

Current PPT exhaust plume models^{1,39-43} rely on accurate experimental measurements of the plume composition and energy distribution for validation. There is nothing more fundamental to a plasmadynamic model of the exhaust plume than the identities and velocities of the species contained within it. This being said however, there are good reasons behind why PPT exhaust plume studies have failed to characterize these properties so far.

The PPT exhaust plume composition and energy distribution data that currently sees the most widespread use comes from spectroscopy (see Table 2). Unfortunately, such

spectroscopic analysis usually contains some error as a result of the unsteady and nonuniform flow conditions in the PPT plume which cause different plasmas to be observed along the optical path.¹ While electrostatic probes can be used to verify spectroscopic data, they often suffer from their own inaccuracies as a result of being placed in the transient, hypersonic flow of the plume.¹ What is needed is a single device which can simultaneously determine particle identity and energy in the plume. Apart from spectroscopy, the only type of instrument that can make such a measurement is a mass spectrometer. The time-of-flight/gridded energy analyzer used in this study is a type of mass spectrometer, and in being so it can do much to characterize the PPT exhaust plume species and energy distribution.

Before continuing, it should be mentioned that outside of Teflon fed rectangular and coaxial type PPTs, other PPT variations such as the gas-fed and z-pinch have been studied.^{39,40} For the purposes of this study however, the focus was kept on Teflon fed coaxial and rectangular type PPTs because of the close similarities in their exhaust plumes, and because a flight qualified version of each has been developed.

Chapter 2: Experimental Setup

The reported research was conducted entirely in a vacuum facility located in the University of Washington's Aerospace & Energetics Research Building (AERB). No major piece of hardware was purchased for this study. Instead, many of the required elements were obtained from either the Dawgstar nanosatellite program or the UW plasma sciences group. The researchers fabricated any remaining elements. This chapter gives a description of the PPT, vacuum facility, and data acquisition system used in this study.

2.1 Dawgstar Pulsed Plasma Thruster

A thorough description of the Dawgstar PPT and its general operating characteristics can be found in Rayburn⁴⁶; for convenience a summary of the description and characteristics appears here.

The University of Washington's Dawgstar nanosatellite is one of three nanosatellites built by separate universities for the Ionospheric Observation Nanosatellite Formation (ION-F) mission. Utah State University has built USUSat for the mission, and Virginia Polytechnic Institute has built HokieSat. The mission objectives for the ION-F nanosatellites are to take spatially distributed measurements of the ionospheric electron density, demonstrate formation flying, and use a micro-PPT for attitude and orbit control.

Initially, both cold gas thrusters and PPTs were considered for propulsion aboard Dawgstar.¹⁰ After a comparison study, PPTs were chosen over the cold gas thrusters because of their ability to have a lower impulse bit (allowing more precise control) at a higher specific impulse. The Dawgstar design includes eight PPTs that are oriented to provide two-axis translational control and three-axis rotational control. Virginia Tech

also uses four PPTs, identical to those designed for the Dawgstar, to provide two-axis translational control of the HokieSat.

A schematic of the final design of the Dawgstar PPT is presented as Figure 3. Each Dawgstar PPT is actually part of a module containing two PPTs that are powered by one capacitor. While this design does not allow both the PPTs contained in one module to fire simultaneously, it does allow all eight PPTs to fit inside the considerable mass and volume constraints posed by the overall Dawgstar spacecraft design.

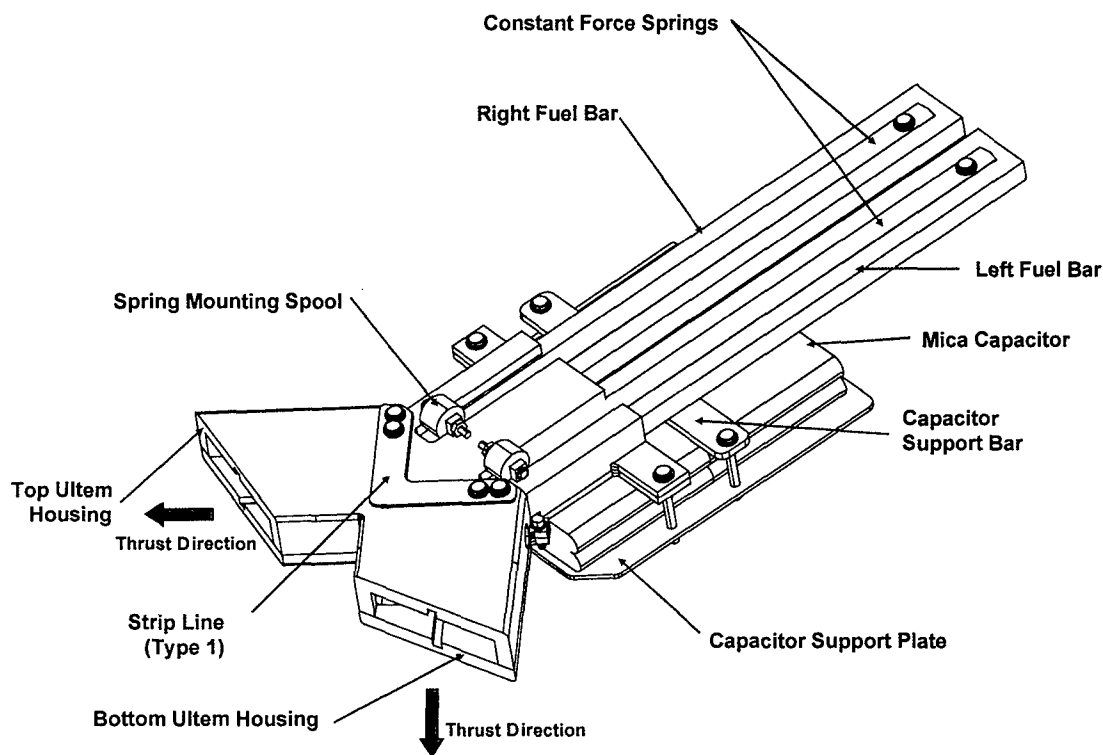


Figure 3: Dawgstar Pulsed Plasma Thruster Module

The capacitor lies along the base of the unit and is a Unison Industries mica-paper/foil model that provides 5 μF at 1466 V. Above the capacitor, the TeflonTM fuel bars are fed into the thruster housing by constant force springs. The housing consists of two pieces of UltemTM thermoplastic machined to provide an exhaust channel for each PPT. Two

boron nitride insulators inside each exhaust channel contain the initial plasma creation. The two insulators are separated by a labyrinth to prevent shorting of the current arc across the surface of the insulator. The copper cathode for each PPT is tied to the other cathode by copper strip lines across the top and bottom of the housing; the bottom strip line also connects them to the capacitor. One stainless steel anode serves both PPTs, and is connected to the capacitor via a strip line along the bottom of the housing. The igniter for each PPT is a 1/4" diameter Unison model that is mounted in the each cathode.

Using theoretical calculations the Dawgstar PPT was estimated to have 73% of its thrust produced by gas dynamic acceleration, with the remaining 27% coming from electromagnetic acceleration. Experimentally determined parameters of the thruster are listed in Table 3.

Table 3: Dawgstar PPT Specifications

Stored Energy	5.2 J	Total Thruster Mass	4.2 kg
Impulse Bit	56.1 $\mu\text{N}\cdot\text{s}$	Electronics Mass	0.5 kg
Specific Impulse	483 s	Fuel Mass	0.59 kg
Ablated Mass/Pulse	11.8 μg	Capacitor Mass	1.39 kg
Propulsive Efficiency	2.60 %	Structure Mass	1.72 kg
Capacitor Voltage	3 kV	Max Pulse Rate	2 pps
Igniter Voltage	1.2 kV	PPU Efficiency	80 %
Igniter Energy	0.20 J	Fuel Surface Area	2.3 cm^2
Peak Current	8 kA	Bus Power at 0.25 pps	3.3 W

The Dawgstar PPT module used for the reported research was identical to those fabricated for flight aboard the Dawgstar, except that the spark plug of the PPT not exhausting towards the diagnostic was removed. The PPT module was powered and fired using a "flight spare" power processing unit (PPU) that had been built for flight aboard

the Dawgstar. The PPU was placed on top of the vacuum tank and connected to the PPT via BNC connectors in a Plexiglas bulkhead covering one port of the tank. The PPU was powered by a 28 V laboratory power supply, and controlled by a computer.

2.2 Vacuum Facilities

All experiments reported were performed in a 1.05 m long by 0.9 m diameter steel vacuum chamber, shown in Figure 4. A schematic of the chamber is shown in Figure 5. A 304.8 mm diameter pipe section connects the vacuum chamber to the roughing line and butterfly valve. The butterfly valve in turn connects the pipe section to the liquid nitrogen trap and diffusion pump. Attached to the one port of the chamber is a 3.2 m long by 88.9 mm diameter stainless-steel tube that was fabricated specifically for the reported research. The 6.35 mm thick tube is broken into four sections: two 1.524 m long sections, and two 152.4 mm long sections. All pressure seals on the vacuum facility are made with Viton o-rings, with the exception of the ionization gauge, which is sealed with a copper gasket.



Figure 4: Vacuum Facility

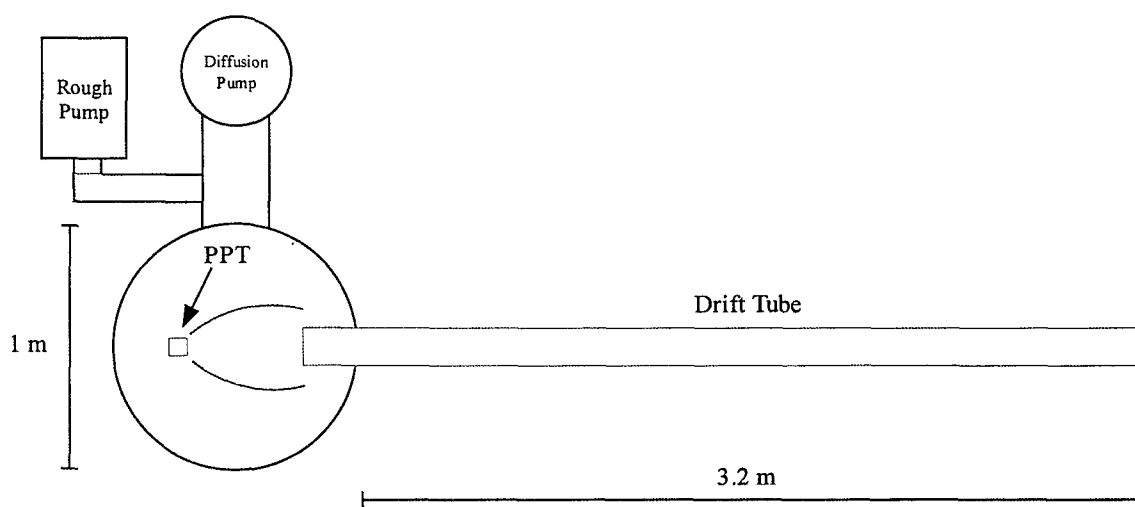


Figure 5: Schematic of Vacuum Facility

The facility is pumped down using a CVC PMCS-10C 10" diameter diffusion pump. Available documentation on the diffusion pump suggests a rating between 4000-4300 l/s on air, but this could not be verified, as the manufacturer no longer exists. The diffusion pump is backed by a Welch Scientific Model 1398 rough pump rated at 1500 l/s. An Aero-Vac liquid nitrogen trap connects the diffusion pump to the butterfly valve, and contains two sets of baffles. The first set of baffles downstream from the butterfly valve is liquid nitrogen cooled, while the second set of baffles is water cooled. Because of the prohibitive cost of liquid nitrogen (in relation to our small budget), the first set of baffles was not cooled during the reported research. Assuming the net effect of the liquid nitrogen trap is negligible on the pumping speed, the effective pumping speed at the tank is 2200 l/s.

Chamber pressure is measured with a MDC ionization gauge controlled by a Cooke Vacuum Products, Inc. IGC20 ionization gauge controller. The ionization gauge is located on a port between the butterfly valve and liquid nitrogen trap. The chamber base pressure is around 5×10^{-7} Torr when the PPT is not pulsed. The background pressure during pulsing of the PPT could not be obtained due to the danger to the ionization gauge filament, but each PPT pulse was spaced far enough apart to allow adequate time for the vacuum vessel to pump back down to near the base pressure. Pump down time from atmospheric pressure to the base pressure is approximately 12 hours.

It should be noted that just prior to the conducting of this study the vacuum facility suffered an accident that led to the moving of the facility, a thorough cleaning of all its elements, and the overhauling of the diffusion pump. Fortunately, the refurbished facility performs even better than it did prior to the accident.

2.3 Data Acquisition

A desktop PC using a Windows operating system was used both for the control of the PPT and data acquisition. PPT control was done via a LabVIEWTM program written by Chris Rayburn. LabVIEW connected to the PPU via a National Instruments multifunction DAQ card (model PCI-6024E) routed through a configurable signal conditioning enclosure (model CA-1000). All data signals were recorded using a Tektronix TDS 420A digital storage oscilloscope. The TDS 420A operates at 200 MHz and was connected to the computer via a GPIB interface. Data was logged from the oscilloscope at the computer using a DOS-based program supplied by Tektronix.

Chapter 3: Time-of-flight/Gridded Energy Analyzer Design

A number of methods and instruments exist to allow one to study the species and energy distribution in the exhaust plume of a PPT. At the top of the list in terms of monetary expense is a commercial plasma process probe, which can determine the ionic and neutral species of a plasma as well as do energy analysis. Unfortunately, the cost of a commercial process probe in relation to the minimal operating budget of this study was ludicrous.

At its heart a commercial process probe is just a modified mass spectrometer; and there exist several much less expensive mass spectrometry techniques. A good description of the four primary types of mass spectrometers, as well as their history, can be found in texts by Jayaram⁴⁷ and Duckworth, et al.⁴⁸ The magnetic-sector type mass spectrometer is simplest and oldest mass spectrometry technique. This instrument deflects ions through a static magnetic field, and uses the resultant mass-dependent trajectory of each ion species to separate and collect the ions. In contrast, the three remaining types of mass spectrometers all use dynamic fields for mass analysis.

Cyclotron-resonance type mass spectrometers measure the cyclotron frequency of an ion in a homogenous magnetic field, which varies inversely with the ion mass, to identify each ion species. Quadrupole mass analyzer (QMA) type mass spectrometers cause the trajectory of an ion passing through the instrument to oscillate by superimposing an rf electric quadrupole field on a dc electric quadrupole field. QMAs can be set such that only ions of a specified mass will stay on a stable trajectory through the instrument, while ions not of that mass will go on unstable trajectories and be lost. Time-of-flight (TOF) type mass spectrometers operate by measuring the amount of time it takes for an ion of known energy to travel some specified distance; using the principle that ions at the same

retarding potential but with different mass-to-charge ratios will travel at different velocities.

The most popular and commercially available type of mass spectrometer today is the QMA. Unfortunately, the cost of a QMA was again far beyond our operating budget. Of the remaining mass spectrometer types, the TOF was the simplest, and the pulsed ion generation that it required fit well with the pulsed nature of the PPT. Recent improvements in transient recorders (such as digital oscilloscopes) have also greatly improved the resolution of TOF mass spectrometers, which has in turn led to the use of TOF mass spectrometers in a variety of fields and environments.^{49,50} For these reasons, the decision was made to build our own TOF mass spectrometer to analyze the PPT exhaust plume.

This chapter provides the theory of operation behind the instrument, the basic principles and practical considerations used in its design, and a full description of the final design.

3.1 Theory of Operation

The original proposal for this study was to build a TOF mass spectrometer similar in design to those used by King⁵¹ to study the SPT-100 Hall thruster and by Pollard⁵² to study the T5 Ion thruster. The ion potential is specified in these two designs by an electrostatic energy analyzer oriented 45° to the plasma flow, which uses a homogenous electric field to deflect ions of the specified retarding potential into a channel electron multiplier. However, as the study progressed it was realized that this design was too complex and costly to be fabricated in the time allotted for the study.

The instrument that was finally fabricated for the reported research uses the principles of TOF mass spectrometry with that of the gridded energy analyzer (GEA). In TOF analysis mode the GEA serves a similar function to the 45° electrostatic energy analyzer,

except it allows all ions above a certain retarding potential to reach the detector rather than just ions exactly at that retarding potential. The GEA can also be used all by itself to calculate the ion retarding potential distribution function.

3.1.1 Time-of-Flight Mass Spectrometry

As previously stated, TOF mass spectrometry is based on the principle that charged particles at the same retarding potential but different mass-to-charge ratios will travel at different velocities. It is no surprise then that in a TOF mass spectrometer a retarding potential is specified, a velocity is determined, and then a mass-to-charge ratio is calculated. The velocity determination comes from finding how long it takes the charged particle to travel a known path length,

$$v = \frac{L}{t} \quad (1)$$

where v is the particle velocity, L the path length, and t the travel time. The velocity relates to the particle's energy through

$$v = \sqrt{\frac{2qV}{m}} \quad (2)$$

where q is the electronic charge, V the particle retarding potential, and m the particle mass. Combining the two equations allows calculation of a property that is specific to each ionic species, the charge-to-mass ratio

$$\frac{m}{q} = 2V \left(\frac{t}{L} \right)^2. \quad (3)$$

The TOF mass spectroscopy technique relies on a pulsing of the ion source for the travel time to be accurately determined. Pulsing the ion source can also limit the overall sample size enough to allow ions at the same potential to separate into distinct groups of the same mass-to-charge ratio via Eq. (3), which may then be resolved separately over time by a detector at the end of the particle path. For an ion source that usually operates in steady-state, an electrostatic gate or solid barrier must be used to pulse the ion source.

Even for an ion source whose normal operation mode is pulsed, like the PPT, a gating mechanism may increase the resolution of the TOF mass spectrometer that is being applied.

The TOF mass spectrometer design for this study uses a gridded energy analyzer (GEA) to determine the ion travel time and retarding potential. A detailed description of the GEA operating theory follows in the next subsection; but when used as part of the TOF mass spectrometer, the GEA simply measures the current collected over time as ions at retarding potentials above the GEA's ion repelling potential (V_G) reach its collector. When the time of current collection at the GEA is compared to the time of plasma creation in the PPT, the ion travel time can be determined. The path length is the distance from the PPT electrodes to the collector of the GEA.

3.1.2 Gridded Energy Analyzer

The gridded energy analyzer, also known as the retarding potential analyzer (RPA), is the simplest existing device to measure an ion velocity distribution. In this function, the GEA has long been used by the plasma sciences community to analyze both laboratory and space plasmas, but its use on electric propulsion device exhaust plumes has occurred only recently. In the last several years GEAs have been used to determine ion velocity distributions of electric propulsion devices in the lab,^{51,53-55} and also as part of diagnostic packages to analyze the operation of flight electric propulsion devices in space.^{56,57} No record was found during the conducting of this study of previous use of the GEA to specify retarding potential in a TOF mass spectrometer, but the widespread use of the TOF mass spectrometry and GEA concepts across a variety of scientific fields would lead one to believe that this configuration is not necessarily unprecedented.

Thorough descriptions of the operational theory of the GEA can be found in numerous papers and texts.^{17,51,58,59} The instrument generally consists of an aperture, at least three

grids, and a collector plate. Each grid creates an equipotential plane oriented perpendicular to the plasma flow path that repels all charged particles except those who meet the criteria

$$v > \sqrt{\frac{2qV_G}{m}} \quad (4)$$

where V_G is the ion repelling grid potential; and m , v , and q are the particle's mass, velocity along the flow path, and electronic charge, respectively. As shown in Figure 6, the first grid encountered by the plasma flow is held at some negative potential large enough to repel all the electrons in the flow. The second grid is held at a variable positive potential to repel all ions in the flow except those whose retarding potential is greater than that specified by the grid potential. Ideally, after passing through the first two grids only high retarding potential ions would be left in the flow, but some ions collide with the ion and electron repelling grids and liberate electrons via secondary emission. These electrons are prevented from reaching the collector by the third grid, which acts as a secondary electron suppressor. The collector is either left floating or biased slightly negative to ensure it collects the remaining ions.

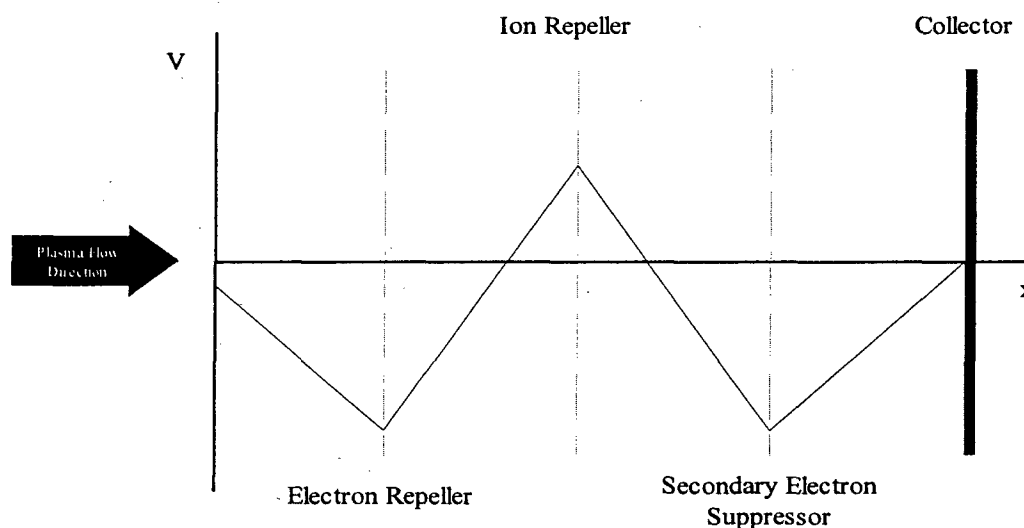


Figure 6: Plot of Potential of Gridded Energy Analyzer Elements

A description of the operation of the GEA as the accelerating voltage filter of a TOF mass spectrometer was given in the previous subsection; what follows describes its use to determine an ion retarding potential distribution. The current generated by the ions that reach the collector can be represented as

$$I(v_i) = A_c q n_i v_i \quad (5)$$

where v_i is the ion velocity, n_i is the ion number density, and A_c is the collector surface area. If we let v_i represent the bulk flow of the ions, and assume a homogenous velocity distribution $f(v)$ in the x-y plane oriented perpendicularly to the flow path z, then the current can also be defined by

$$I(v_i) = A_c q n_i \left(\frac{1}{n_i} \int_{\sqrt{2qV_G/m_i}}^{\infty} f(v_i) v_i dv_i \right). \quad (6)$$

Because velocity varies with mass-to-charge ratio, it is preferable to find the current as a function of the ion accelerating voltage. This can be done using a transformation of variables of Eq. (2)

$$dv_i = \frac{1}{2} \sqrt{\frac{2q}{m_i}} V^{-1/2} dV. \quad (7)$$

Using Eq. (2) and Eq. (7), the collected current now becomes

$$I(V) = A_c q \int_{V_G}^{\infty} \sqrt{\frac{2qV'}{m_i}} \frac{1}{2} \sqrt{\frac{2q}{m_i}} V'^{-1/2} f(V') dV' \quad (8)$$

$$I(V) = \frac{A_c q^2}{m_i} \int_{V_G}^{\infty} f(V') dV' \quad (9)$$

Taking the derivate of both sides of Eq. (9) in relation to the retarding potential allows an expression for the retarding potential distribution function, $f(V)$, to be obtained

$$f(V) = \frac{m_i}{A_c q^2} \left(-\frac{dI(V)}{dV} \right). \quad (10)$$

The GEA determines $dI(V)/dV$ by comparing the current collected at different values of ion repelling potential. The ion mass and electronic charge used to calculate the ion

retarding potential function must come from another form of analysis (such as TOF mass spectrometry) or conjecture.

3.2 Design Principles

Understanding why the gridded energy analyzer is also referred to as the retarding potential analyzer is key to an understanding of the issues that determine the resolution of the combined TOF/GEA instrument. When it is used to examine a plasma that consists entirely of ions of the same mass and charge, the output of the GEA is (as its name implies) an ion energy distribution. If the plasma contains ions of varying mass and charge however, then the GEA is only capable of producing an ion retarding potential distribution. In other words, if the flow into a GEA contains multiple ionic species, then the $dI(V)/dV$ curve produced from the GEA data will no longer be directly proportional to the ion energy distribution. This fact is borne out by Eq. (10). Fortunately, obtaining an ion energy distribution for plasma that contains multiple ion species is possible with the combined TOF/GEA instrument, as long as the mass resolution of the TOF apparatus is adequate enough.

A TOF/GEA spectra with a mass resolution “adequate enough” to allow an energy distribution for each ionic species to be determined is shown in Figure 7. Each current pulse corresponds to a different group of ions of the same mass-to-charge ratio arriving at the collector of the GEA. This particular spectra is considered good because each of the current pulses is distinct and not overlapping, which allows each pulse to be evaluated separately. Of course these properties must be found in each TOF/GEA spectra across the range of GEA ion repelling potentials applied, as required to produce the $dI(V)/dV$ curve separately for each mass-to-charge ratio group.

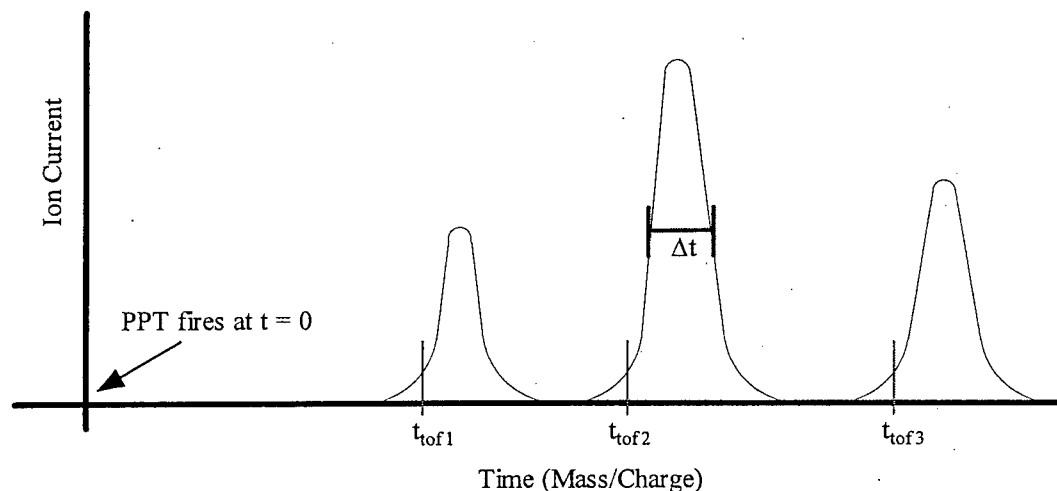


Figure 7: Ideal TOF Spectra

In equation form, the mass resolution of a TOF mass spectrometer in which ions travel at constant energy is given as

$$\frac{m}{\Delta m} = \frac{2t_{tof}}{\Delta t} \quad (11)$$

where m is the ion mass, Δm the range of masses resolved, t_{tof} the flight time, and Δt the full width at half maximum (FWHM) of the signal received (see Figure 7). While the ions in the TOF/GEA instrument used on the PPT in the reported research do not necessarily travel at constant energy, it can be assumed that they travel near enough to it to consider the mass resolution given by Eq. (11) approximately correct in this case. As explained by Cotter in his texts,⁴⁹⁻⁵⁰ t_{tof} and Δt (and therefore the mass resolution) are determined by issues associated with three types of ion distributions: the temporal, initial kinetic energy, and spatial.

The temporal distribution describes how the ions reach the detector and are recorded over time. It is determined in a TOF device by the ion travel length, time of ion formation, gating of the ion flow, and limitations of the detection and recording devices. The ion travel length is the distance between the ion generation source and the detector,

and it dictates the total ion flight time. Thus, the ion travel length is directly proportional to the mass resolution.

The time of ion formation at the ion generator affects the temporal distribution and mass resolution more subtly by undermining the assumption used in a simple TOF spectra (like Figure 7) that all ions were created at the same moment. As shown in Figure 8, ions of the same mass-to-charge ratio created at different times can appear to be of different mass-to-charge ratio if only one creation time is considered. Recent research has suggested that the PPT may create two groups of ions corresponding to an initial current flow and a subsequent current reversal during the pulse,¹⁹ so the variation in the time of ion formation must be carefully considered when interpreting the TOF/GEA data.

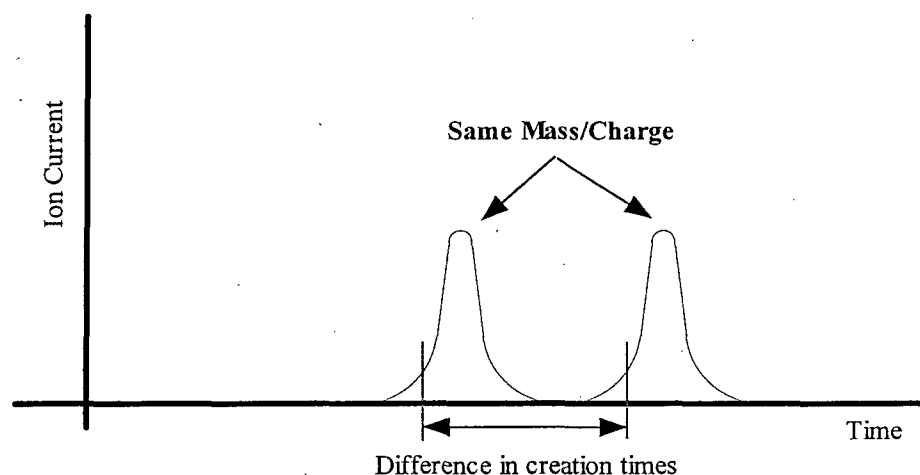


Figure 8: TOF Spectra With Two Ion Creation Times

The temporal distribution can also be affected by a gating mechanism, such as a physical barrier that moves in and out of the ion flow or an electrostatic deflector that is pulsed on and off. Gating affects the temporal distribution by allowing only particles at a certain range of velocities to reach the detector, which reduces the sample size. In this manner gating reduces Δt at the detector to length of time the gate is left open (t_{gate}), as shown in Figures 9 and 10. If a gate is open for too short a time for any part of the slowest ionic

species velocity distribution to pass all the way through it, then gating can also reduce the range of masses resolved (Δm). In any case, by reducing Δt and possibly Δm , gating increases the mass resolution. The drawback with gating is if it is done so quickly that Δm is reduced, then multiple measurements must be taken with different gate opening times.

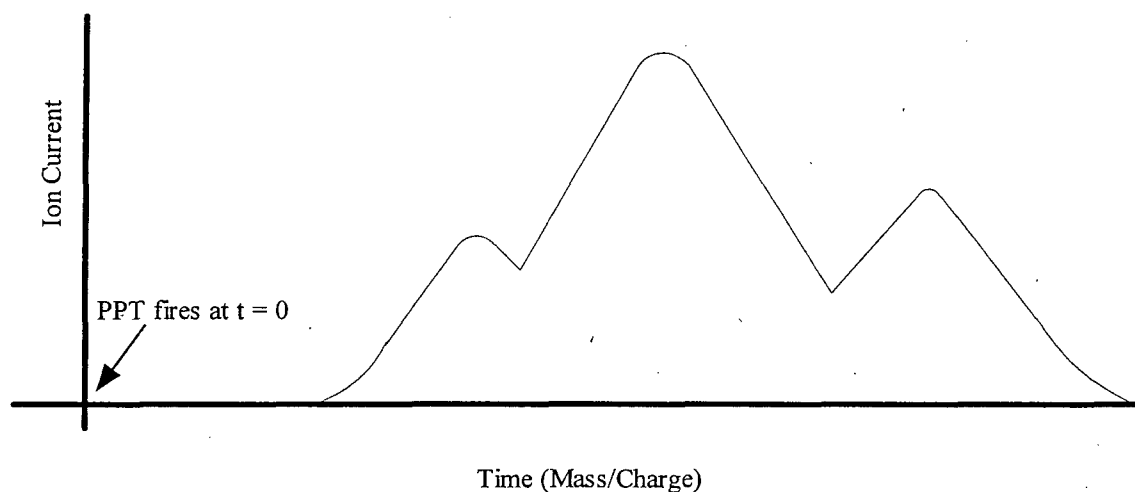


Figure 9: TOF Spectra With No Gating

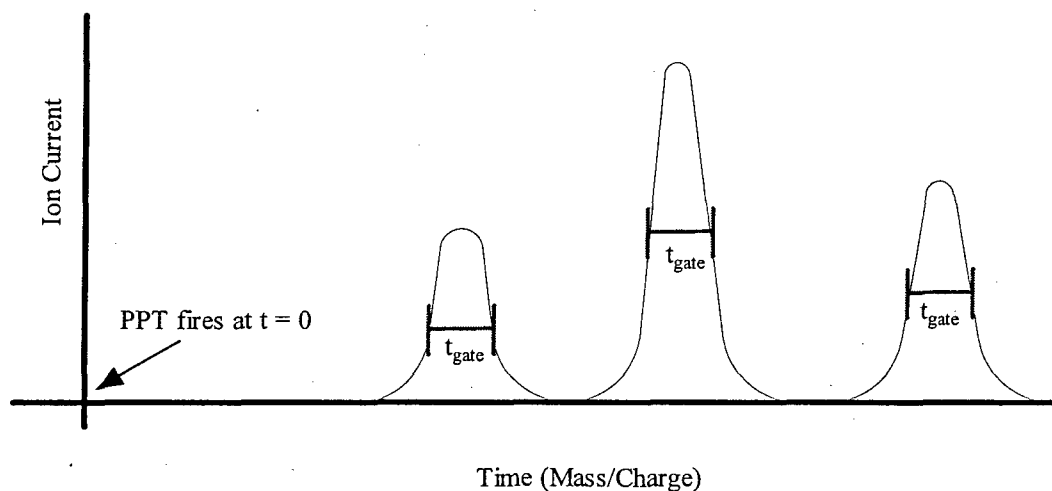


Figure 10: TOF Spectra With Gating

The last temporal distribution issue affecting resolution is the limitations of the device being used to monitor the detector's signal, which usually is a digital oscilloscope connected to the detector via some form of cabling. The limitations of an oscilloscope to convert the ion current incident on the detector into data can be characterized by the device's bandwidth, sampling rate, record length, and dynamic range. The cabling's ability to get the undistorted detector signal to the oscilloscope also plays a large role. A good oscilloscope and cabling can reduce Δt considerably, and in turn increase the mass resolution.

The initial kinetic energy distribution also plays a role in determining the mass resolution. Nominally, it is assumed that all the ions are created with nearly the same initial kinetic energy distribution, which translates to each mass-to-charge ratio having around the same velocity. The degree to which this is true determines the range of velocities that reach the detector for each ionic species, which is just the Δt . If the initial kinetic energy distribution is spread-out, as in Figure 9, then the mass resolution can go down significantly. Further complicating this issue is the fact that ions created at different times, such as during current reversals during the PPT pulse, may also have different initial kinetic energy distributions. Thus, the initial kinetic energy distribution must be considered in any TOF/GEA data interpretation.

Another sometimes complicated issue surrounding mass resolution is the spatial distribution. The spatial distribution describes the location of ion formation, which by turns decides the ion travel distance and mass resolution. Luckily for the TOF/GEA instrument used in this study, the region of ion formation is in such close proximity to the fuel bar surface of the PPT that the spatial distribution can be considered to be extremely narrow and therefore relatively unimportant to the mass resolution.

Apart from the distribution issues, one issue unique to the TOF/GEA instrument and its use on the PPT also affects its overall resolution. As previously stated, the GEA requires

the differentiation of multiple pulses of the PPT with different applied ion repelling potentials to form the $dI(V)/dV$ curve. If the PPT created the exact same plasma each time it fired this would be no problem, but by its nature the PPT igniter has a shot-to-shot variation whose effect can propagate into variations in the discharge pulse.¹ Significant variations in PPT performance over the course of a number of pulses with different GEA ion repelling potentials can render the $dI(V)/dV$ curve inaccurate. Thus, variations in PPT performance must be monitored and studied before the data from the TOF/GEA instrument may be trusted.

3.3 Practical Design Considerations

With theory and design principles in hand, a consideration of the hardware and materials available was the last step remaining before the final specifications of the TOF/GEA design were decided. It should be noted that the small operating budget of this study limited us primarily to materials and hardware that were either borrowed or had been discarded by other studies in the University of Washington's Department of Aeronautics and Astronautics. This made the practical design of the TOF/GEA much different than the ideal design in many areas, and those areas have been noted throughout this section.

The linchpin of any TOF mass spectrometer design is the data recorder, which in our case was a digital storage oscilloscope. The data recorder has such a status because compensation for its capabilities and limitations is often what drives a majority of TOF device design decisions. As such, the relatively slow sampling rate and small bandwidth of the oscilloscope used in this study (in relation to the oscilloscope employed in King's study⁵¹) dictated that the mass resolution be increased by other aspects of the overall design.

The simplest aspect of a TOF device design to change in order to increase the mass resolution is the ion travel length. In fact, the ion travel length is usually only limited by

the practical length of the vacuum vessel and the record length of the oscilloscope. The practical length of the vessel turned out to be the limiting factor in the TOF/GEA design, as existing material to lengthen the vacuum vessel set the distance from the PPT fuel bar face to the GEA collector at 3.68 m. With the fastest ion velocity ever recorded from a PPT similar in configuration to the Dawgstar PPT being 60 km/s,¹⁹ this yielded a fastest possible flight time for the TOF/GEA of 61 μ s.

Another method of directly increasing the mass resolution is to employ a gating device. As previously mentioned, the pulsed nature of the PPT does not require that the TOF/GEA instrument be gated. In order to avoid unnecessary complexity in this study's initial application of the instrument to the PPT then, no gating mechanism was developed.

Apart from increasing the mass resolution, other practical design considerations focused on how the ions were to travel from the PPT exhaust channel to the collector of the GEA. One of the principal assumptions in the GEA operating theory is the ions have a homogenous velocity distribution in the plane perpendicular to the flow path. This assumption requires the PPT exhaust plume be collimated before reaching the GEA, as its velocity distribution at the exhaust channel exit is divergent enough to invalidate the assumption. Collimation in the TOF/GEA design was achieved via two 3.6 mm orifices spaced 3.2 m apart along the ion flow path from the PPT to the GEA.

Ensuring the vacuum vessel had time to pump out all the PPT exhaust products between pulses was another important consideration. Not allowing for adequate pump out time can cause the ions from the PPT to collide with neutral particles from previous pulses, which perturbs the ion velocity distribution. As the ionization gauge could not be used to monitor pressure in the vacuum vessel during the PPT pulses, the pump down time had to be estimated using vacuum conductance and equivalent pumping speed calculations.⁶⁰ At an initial pressure of 5×10^{-7} Torr, and using a conservative estimate of a pressure rise to

1×10^{-3} Torr following a PPT pulse, the time required to pump down within an order of magnitude of the initial pressure is approximately one minute. Thus, the TOF/GEA requires at least one minute between PPT pulses for the exhaust products from previous pulses not to interfere with ion travel from the PPT to the GEA.

Once having arrived at the GEA, the ions must still travel through the repelling grids before reaching the collector plate. While the grids are meant to only provide an equipotential barrier, by their nature they are also a physical barrier. In an ideal grid, the wires would be infinitely thin and close together, insuring that every charged particle in the plasma flow came within at least one Debye length (λ_D) of a grid wire without actually striking the wire. Debye length is the maximum distance from a wire at which the plasma is effected by the potential on the wire, and is given by

$$\lambda_D = \sqrt{\frac{T_e \epsilon_0}{n_\infty q_e^2}} \quad (12)$$

where T_e is the electron temperature in eV, ϵ_0 is the dielectric constant of free space (8.85×10^{-12} farads/m), n_∞ is the electron density far from the perturbing potential, and q_e is the charge of the electrons (1.6×10^{-19} C). The Debye length of the Dawgstar PPT exhaust plume when it reaches the GEA can be estimated using data on electron temperature and density obtained from a similar rectangular PPT operating at 5 J.¹⁹ At a point along the thrust centerline 20 cm from the fuel bar surface, the electron density was $1 \times 10^{19} \text{ m}^{-3}$ and the electron temperature was 1 eV. This yields a Debye length of 2.35 μm . While the Debye length of the collimated exhaust plume 3.68 m away from the PPT will almost certainly be greater than this (due to a drop in electron density), 2.35 μm is a good baseline design point.

Only very fine meshes formed via chemical etching or electroplating have wire spacings on the order of our Debye length. One characteristic of grids produced in this method is that as the spacing between wires is decreased, the transmission (percentage of the grid that is open area) decreases even more drastically.⁶¹ Reducing the grid transmission

reduces the number of ions and electrons which can travel through the grid without striking it. This leads to a smaller ion and electron density on the backside of the grid, which means that less current will be generated on the collector than if a grid with higher transmission had been used. Of course reducing the electron density also increases the Debye length, which makes the grids downstream more effective at repelling ions and electrons. Thus, a compromise must be struck between transmission and wire spacing in each of the grids selected for the GEA.

Apart from the wire spacing in the grids, the spacing between the grids is also of concern because of possible space charge effects. If either the electron or ion density is allowed to build up in front of any of their respective repelling grids in the GEA, then a space charge from these increased densities can increase the potential in the area around the grid above that of the grid itself. Ion or electron distributions encountering these repulsive hills will not create as large of a current on the collector as they would if the space charge effects were not present. Hutchinson¹⁷ recommends a grid spacing of $\sim 4 \lambda_D$ to limit space charge effects, but for the baseline Debye length used in this study such a grid spacing is impractical. In reality, the grid spacing is usually limited by the capability of the electrical insulation between the grids to resist arcing across its surface.

3.4 Description of Apparatus

The final design of the TOF/GEA instrument has four primary components, shown in their operating configuration in Figures 11 and 12. The largest component is the drift tube, whose purpose is to lengthen the ion travel path from the PPT to the GEA and collimate the PPT exhaust plume. The tube itself is 101.6 mm outer diameter, 6.35 mm thick 304 stainless steel pipe in four sections. Flanges welded to either section end are used to connect the sections together via a six-bolt pattern. The first drift tube section is 152.4 mm long and contained entirely in the original vacuum tank. It is capped on the end facing the PPT by a stainless steel plate with the first 3.6 mm collimating orifice.

The second section is 1.524 m long and creates a vacuum seal with the tank on one end, and with the third section via a centering ring on the other. The third section is also 1.524 m long, and creates a vacuum seal to the fourth section via a centering plate that contains the second 3.6 mm collimating orifice. The fourth section is 152.4 mm long and capped by a Plexiglas bulkhead. The GEA is mounted to the bulkhead, and the electrical feedthrough used to operate the GEA is contained in the bulkhead.

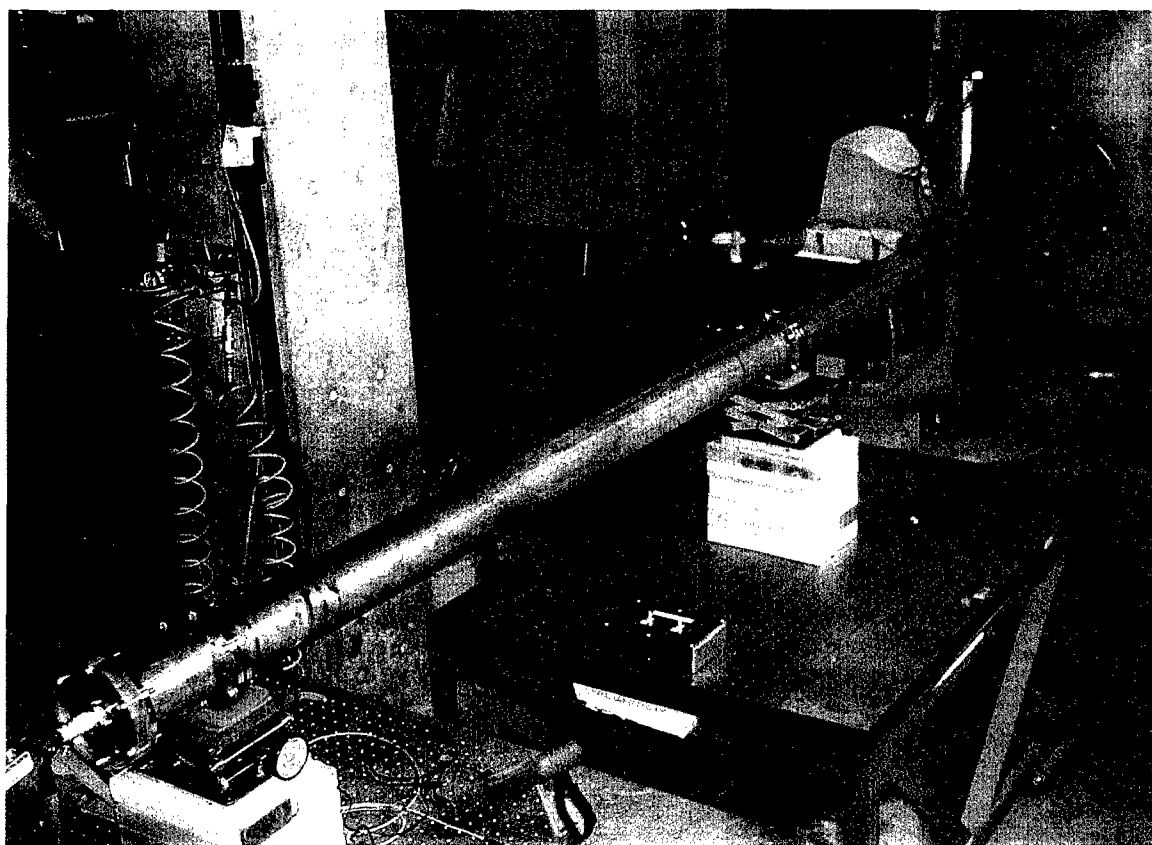


Figure 11: TOF/GEA Instrument

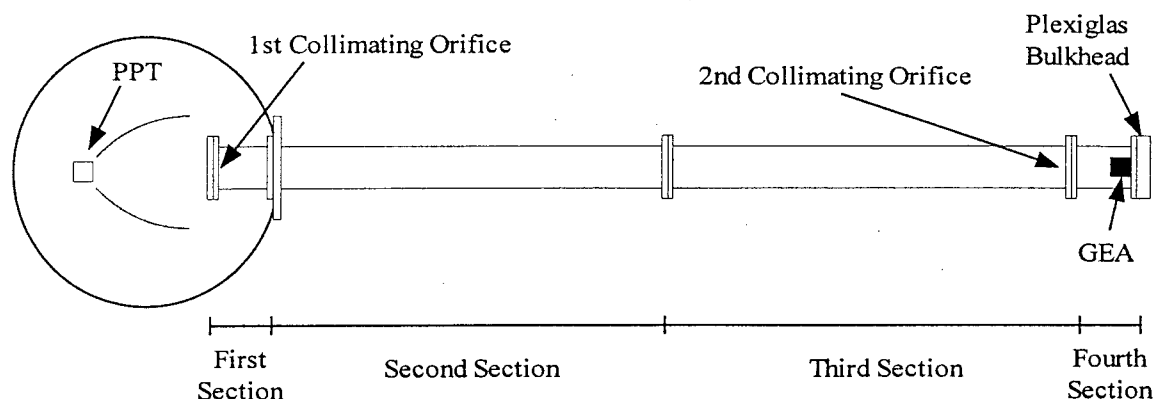


Figure 12: Schematic of TOF/GEA Instrument

The Dawgstar PPT is oriented on a mounting table with the center of its exhaust channel 254 mm away from the first collimating orifice. The exhaust channel exit is also oriented so that it is parallel to the plate containing the collimating orifice, as shown in Figure 13. A Rogowski coil has been placed around the upper stripline of the PPT in order to monitor its current during the pulse of the thruster. While the current through the upper stripline is only a fraction of the entire discharge current, Rayburn found it to consistently be 34%.⁴⁶

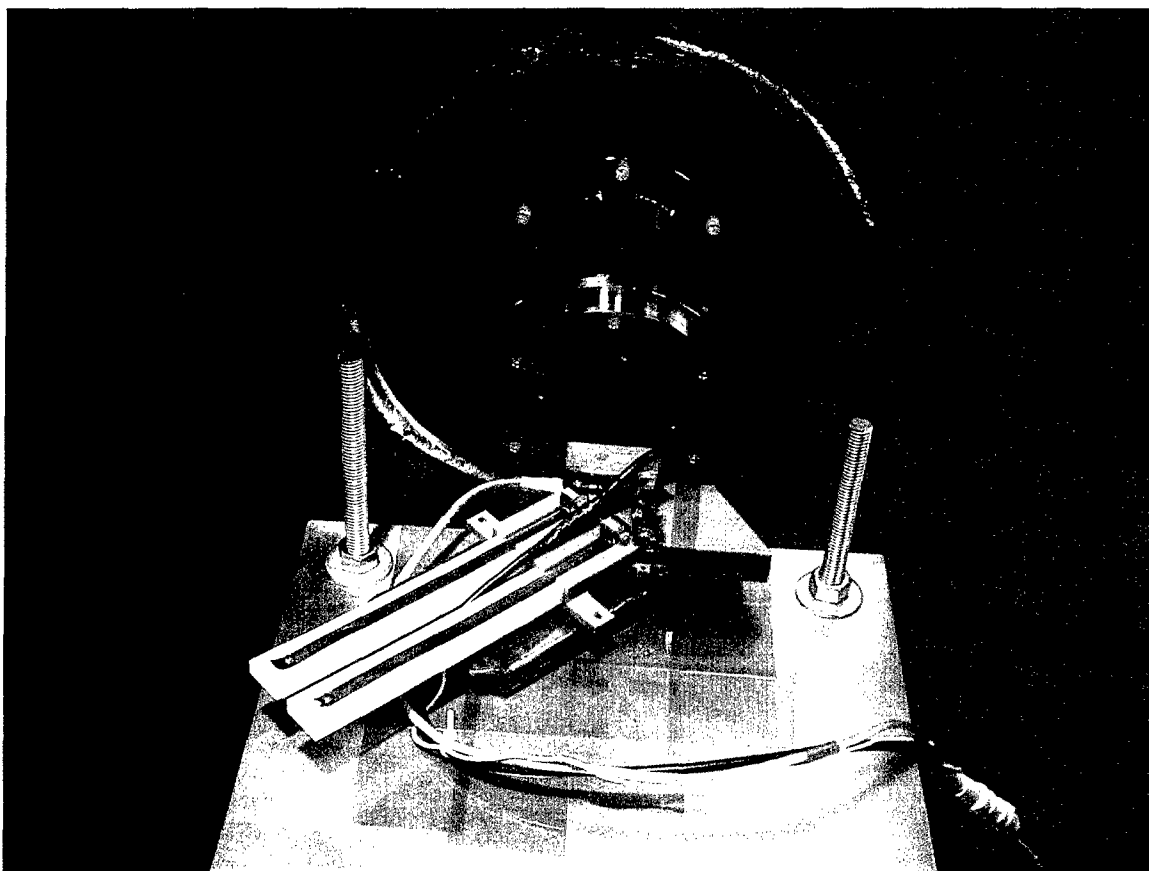


Figure 11: PPT and First Section of Drift Tube. The PPT was actually placed much farther away (254 mm) from the first collimating orifice for this study.

An exploded view of the components of the GEA is shown in Figure 14, and a photograph of the assembled GEA is shown in Figure 15. The GEA housing is constructed of 304 stainless steel, and its entrance has a 19.05 mm diameter. This entrance diameter is maintained through the length of the GEA, giving the collector face the same diameter. Each of the grids is supported on one side by a stainless steel ring; and all of the grids and the collector are connected to their electrical leads by copper rings. The grids, collector, and their associated rings are electrically isolated from each other and the housing by six Teflon disks. A six-hole pattern passes through each Teflon disk, the housing, and a stainless steel compression ring. Three of the holes are used to secure the GEA to the drift tube's Plexiglas bulkhead, while the other three holes allow

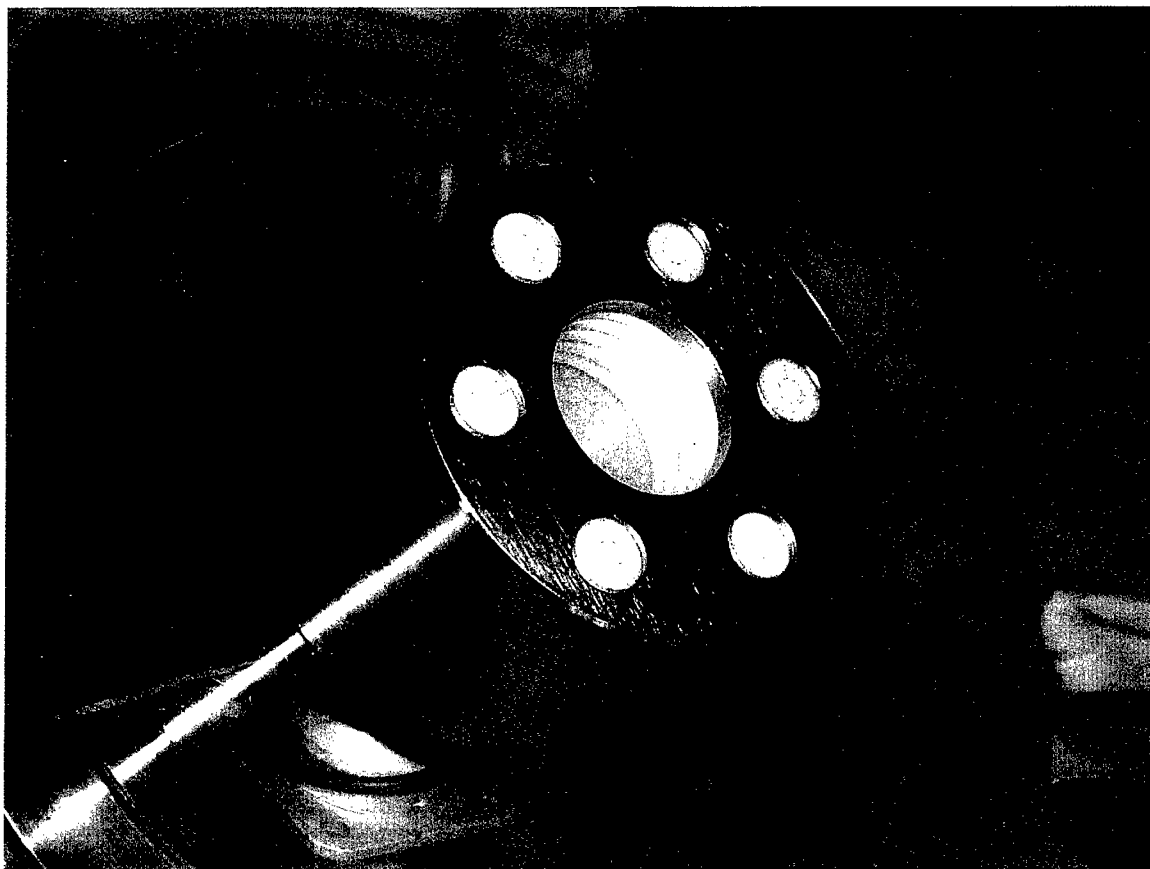


Figure 13: The Gridded Energy Analyzer

The grids are made of electroformed nickel mesh and secured to the copper and stainless steel rings through compression only. The grid closest to the GEA entrance has a much smaller transmission than the other three, and is used primarily to reduce the electron and ion density so that the plasma has a much higher Debye length when it encounters the last three grids. This first grid is electrically connected to the GEA housing at the back of the device. The last three grids (the repelling grids) are configured identically to those shown in Figure 6. Specifications of the grids are contained in Table 4.

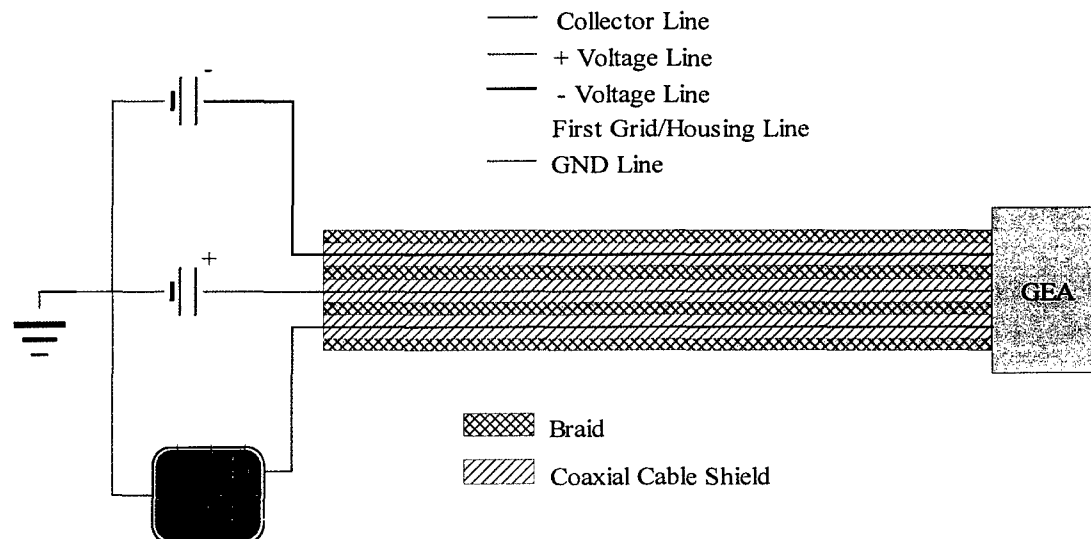
Table 4: GEA Grid Specifications

	Mesh	Transmission	Hole Size (μm)	Wire Width (μm)
First Grid	1000	50	18	7.4
Repelling Grids	100	85	234	19.8

As a result of the grid transmissions selected, the effective collection area of the collector is 87.52 mm^2 .

Teflon (PTFE) was chosen as the electrical insulator because of its ability to be compressed around the grids and how easily it is machined. Electrical isolation of each grid was accomplished by recessing a channel into each Teflon disk in which the grids and rings could be held. In determining how little Teflon could be used to separate the grids from each other, the limiting electrical property of the material was its resistance to arcing across its surface rather than its dielectric strength. Unfortunately, the ASTM test (D495-99) that it is commonly used to test an electrical insulator's arc resistance measures how long a high-voltage, low-current arc can be held above the surface of the insulator without causing a conduction path to form along that surface.⁶² Such a measurement is helpful in comparing insulators, but it does not allow one to scale the size of the insulator between the grids based on it. In the end the grid separation distance was just selected to be on the range of other GEAs that used Teflon insulation disks.^{53,63} Except for the distance between the housing and first grid (which is 1.93 mm), each grid and the collector are separated from one another by 3.34 mm. This distance includes the thickness of one Teflon disk and set of support rings.

The final instrumentation line set-up used to control the GEA through the vacuum electrical feedthrough can be found in Figure 16. In this set-up three coaxial cables are kept inside a wire braid is connected only to the first grid/housing of the GEA. The shields of the coaxial cables are connected to the braid at a point near the vacuum electrical feedthrough, which causes the braid and coaxial cable shields to act as a double electrostatic shield for the coaxial cable inner conductors. The inner conductors are



The ion current incident on the GEA collector is determined by comparing the current through the collector line to that through the first grid/housing line if the GEA is floated, or to ground if it is not. The former method is known as differential amplification, and it can be done by either subtracting one signal from the other in the oscilloscope (also known as quasi-differential amplification) or through an external differential probe or amplifier. Several different differential amplifiers were used to record the collector current when the GEA first grid/housing was floated, and these efforts are documented in the next chapter.

The oscilloscope (TDS 420A) used throughout this study has already been briefly described, but as its specifications played a large role in determining the quality of the GEA collector signal recorded, a more thorough description is needed. The fastest sampling time the TDS 420A can offer is 1×10^8 samples a second, while the longest record length is 30,000 data points. This translates to one sample every 10 ns over a period of 300 μ s if the oscilloscope is run at top speed and record length. At the voltage sensitivities (5-20 mV/division) used in this study, the oscilloscope has a rise time of 2.3 ns and a dynamic range of ± 5 divisions.

Chapter 4: Data Analysis

From the first measurement taken on the TOF/GEA, it was clear that the PPT is a strong source of electromagnetic interference (EMI). This was not surprising, as several studies have been committed to testing for EMI from PPTs and then finding methods to shield the spacecraft from it.^{1,3,4} Still, much more time was spent in this study characterizing the effects of EMI from the Dawgstar PPT upon the GEA and finding methods to lessen its influence than was initially planned.

Although the GEA was located 3.68 m away from the EMI source, during the first PPT pulses taken on the TOF/GEA any floated part of the device or lines attached to it picked up enough EMI to totally obscure the signal of the collector plate through capacitive coupling. Another measure of the EMI generated by the PPT pulse was that an oscilloscope placed a similar distance away from the thruster as the GEA could be triggered by the pulse, even with nothing attached to any of its input channels.

Methods of lessening the EMI pickup in the collector line attempted included changes to the GEA instrumentation cabling and the use of differential amplifiers. The first and least successful cabling set-up used five insulated electrical lines (one for each repelling grid, the first grid/housing, and the collector) inside an unshielded cable that was approximately 6.4 m long. Power was supplied to the repelling grid lines using a laboratory power supply. This cabling was found to pick up far too much electromagnetic noise even when the PPT was not being pulsed.

Another cabling set-up that was tried involved four coaxial cables inside a wire braid. The shields of the coaxial cables and the braid were connected only at the oscilloscope end of the cabling, where they were tied to ground. The inner conductors of the coaxial cable were connected to the first grid/housing, collector, ion repeller, and both electron

repellers, respectively. Additionally, the laboratory power supply was replaced by 45 V batteries whose potential was varied using a voltage divider. The primary goal of this set-up was to allow the GEA first grid/housing to be floated, and the collector and first grid/housing lines to be compared to find the collector current. Once again however, the EMI pick-up from the PPT current discharge was found to obscure the collector current signal. Specifically, the EMI would induce such a high current in the collector and first grid/housing lines that the dynamic range of the oscilloscope was exceeded.

The GEA instrumentation cabling set-up described in the last chapter and diagramed in Figure 16 shielded out enough of the EMI for a fairly consistent current signal to be seen on the collector when the shield of the collector coaxial line (and in turn the other coaxial shields, braid, and first grid/housing) was tied to ground. Getting a signal without tying the collector coaxial line to ground in this configuration was much more troublesome, though several different methods of differential amplification were tried in order to do so.

The first method of differential amplification attempted was quasi-differential, and it just consisted of subtracting the digital signal of the collector line from the first grid/housing line (the collector line shield). Results using this method were inconclusive, so a Tektronix P5205 high voltage differential probe was used to compare the analog signals of the two lines. Unfortunately, the minimum attenuation of the probe (50x) was far too high to allow the signal to be seen. The next differential amplifier used was built on a protoboard by Dr. Tom Mattick using an INA118 instrumentation amplifier. This differential amplifier showed much promise, especially when housed in a metal box, but time ran out in the study before a consistent collector current signal could be received.

As a result of the EMI pick-up and failure to find an appropriate differential amplifier in the time allotted, the GEA first grid/housing was grounded for all of the data presented in the reported research. Grounding the first grid/housing likely led to some perturbations

in the PPT exhaust plume as it arrived at the GEA, but the high flow velocity of the plume most likely made the effect of these perturbations very small.

4.1 Measurements on a Dawgstar PPT

Two complete surveys of the ion repelling grid potential were recorded using the TOF/GEA instrument on the Dawgstar PPT. The potential needed to repel all the electrons in the flow was determined using Eq. (2) and a maximum flow velocity¹⁹ of 60 km/s to be -10 mV. Because the wire spacing of the electron and secondary electron repelling grids is quite a bit bigger than the Debye length, the potential of the grids for the first data set was between -44 V and -45 V (the variation being due to voltage draw down on the batteries over time). For the second set of data the same grids were held at -42 V.

In the first survey, the ion repelling grid potential was increased by one volt each PPT pulse until data was obtained for almost every integer ion repelling grid potential between 5 and 200 V. The oscilloscope was triggered by the EMI from the PPT pulse recorded on an unconnected input channel, and this event was set as time zero. The collector current recorded for each pulse was examined using the standard filter function in Matlab to remove the high frequency noise. The maximum current, time of initial current rise, and average value of the current fiducial (defined as the current between where the EMI pulse dies out at 5 μ s and 40 μ s later, well before any ions were seen to arrive) were recorded. The maximum current as a function of the ion repelling grid potential for the first data set is shown in Figure 17.

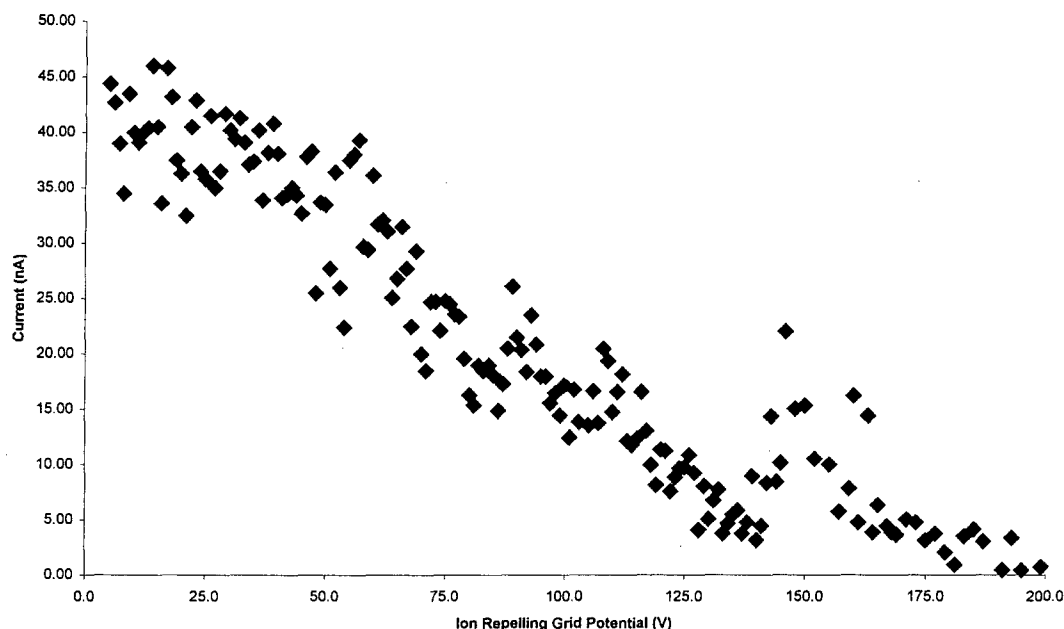


Figure 15: First Survey Maximum Collector Current vs. Ion Repelling Grid Potential

The first survey is comprised of data taken on five separate days over the course of an eight day period. This created some inconsistencies in the overall data set because (as was found afterwards) it generally took about a dozen PPT pulses to build up an equilibrium pressure in the vacuum tank that was consistent for all pulses. Maximum collector current measurements taken at one ion repelling grid potential before the equilibrium pressure was reached tended to be much higher than they were after the equilibrium pressure had been established. This lack of equilibrium pressure is believed to be why there is a bump in Figure 17 around 150 V, as these data were taken at the start of one day's testing.

For the second survey, five PPT pulses were performed at every five volts in the ion repeller potential range 5-150 V. To ensure variations in vacuum tank pressure did not affect the data, the PPT was fired every three minutes for the duration of the data collection; and data were not collected at the start of each day until the tank equilibrium

pressure had been built up by at least a dozen PPT pulses. The oscilloscope was triggered by the voltage rise in the Rogowski coil around the top stripline of the PPT, and this event was set as time zero. Again, the collector current recorded for each pulse was examined using the standard filter function in Matlab to remove the high frequency noise. The maximum Rogowski and collector currents, time of initial current rise, and the current fiducial were recorded. The five maximum current measurements at each ion repelling grid potential were used to calculate the standard deviation, which is represented as the length of either side of the error bars from the average current in Figure 18.

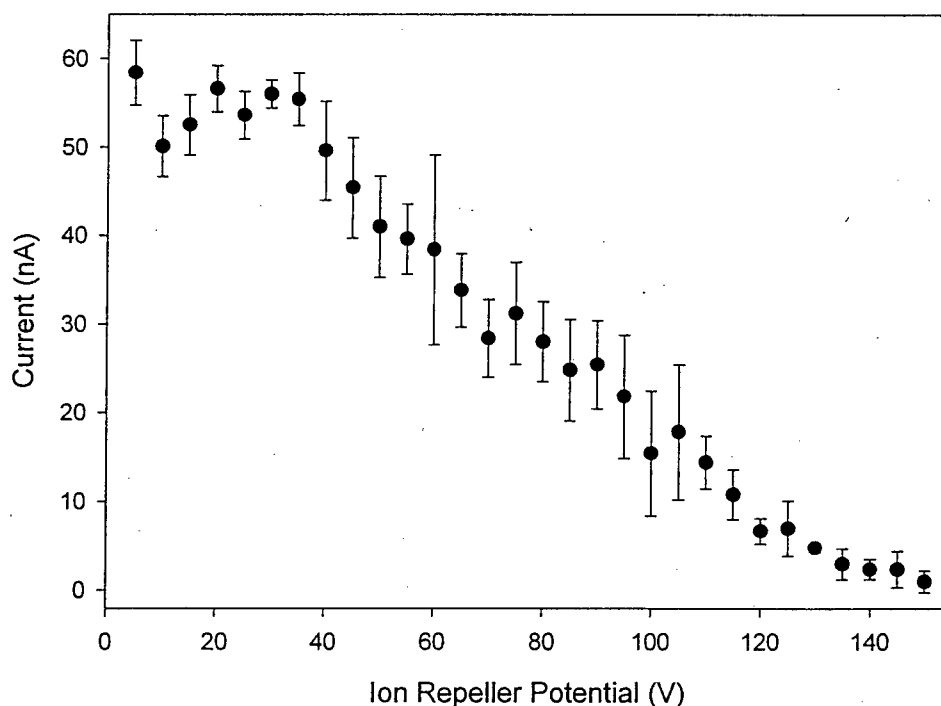


Figure 18: Second Survey Maximum Collector Current vs. Ion Repelling Grid Potential

Additional data were taken with the TOF/GEA following the second survey using the same parameters and methods. The only changes were in how many PPT pulses were taken at each ion repelling grid potential, and in the range of ion repelling grid potentials applied (either 0 V or >150 V). This data set was used to calculate the maximum velocity and identity of the PPT exhaust plume ions with the highest retarding potentials, as detailed in the next section.

4.2 Discussion of Results

Determining the maximum current of each run proved to be a relatively simple task, but determining the time of initial collector current increase was somewhat more difficult. When the data for both surveys were first examined, the time of initial collector current increase was defined to be the time following time zero where the current began to display a sharp, continual increase. This method yielded widely varying times, even at the same ion repelling grid potential.

A more rigorous method of determining the time of initial collector current increase was found by using the intersection between a line drawn through where the current passes through 25% and 75% of its maximum value and another line drawn through the average slope of the current fiducial. An example of using this method to determine the time of initial current increase is shown in Figure 19. This time, minus the time of the peak discharge current from the integrated Rogowski coil voltage, is the ion flight time.

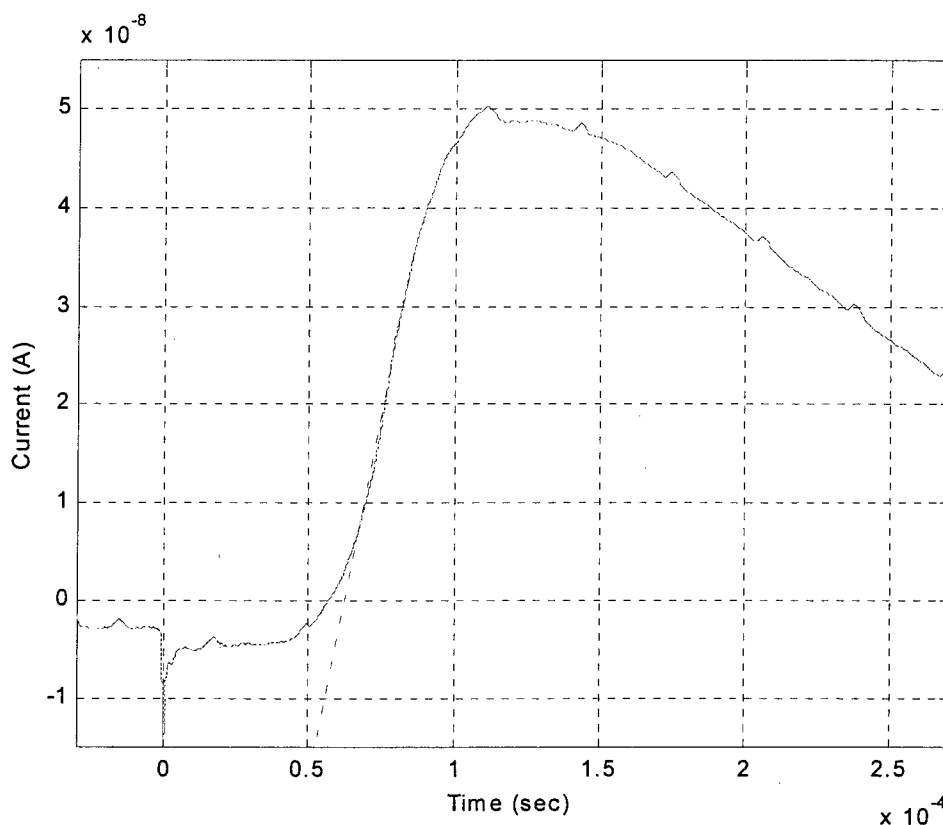


Figure 19: Example of Technique Used To Measure Time Of Initial Collector Current Increase

To measure the maximum ion velocity of the PPT exhaust plume, the PPT was fired seven times with the ion repeller potential set to zero (the ion repeller electrical lead was terminated through a 1 M Ω resistor). Using the intersecting slope lines method, the maximum ion velocity was found to be 64 ± 3.6 km/s.

To perform mass spectral analysis on the plume using TOF/GEA, the ion repeller potential was set high enough to only let the ions with the highest retarding potentials through. The ions that reach the collector at such high ion repeller potentials can be assumed to have retarding potentials near that of the ion repeller. Thus, the ion repeller potential specified and the ion flight time measured can be used in Eq. (3) to directly calculate the mass-to-charge ratio of the ions with the highest retarding potential.

To ensure only the highest retarding potential ions were seen, the ion repeller potential was initially set high enough to not allow any ions to reach the collector. The ion repeller potential was then slowly lowered until a definite current rise corresponding to ion arrival was seen on the collector. Somewhat in conflict with this desire to sample only the ions with highest retarding potentials was the need to have a large enough signal (in relation to the electromagnetic noise) to easily and consistently determine the ion flight time. The ion repeller potential that was found to balance these two desires was 150 V.

Five PPT pulses were taken at an ion repeller potential of 150 V as part of the second ion repeller potential survey. The collector current vs. time for each of those pulses is presented as Figures 20-24.

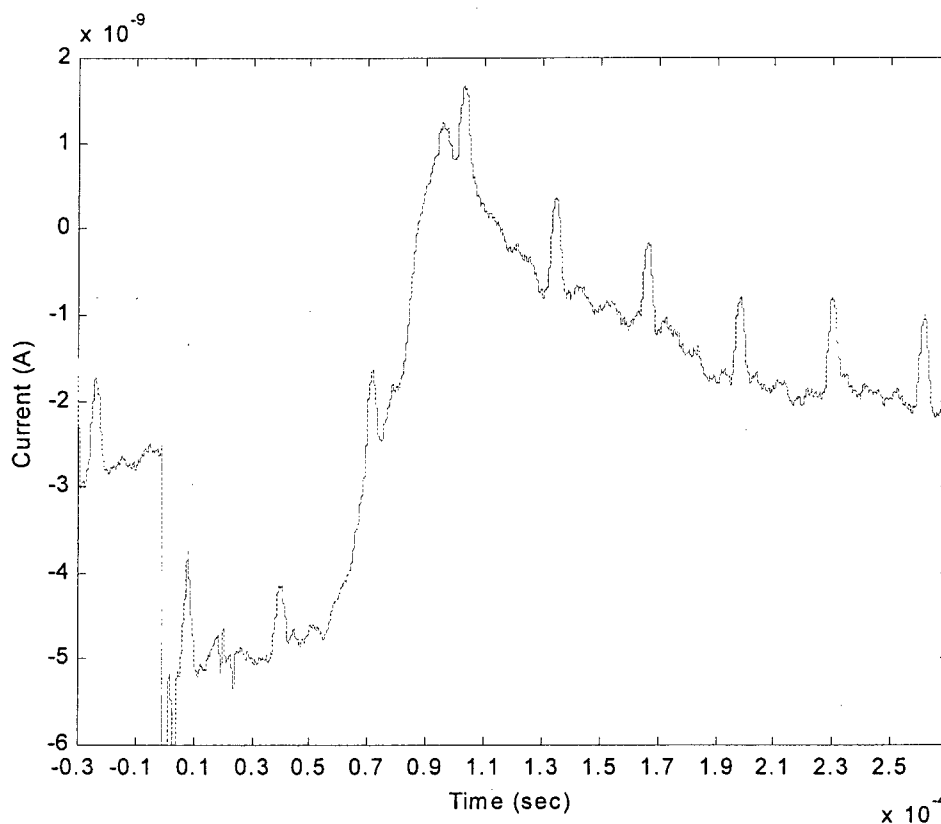


Figure 20: Collector Current at Ion Repeller Potential of 150 V, PPT Pulse 1

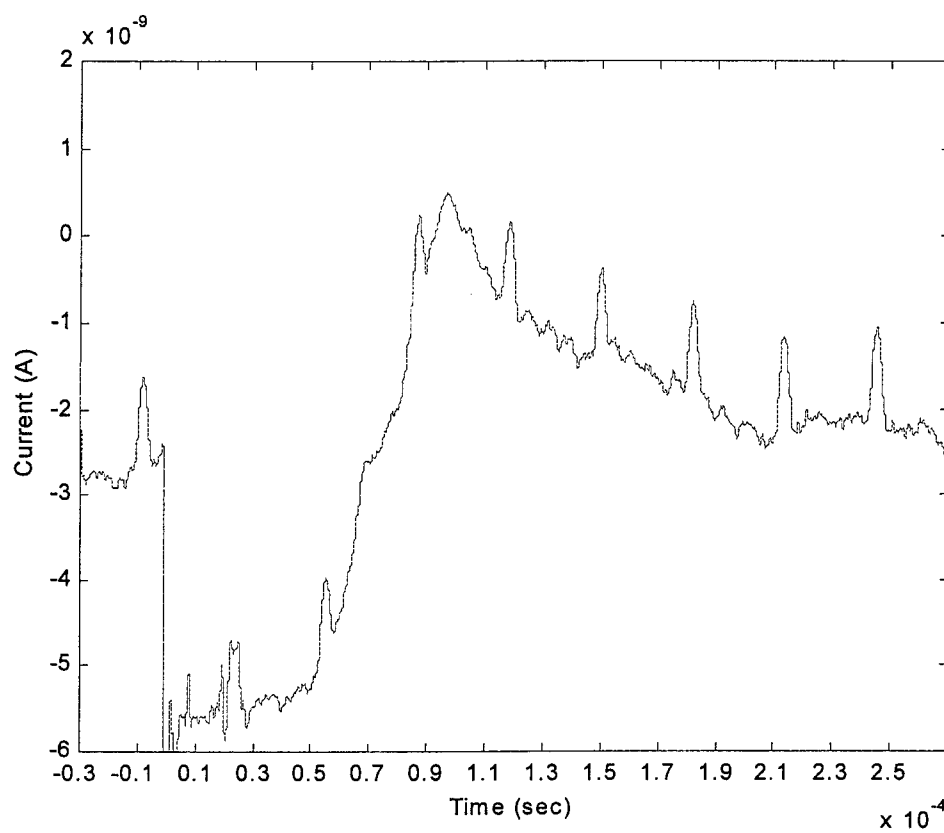


Figure 21: Collector Current at Ion Repeller Potential of 150 V, PPT Pulse 2

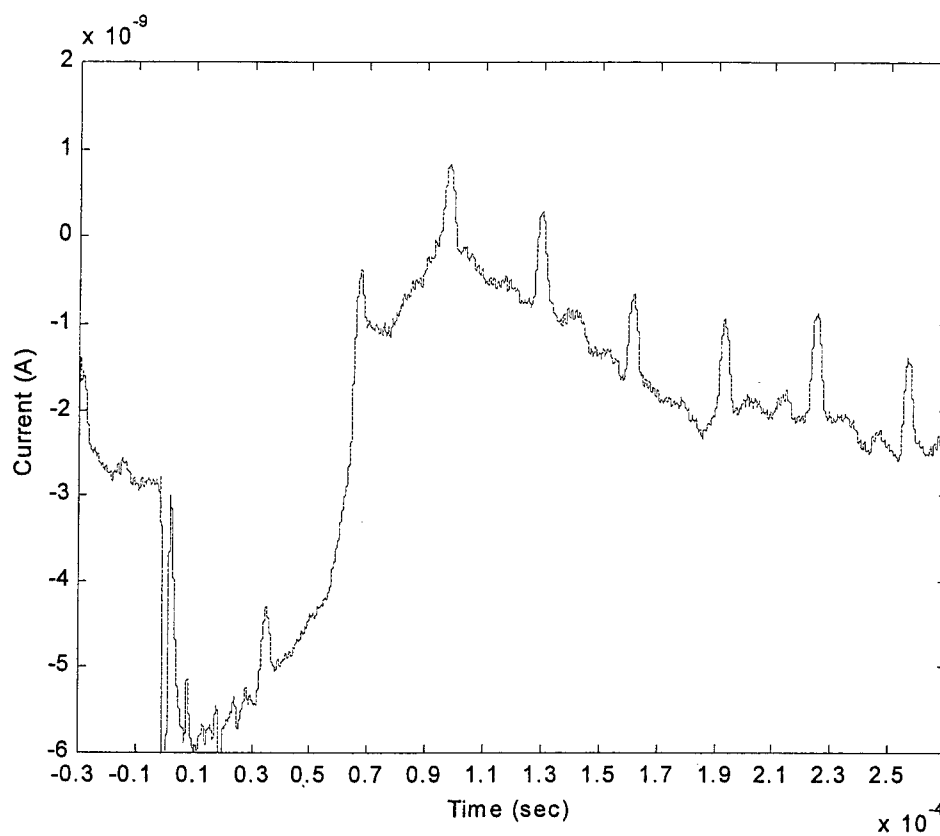


Figure 22: Collector Current at Ion Repeller Potential of 150 V, PPT Pulse 3

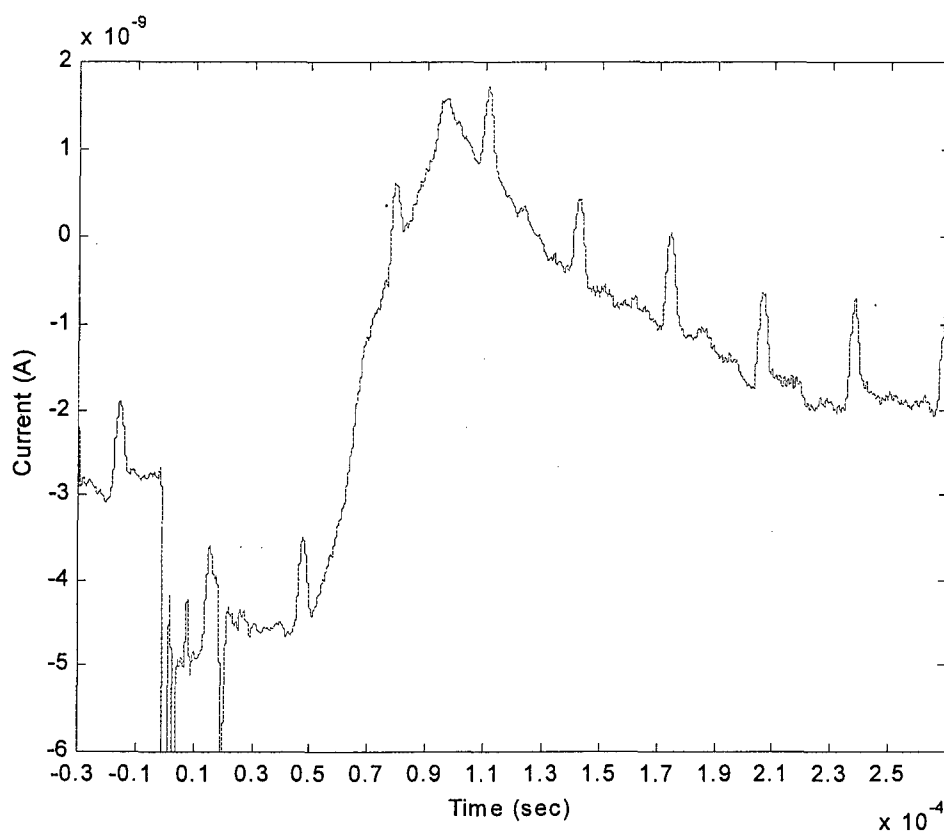


Figure 23: Collector Current at Ion Repeller Potential of 150 V, PPT Pulse 4

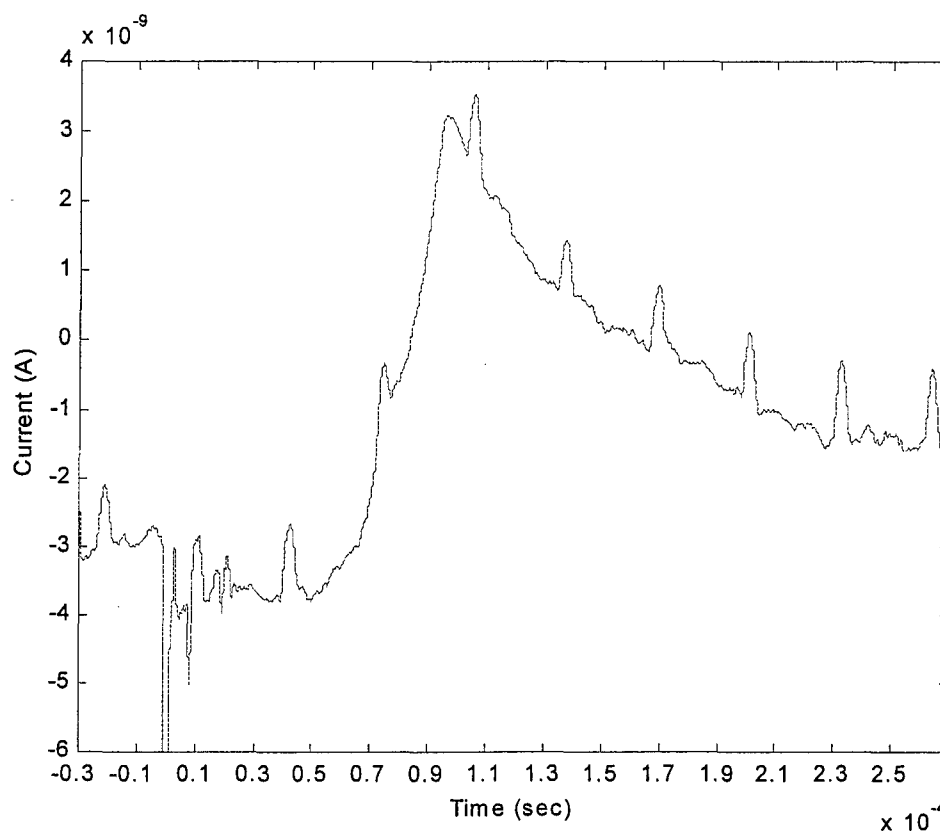


Figure 24: Collector Current at Ion Repeller Potential of 150 V, PPT Pulse 5

For pulses 1-3, the slope of the current fiducial makes it difficult to determine at what time the current begins to rise as a result of ion arrival at the collector. Further complicating this measurement is the 1 nA noise at 32 kHz, as it obscures what appears to be the initial current rise in pulses 1-3. Luckily, the time of initial current increase is fairly distinct in pulses 4 and 5. The noise in both signals makes using the method of intersecting slope lines inaccurate, so the time at which the slope of the current becomes positive and stays positive (ignoring the 32kHz noise) until the maximum current is reached was defined as the time of initial current increase. In contrast to previous efforts using this method with larger current signals, the ion travel time for pulses 4 and 5 were fairly close together, 50.6 μ s and 49.7 μ s respectively. If it is assumed the ions that arrived for both of these pulses had a retarding potential in the range 150-190 V (above 190 V almost all the ions are repelled, see Figure 17), the mass-to-charge ratio of these

ions is around $5.47 - 7.18 \times 10^{-8}$ kg/C. The ion mass-to-charge ratio of the elements that comprise the Teflon propellant can be found in Table 5. Based on these known mass-to-charge ratios and the ratios found, it appears that C^{++} and/or F^{+++} are present in the PPT exhaust plume, and have the highest retarding potentials of the species in the plume.

Table 5: Mass-to-Charge Ratios of Ionic Elements of Teflon

Species	m/q (kg/C)
C^+	1.24×10^{-7}
C^{++}	6.22×10^{-8}
C^{+++}	4.15×10^{-8}
F^+	1.97×10^{-7}
F^{++}	9.84×10^{-8}
F^{+++}	6.56×10^{-8}

It should be noted that the ion travel times found for pulses 4 and 5 yield ion velocities around 10 km/s faster than the measured maximum ion velocity found using an ion repeller potential of zero. Because the ions being measured in pulses 4 and 5 generate such a small current it is reasonable to assume they are present in the pulses taken with the ion repeller set to zero, but are not seen because the current rise dominated by ions with lesser retarding potentials is so much greater in magnitude.

Initially it was hoped that each PPT pulse would produce sufficiently reproducible signals on the collector, allowing the current at each retarding potential to be found by subtracting signals found at different ion repeller potentials. Being able to specify the retarding potential in this method would allow mass spectral analysis at retarding potentials below the maximum found in the plume, and provide a highly accurate way to calculate $dI(V)/dV$. Unfortunately, as given evidence for in Figure 18, there was too much variation in the current collected from pulse to pulse at the same ion repeller potential for this method to be accurate.

The $dI(V)/dV$ curve may still be calculated based solely on the maximum current recorded at each ion repelling potential. As this is a differential measurement, it is essential the magnitude of the random variations in the maximum current recorded from pulse to pulse not be greater than the magnitude of any trends in those same data that may indicate the general shape of the retarding potential distribution. The $dI(V)/dV$ curve for the first ion repeller survey is presented in Figure 25, and the curve for second survey is presented in Figure 26. Attempts to smooth and filter these curves did not produce any distinguishable structure.

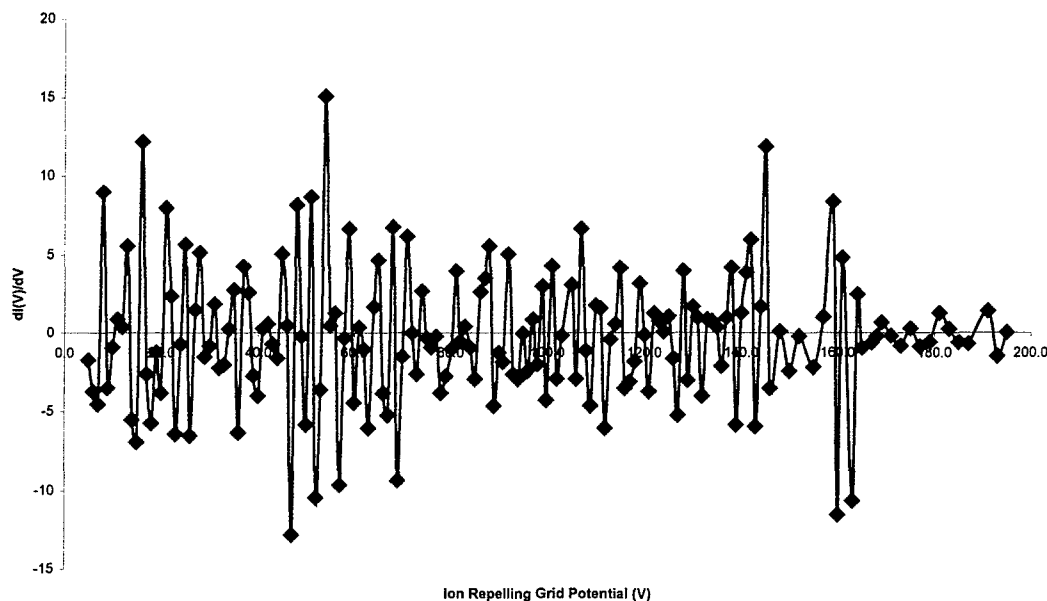


Figure 25: $dI(V)/dV$ Data For Maximum Collector Current In First Survey

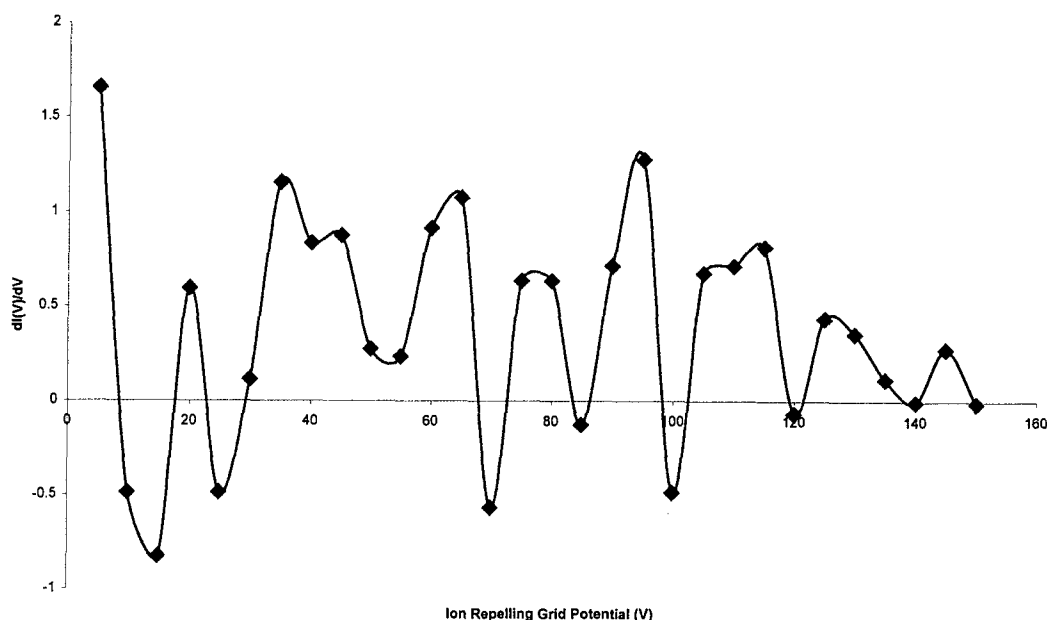


Figure 26: $dI(V)/dV$ Data For Average Maximum Collector Current In Second Survey

While not necessarily useful in producing the ion retarding potential distribution directly, the first and second surveys can still be used to define the minimum ion retarding potential. Using Figures 17 and 18, the minimum retarding potential is where the slope of the $I(V)$ curve begins to become negative, indicating that some ions are starting to be repelled. For both surveys, the minimum retarding potential appears to be around 35 V.

The first and second surveys also yield some information about the general shape of the retarding potential distribution when the logarithm of the maximum collector current is plotted in Figure 27. As the PPT exhaust plume has been documented to have an ion temperature of only a few eV,¹ were the plume also mono-energetic one would expect the $I(V)$ curve drop rapidly to zero once the minimum retarding potential of the plume was exceeded by the ion repeller potential. Figure 27 displays that this is not the case, and based on the slope of the $\log I(V)$ curve, the PPT exhaust plume has a retarding potential spread of around 100 V. This retarding potential spread could indicate that the ions in the

plume are created with a widely spread velocity distribution, or that the velocity distribution spreads as the exhaust plume travel farther away from the PPT. The spread could also be representative of several species-specific retarding potential distributions each contributing to the overall spread separately.

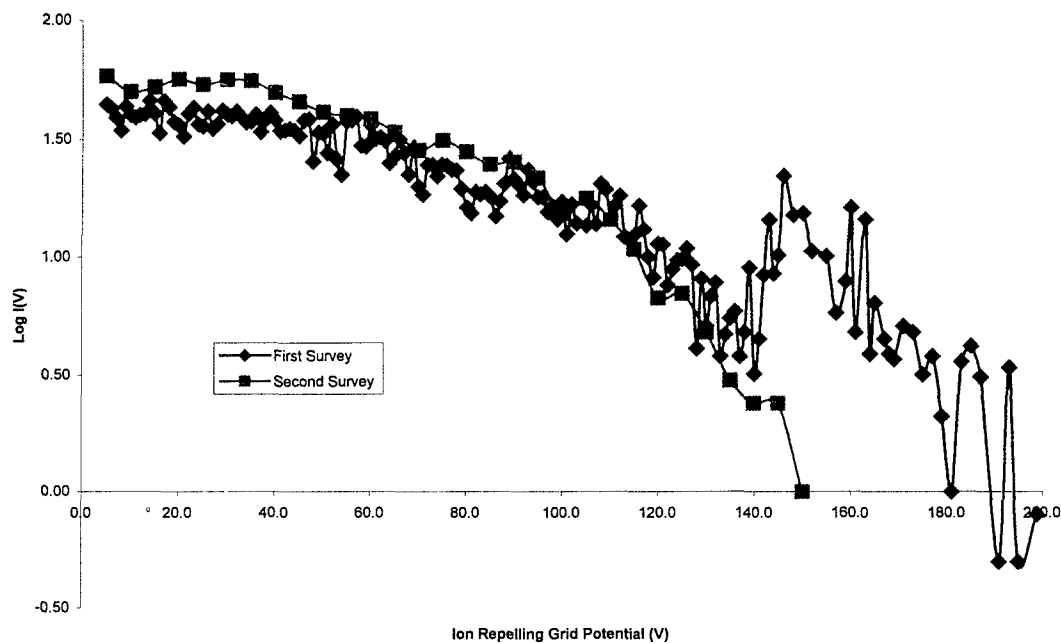


Figure 27: Log Plot of I(V) For Both Surveys

Chapter 5: Conclusions

The body of this report details the design and implementation of a time-of-flight/gridded energy analyzer instrument to analyze the species and energy distributions in the exhaust plume of a pulsed plasma thruster. The motivation behind this study came from a desire to both better understand the contamination threat from the PPT exhaust plume and to help validate computational models of the plume. A survey of previous experimental investigations into the PPT exhaust plume determined that no successful attempt has been made to date to analyze the composition and energy distribution of the plume using anything other than spectroscopic methods.

The TOF/GEA instrument works in two modes. In mass spectrometer mode, the instrument specifies the minimum retarding potential and measures the ion flight time to determine the species mass-to-charge rate. In retarding potential analyzer mode, the maximum currents collected at different ion repeller potentials are compared to one another to determine the ion retarding potential distribution.

The TOF/GEA instrument was used to examine the exhaust plume of the 5 J, rectangular Dawgstar PPT. Without repelling any ions out of the plasma flow, the maximum ion velocity of the plume was found to be 64 ± 3.6 km/s. When the ion repeller potential was increased to repel almost all of the ions out of the flow, a mass-to-charge ratio of the remaining ions was estimated as $5.47 - 7.18 \times 10^{-8}$ kg/C. This mass-to-charge ratio range indicates the presence of C^{++} , F^{+++} , or both, in the exhaust plume. Two separate surveys of the collector current as a function of the ion repeller potential were conducted, but the current collected was too small in relation to the error introduced from PPT pulse to pulse to allow numerical differentiation of the surveys and determination of the ion retarding potential distribution. Both surveys indicated an exhaust plume minimum ion retarding potential of around 35 V, and a kinetic energy spread of approximately 50 eV.

Chapter 6: Future Work

This work began with the objective of characterizing the species and energy distribution of the PPT exhaust plume, and that objective remains. Much work can be done to improve the performance of the TOF/GEA instrument in its current configuration. This work includes investigating better EMI shielding techniques, changing the hole size and transmission of the GEA grids, and simply upgrading to an oscilloscope with better dynamic range (which would allow smaller signal sensitivities to be used). Another goal of this work should be to find a differential amplifier that allows measurements to be taken with the GEA first grid/housing left floating. Once the measurement technique is improved, the off-centerline properties of the PPT plume should be investigated by changing the orientation of the PPT exhaust channel in relation to the first collimating orifice. Shortening the ion travel length by removing the third section of the drift tube should also be attempted, so that how the retarding potential distribution changes as it travels down the tube may be observed.

The next step, following further work with the GEA, is to build a 45° electrostatic energy analyzer of the type used by King⁵¹ and Pollard⁵² for the existing drift tube. This will greatly increase the retarding potential resolution over that currently offered by the GEA. The 45° electrostatic energy analyzer is presented schematically in Figure 28.

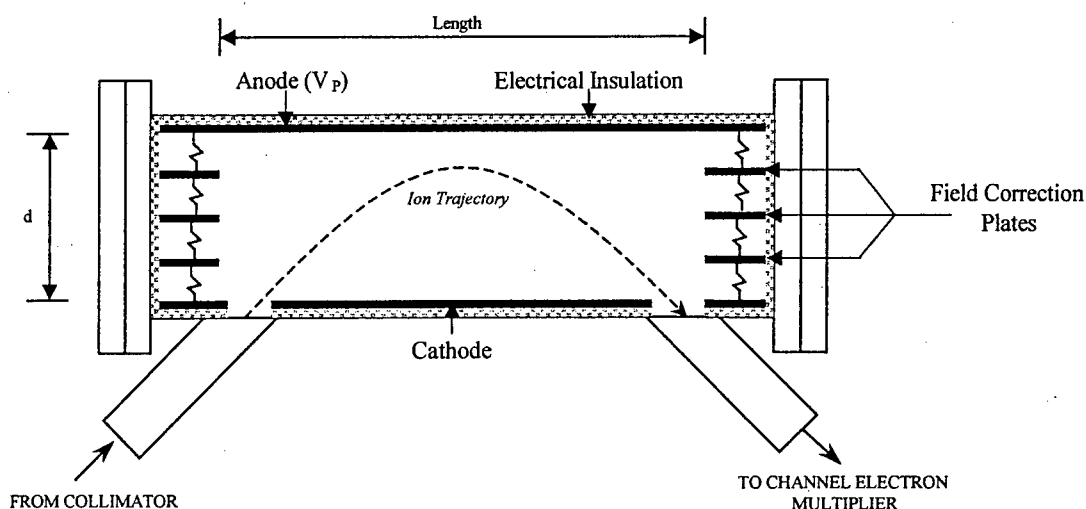


Figure 28: Schematic of 45° The Electrostatic Energy Analyzer

The PPT exhaust plume will enter the analyzer from the current second collimating orifice after traveling through the existing drift tube up until that point. Consisting of a back plate at a potential V_p , and a front plate at ground, the electrostatic energy analyzer creates a uniform, constant electric field V_p/d between the two plates (d being the distance between the plates). The field is made uniform by field correction plates along the perimeter of the analyzer. Ions enter through one slit in the analyzer and are deflected by the electric field on a curved trajectory. Ions with the appropriate energy per charge value are admitted through the exit slit of the analyzer and into the channel electron detector, which records their arrival as a current pulse. The current pulse from the channel electron detector is proportional to the number of ions impinging upon it, and thus the relative quantities of each ionic species in the exhaust plume at one energy can be found, in addition to the velocities and identities of each of the species in the plume.

Using ion trajectory and kinetic energy analysis through the electrostatic energy analyzer, the slit width, distance between plates, and length of the device can be specified.⁵¹ Placing the origin in the center of the entrance slit, and defining the \hat{i} direction to be

parallel to the plates and \hat{j} perpendicular to them; then the ion trajectory through the analyzer is

$$x\hat{i} + y\hat{j} = vt \cos \theta \hat{i} + vt \sin \theta \hat{j} - \frac{V_p}{2dm} q t^2 \hat{j} \quad (13)$$

where θ is the angle from \hat{i} ; and v , t , m , and q are the ion velocity, time in the analyzer, mass, and charge, respectively. Solving for t in the \hat{i} direction trajectory equation with the knowledge that at $\theta = 45^\circ$, $\sin \theta = \cos \theta$, creates the following expression

$$t = \frac{x}{v \sin \theta}, \quad (14)$$

which can then be plugged into the \hat{j} direction trajectory equation to find a time independent expression for y

$$y = x - \frac{V_p q}{2dm} \left(\frac{x}{v \sin \theta} \right)^2. \quad (15)$$

Setting $\theta = 45^\circ$ and using $v^2 = 2qV_i/m$ (where V_i is the ion retarding potential), Eq. (15) simplifies to

$$y = x - \frac{V_p x^2}{2dV_i}. \quad (16)$$

Defining the exit slit as $y = 0$ and $x = l$ (where l is the length between the two slits) and as a point through which all recorded ions must pass, Eq. (16) can be used to define the spectrometer constant (K_{45})

$$K_{45} \equiv \frac{V_p}{V_i} = \frac{2d}{l}. \quad (17)$$

Thus, the ion retarding potential recorded by the 45° electrostatic energy analyzer is

$$V_i = \frac{V_p}{K_{45}}. \quad (18)$$

To determine d and l (and in turn K_{45}) for an actual instrument, King⁵¹ manipulated Eq. (16) to find that $d > l/4$ and presented the retarding potential resolution as

$$\frac{V_i}{\Delta V_i} = \frac{l}{w \sin \theta} \quad (19)$$

where w is the slit width. If we allow w to be the same as the current collimating diameter of the drift tube (3.6 mm), set θ at 45° to the plasma flow path, and aim for the same retarding potential resolution as King,⁵¹ the distance between slits becomes 636 mm. This makes the distance between plates at least 159 mm, which in turn means that an at least 7" ID tube will have to be found to hold the plates of the analyzer and its associated electrical insulation.

Building the 45° electrostatic energy analyzer should allow a full characterization of the PPT exhaust plume ionic species and their energy distribution, but it will do little to characterize the neutral species in the plume and their energy distribution. Such an investigation of the neutral components of the plume will require novel diagnostics such as King's neutral particle flux probe.⁶³

To provide a point of comparison to other PPT exhaust plumes, a Langmuir probe survey of the Dawgstar PPT exhaust plume would be valuable. By supplying a measure of the electron density and temperature in the exhaust plume, the Langmuir probe survey would also be a nice complement to the data obtained with the GEA.

Bibliography

- ¹ Burton, R. L., and Turchi, P. J., "Pulsed Plasma Thruster," *Journal of Propulsion and Power*, Vol. 14, No. 5, 1998, pp. 716-735.
- ² Kang, X., "An Overview of Electric Propulsion Activities in China," IEPC Paper 01-007, October 2001.
- ³ Hirata, M., and Murakami, H., "Electromagnetic Noise Measurement Study of Pulsed Plasma Engine," AIAA Paper 81-0722, April 1981.
- ⁴ Zakrzewski, C. M., Davis, M., and Sarmiento, C., "Addressing EO-1 Spacecraft Pulsed Plasma Thruster EMI Concerns," AIAA Paper 2001-3641, July 2001.
- ⁵ Spores, R. A., Spanjers, G. G., Birkan, M., and Lawrence, T. J., "Overview of the USAF Electric Propulsion Program," AIAA Paper 2001-3225, July 2001.
- ⁶ Antonsen, E. L., Burton, R. L., and Spanjers, G. G., "High Resolution Laser Diagnostics in Millimeter-Scale Micro Pulsed Plasma Thrusters," IEPC Paper 01-157, October 2001.
- ⁷ Takegahara, H., "An Overview of Electric and Advanced Propulsion Activities in Japan," IEPC Paper 01-004, October 2001.
- ⁸ Reichbach, J. G., Sedwick, R. J., and Martinez-Sanchez, M., "Micropropulsion System Selection for Precision Formation Flying Satellites," AIAA Paper 2001-3646, July 2001.
- ⁹ Polzin, K. A., Choueiri, E. Y., Gurfil, P., and Kasdin, N. J., "Plasma Propulsion for Three Terrestrial Planet Finder Architectures: Free-Flying, Monolithic and Tethered," AIAA Paper 2001-3645, July 2001.
- ¹⁰ Hoskins, W. A., Wilson, M. J., Willey, M. J., Meckel, N. J., Campbell, M., and Chung, S., "PPT Development Efforts at Primex Aerospace Company," AIAA Paper 99-2291, June 1999.
- ¹¹ Dunning, J., "NASA's Electric Propulsion Program: Technology Investments for the New Millennium," AIAA Paper 2001-3224, July 2001.
- ¹² Gallimore, A. D., "Review of EP Activities of US Academia," AIAA Paper 2001-3227, July 2001.

¹³ Gorshov, O. A., Koroteev, A. S., Arkhipov, B. A., Murashko, V. M., Anfimov, N. A., Lukayashenko, V. I., Kim, V., and Popov, G. A., "Overview of Russian Activities in Electric Propulsion," AIAA Paper 2001-3229, July 2001.

¹⁴ Cadiou, A., Gelas, C., Darnon, F., Jolivet, L., and Pillet, N., "An Overview of the CNES Electric Propulsion Program," IEPC Paper 01-008, October 2001.

¹⁵ Brito, H., Elaskar, S., Brito, C., and Ballete, R., "Performance and Design Studies Status of the P4S-1 Thruster," IEPC Paper 01-145, October 2001.

¹⁶ Wentink, T., Jr., "High Temperature Behavior of Teflon," AVCO-Everett Research Laboratory, AF 04(647)-278, Everett, MA, July 1959.

¹⁷ Hutchinson, I. H., Principles of Plasma Diagnostics, Cambridge University Press, New York, 1987.

¹⁸ Myers, R. M., Arrington, L. A., Pencil, E. J., Carter, J., Heminger, J., and Gatsonis, N., "Pulsed Plasma Thruster Contamination," AIAA Paper 96-2729, July 1996.

¹⁹ Gatsonis, N. A., Eckman, R., Xuemin, Y., Pencil, E. J., and Myers, R. M., "Experimental Investigations and Numerical Modeling of Pulsed Plasma Thrusters," *Journal of Spacecraft and Rockets*, Vol. 38, No. 3, 2001, pp. 454-464.

²⁰ Antropov, N., Gomilka, L., Diakonov, G., Krivonosov, I., Popov, G., and Orlov, M., "Parameters of Plasmoids Injected by PPT," AIAA 97-2921, July 1997.

²¹ Hirata, M., and Murakami, H., "Exhaust Gas Analysis of a Pulsed Plasma Engine," IEPC Paper 84-52, May 1984.

²² Guman, W. J., and Begun, M., "Pulsed Plasma Plume Studies," Fairchild Industries, Inc., AD-A036904, Farmingdale, NY, Mar. 1977.

²³ Byrne, L. T., Gatsonis, N. A., and Pencil, E. J., "Triple Langmuir Probe Measurements in the Plume and Backflow Region of a Pulsed Plasma Thruster," AIAA Paper 2001-3640, July 2001.

²⁴ Bushman, S. S., and Burton, R. L., "Heating and Plasma Properties in a Coaxial Gasdynamic Pulsed Plasma Thruster," *Journal of Propulsion and Power*, Vol. 17, No. 5, 2001, pp. 959-966.

²⁵ Dawbarn, R., Steely, S. L., McGuire, R. L., and Price, L. L., "A Study of Test Techniques for Evaluating Ablative Plasma Engines in Vacuum Test Cells," Calspan Field Services, Inc., AD-105875, Arnold Air Force Station, TN, Oct. 1981.

- ²⁶ Rudolph, L. K., and Jones, R. M., "Pulsed Plasma Thruster Contamination Studies," AIAA Paper 79-2106, Oct. 1979.
- ²⁷ Vondra, R., Thomassen, K. and Solbes, A., "A Pulsed Electric Thruster for Satellite Control," *Proceedings of the IEEE*, Vol. 59, No. 2, 1971, pp. 271-277.
- ²⁸ Thomassen, K. I., and Vondra, R. J., "Exhaust Velocity Studies of a Solid Teflon Pulsed Plasma Thruster," *Journal of Spacecraft and Rockets*, Vol. 9, No. 1, 1972, pp. 61-64.
- ²⁹ Thomassen, K. I., and Tong, D., "Interferometric Density Measurements in the Arc of a Pulsed Plasma Thruster," *Journal of Spacecraft and Rockets*, Vol. 10, No. 3, 1973, pp. 163-164.
- ³⁰ Dawbarn, R., Steely, S. L., McGuire, R. L., and Pipes, J. G., "Operating Characteristics of an Ablative Pulsed Plasma Engine," Fairchild Industries, Inc., AD-A118260, Arnold Air Force Station, TN, Jul. 1982.
- ³¹ Spanjers, G. G., and Spores, R. A., "PPT Research at AFRL: Material Probes to measure the Magnetic Field Distribution in a Pulsed Plasma Thruster," AIAA Paper 98-3659, July 1998.
- ³² Popov, G., Antropov, N., Dyakonov, G., Orlov, M., Tyutin, V., and Yakovlev, V., "Experimental Study of Plasma Parameters in High-Efficiency Pulsed Plasma Thrusters," IEPC Paper 01-163, October 2001.
- ³³ Markusic, T. E., and Spores, R. A., "Spectroscopic Emission Measurements of a Pulsed Plasma Thruster Plume," AIAA Paper 97-2924, July 1997.
- ³⁴ Umeki, T., Mikellides, P. G., Kamhawi, H., and Turchi, P. J., "Quantitative Spectroscopic Measurements of a Pulsed Plasma Microthruster," AIAA Paper 00-3259, July 2000.
- ³⁵ Spanjers, G. G., McFall, K. A., Gulczinski, F. S., III, and Spores, R. A., "Investigation of Propellant Inefficiencies in a Pulsed Plasma Thruster," AIAA Paper 96-2723, July 1996.
- ³⁶ Rudolph, L. K., Pless, L. C., and Harstad, K. G., "Pulsed Plasma Thruster Backflow Characteristics," *Journal of Spacecraft and Rockets*, Vol. 17, No. 5, 1980, pp. 447-452.
- ³⁷ Spanjers, G. G., Lotspeich, J. S., McFall, K. A., and Spores, R. A., "Propellant Losses Because of Particulate Emission in a Pulsed Plasma Thruster," *Journal of Propulsion and Power*, Vol. 14, No. 4, 1998, pp. 554-559.

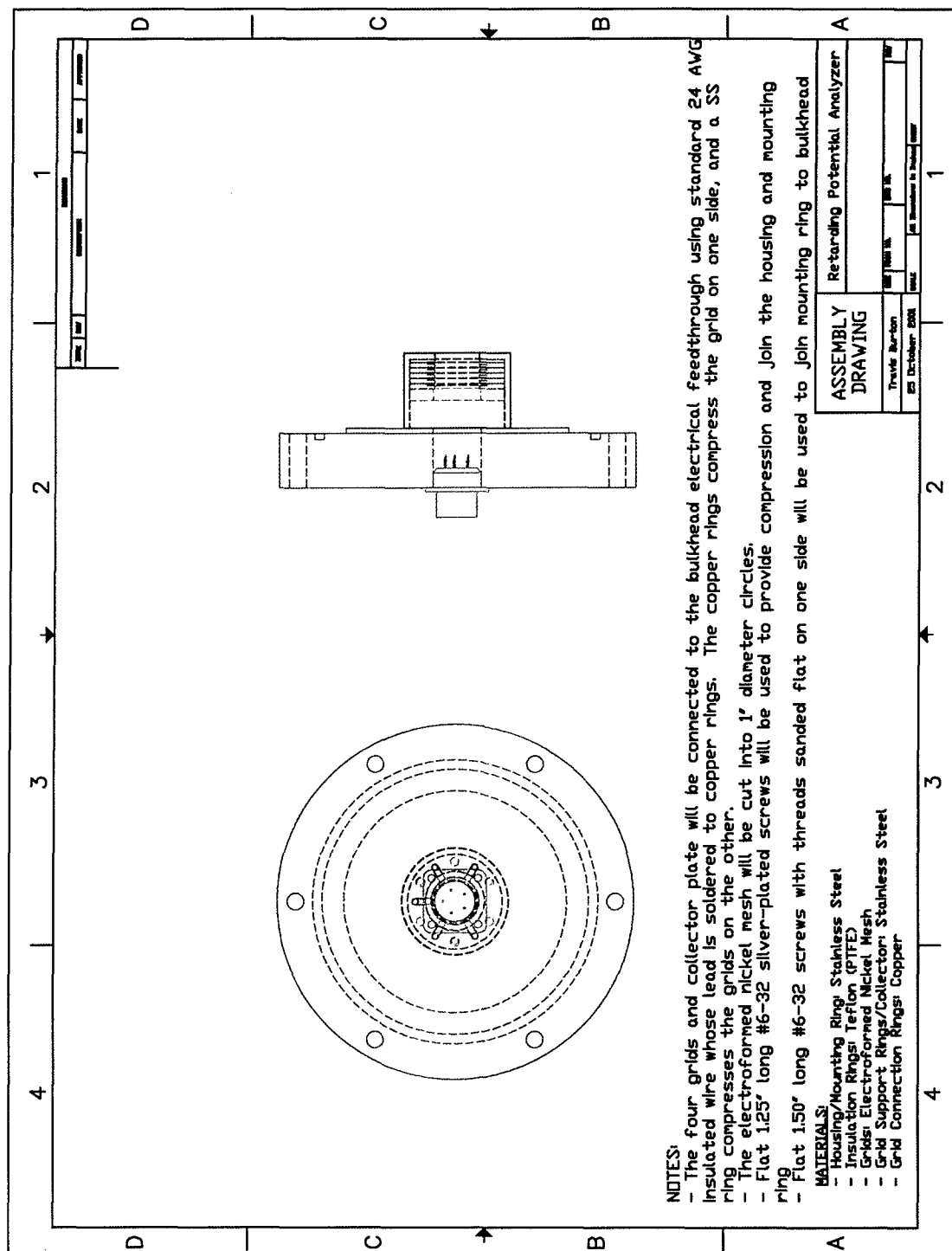
- ³⁸ Arrington, L. A., Marrese, C. M., and Blandino, J. J., "Pulsed Plasma Thruster Plume Study: Symmetry and Impact on Spacecraft Surfaces," AIAA Paper 2000-3262, July 2000.
- ³⁹ Gatsonis, N. A., and Yin, X., "Hybrid (Particle-Fluid) Modeling of Pulsed Plasma Thruster Plumes," *Journal of Propulsion and Power*, Vol. 17, No. 5, 2001, pp. 945-958.
- ⁴⁰ Keidar, M., Boyd, I. D., and Beilis, I. I., "Model of Particulate Interaction with Plasma in a Teflon Pulsed Plasma Thruster," *Journal of Propulsion and Power*, Vol. 17, No. 1, 2001, pp. 125-138.
- ⁴¹ Boyd, I. D., Keidar, M., and McKeon, W., "Modeling of a Pulsed Plasma Thruster From Plasma Generation to Plume Far Field," AIAA Paper 99-2300, June 1999.
- ⁴² Keidar, M., and Boyd, I. D., "Electromagnetic Effects in the Near Field Plume of a Pulsed Plasma Thruster," AIAA Paper 2001-3638, July 2001.
- ⁴³ Rhodes, R., Keefer, D., and Thomas, H., "A Numerical Study of a Pulsed Plasma Thruster," AIAA Paper 2001-3895, July 2001.
- ⁴⁴ Ziemer, J. K., and Choeiri, E. Y., "A Characteristic Velocity for Gas-fed PPT Performance Scaling," AIAA Paper 2000-3432, July 2000.
- ⁴⁵ Keidar, M., Boyd, I. D., Lepsetz, N., Markusic, T. E., Polzin, K. A., and Choueiri, E. Y., "Performance Study of the Ablative Z-Pinch Pulsed Plasma Thruster," AIAA Paper 2001-3898, July 2001.
- ⁴⁶ Rayburn, C. D., The Development of a Pulsed Plasma Thruster for the Dawgstar Satellite, Master's Thesis, University of Washington Dept. of Aeronautics & Astronautics, 2001.
- ⁴⁷ Jayaram, R., Mass Spectrometry: Theory and Applications, Plenum Press, New York, 1966.
- ⁴⁸ Duckworth, H. E., Barber, R. C., and Venkatasubramanian, V. S., Mass Spectroscopy, Cambridge University Press, Cambridge, 1986.
- ⁴⁹ Cotter, R. J., Time-of-Flight Mass Spectrometry: Instrumentation and Applications in Biological Research, American Chemical Society, Washington, 1997.
- ⁵⁰ Cotter, R. J., Ed., Time-of-Flight Mass Spectrometry, American Chemical Society, Washington, 1994.

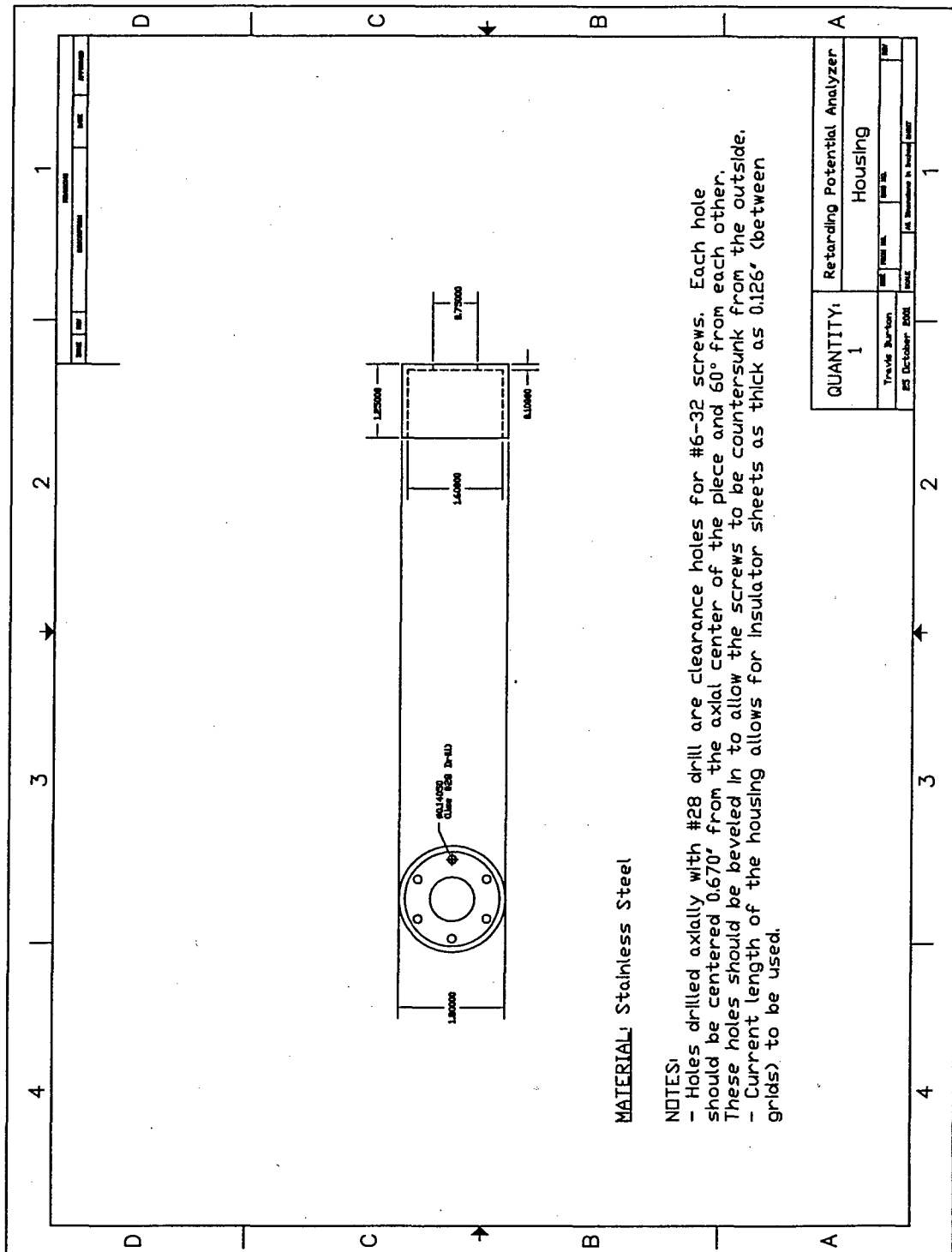
- ⁵¹ King, L. B., Transport-Property and Mass Spectral Measurements in the Plasma Exhaust Plume of a Hall-Effect Space Propulsion System, Doctoral Dissertation, University of Michigan Dept. of Aerospace Engineering, Published through University Microfilm International, 1998.
- ⁵² Pollard, J. E., "Plume Angular, Energy, and Mass Spectral Measurements with the T5 Ion Engine," AIAA Paper 95-2920, July 1995.
- ⁵³ Marrese, C., Gallimore, A. D., Haas, J., Foster, J., King, B., Kim, S. W., and Khartov, S., "An Investigation of Stationary Plasma Thruster Performance with Krypton Propellant," AIAA Paper 95-2932, July 1995.
- ⁵⁴ Pollard, J. E., Diamant, K. D., Khayms, V., Werthman, L., King, D. Q., and de Grys, K. H., "Ion Flux, Energy, and Charge-State Measurements for the BPT-4000 Hall Thruster," AIAA Paper 2001-3351, July 2001.
- ⁵⁵ Crofton, M. W., and Boyd, I. D., "Plume Measurement and Modeling Results for a Hollow Cathode Micro-Thruster," AIAA Paper 2001-3795, July 2001.
- ⁵⁶ Darnon, F., "The SPT-100 Plasma Plume and its Interaction with a Spacecraft, from Modeling to Ground and Flight Characterization," AIAA Paper 2000-3525, July 2000.
- ⁵⁷ Wang, J., Brinza, D. E., Young, D. T., Nordholt, J. E., Polk, J. E., Henry, M. D., Goldstein, R., Hanley, J. J., Lawrence, D. J., and Shappirio, M., "Deep Space One Investigations of Ion Propulsion Plasma Environment," *Journal of Spacecraft and Rockets*, Vol. 37, No. 5, 2000, pp. 545-555.
- ⁵⁸ Lipshultz, B., Hutchinson, I., LaBombard, B. and Wan, A., "Electric Probes in Plasmas," *Journal of Vacuum Science and Technology A*, Vol. 4, No. 3, 1986, pp. 1810-1816.
- ⁵⁹ Böhm, C., and Perrin, J., "Retarding-field Analyzer for Measurements of Ion Energy Distributions and Secondary Electron Emission Coefficients in Low-pressure Radio Frequency Discharges," *Review of Scientific Instruments*, Vol. 64, No. 1, 1993, pp. 31-44.
- ⁶⁰ Harris, N. S., Modern Vacuum Practice, McGraw-Hill, London, 1989.
- ⁶¹ Shell, J. R., and Enloe, C. L., "Optimizing the Energy Resolution of Planar Retarding Potential Analyzers," *Review of Scientific Instruments*, Vol. 63, No. 2, 1992, pp. 1788-1791.
- ⁶² "Standard Test Method for High-Voltage, Low-Current, Dry Arc Resistance of Solid Electrical Insulation," Annual Book of ASTM Standards, Vol. 10.01, 1999.

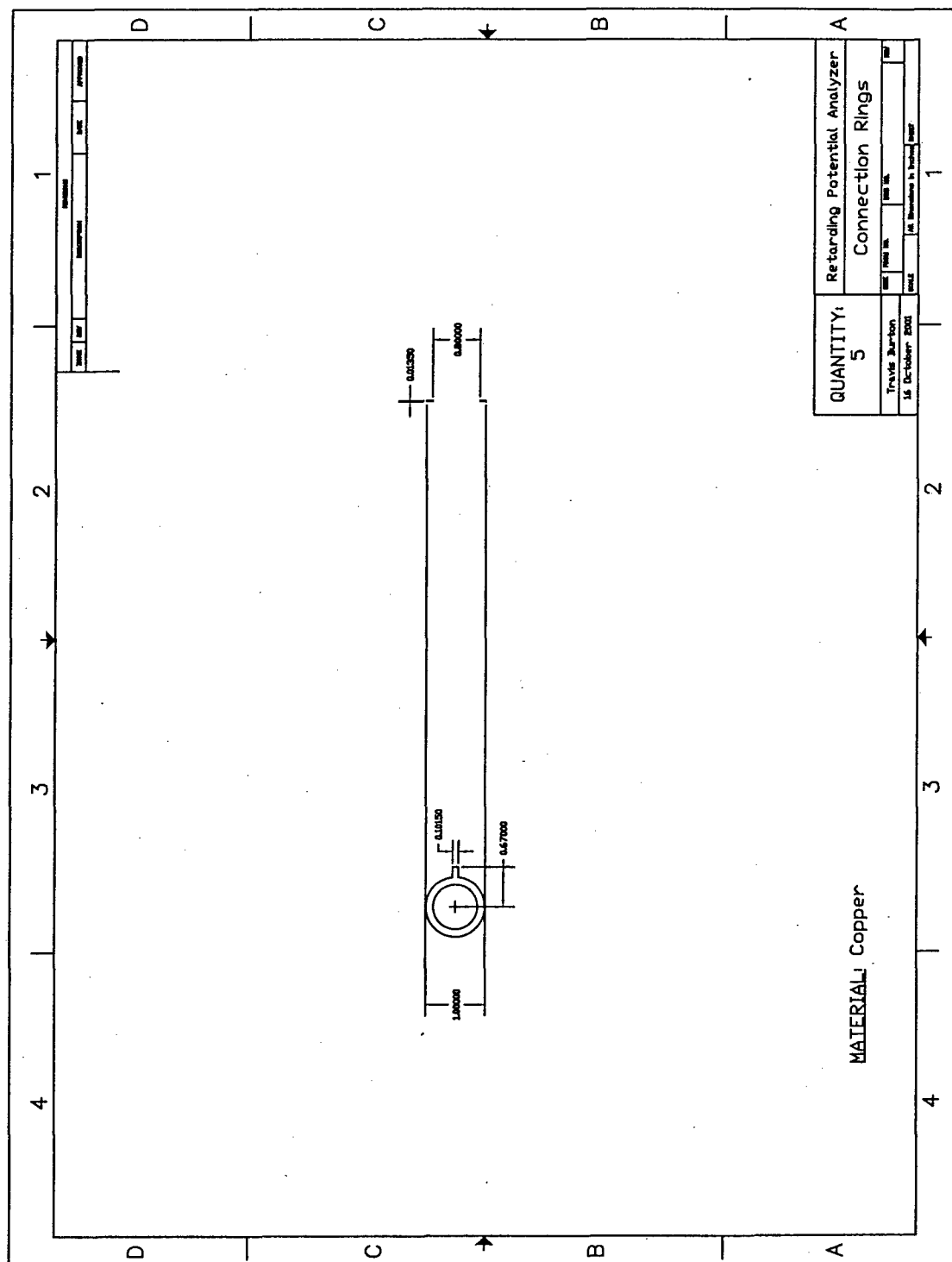
⁶³ King, L. B., and Gallimore, A. D., "Gridded Retarding Pressure Sensor for Ion and Neutral Particle Analysis in Flowing Plasmas," *Review of Scientific Instruments*, Vol. 68, No. 2, 1997, pp. 1183-1188.

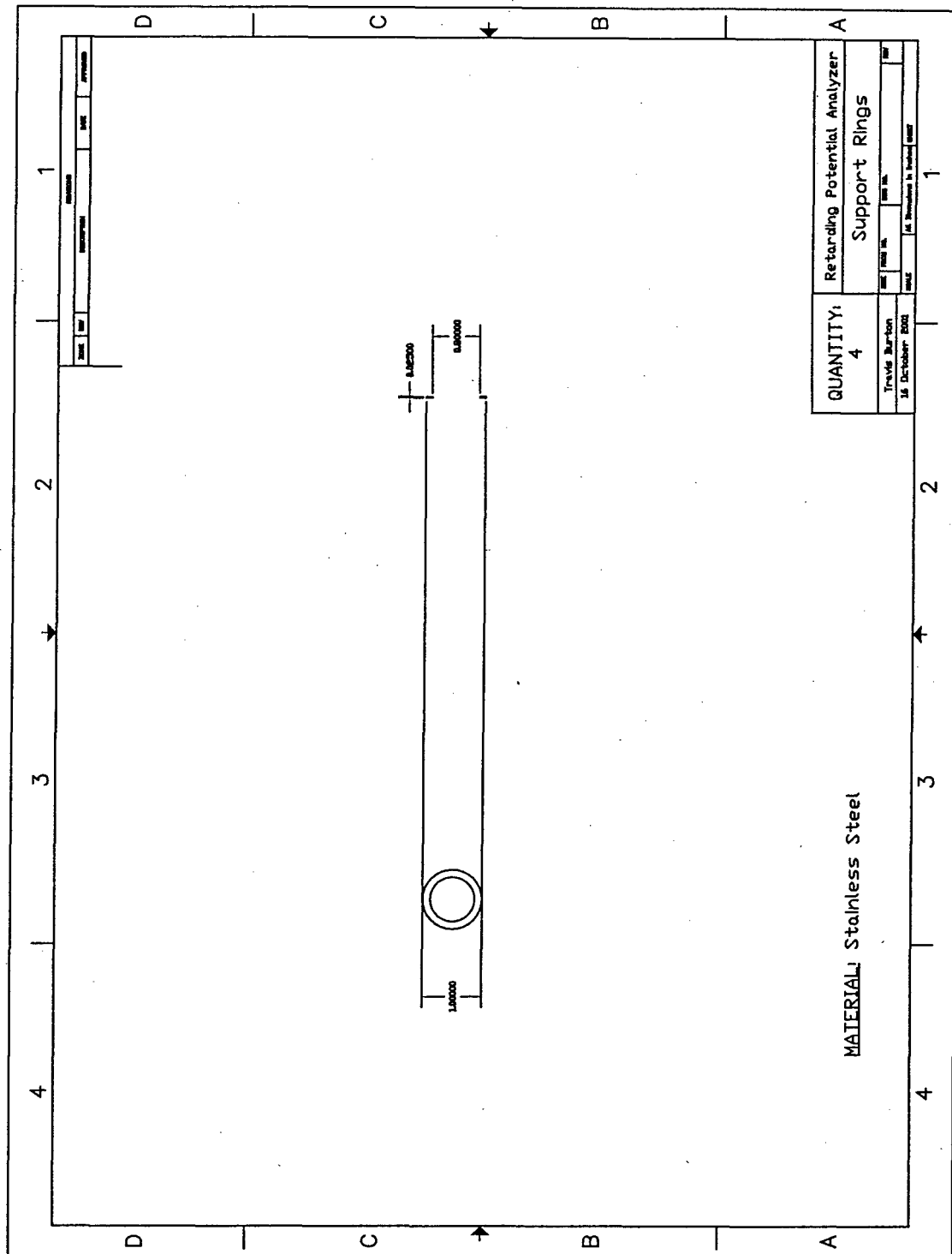
Appendix: Mechanical Drawings

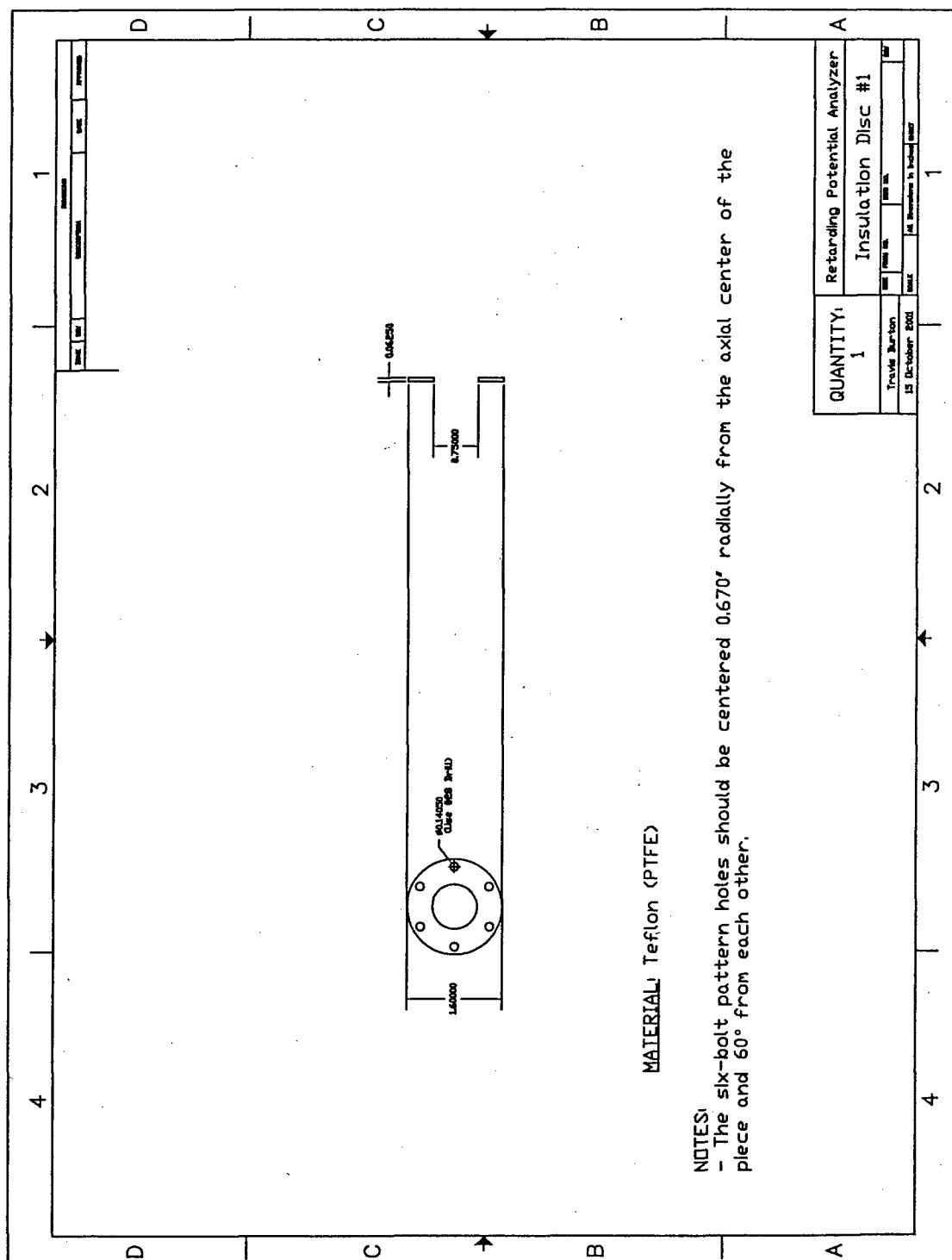
Attached are the mechanical drawings used in the fabrication of the Time-of-Flight/Gridded Energy Analyzer instrument.

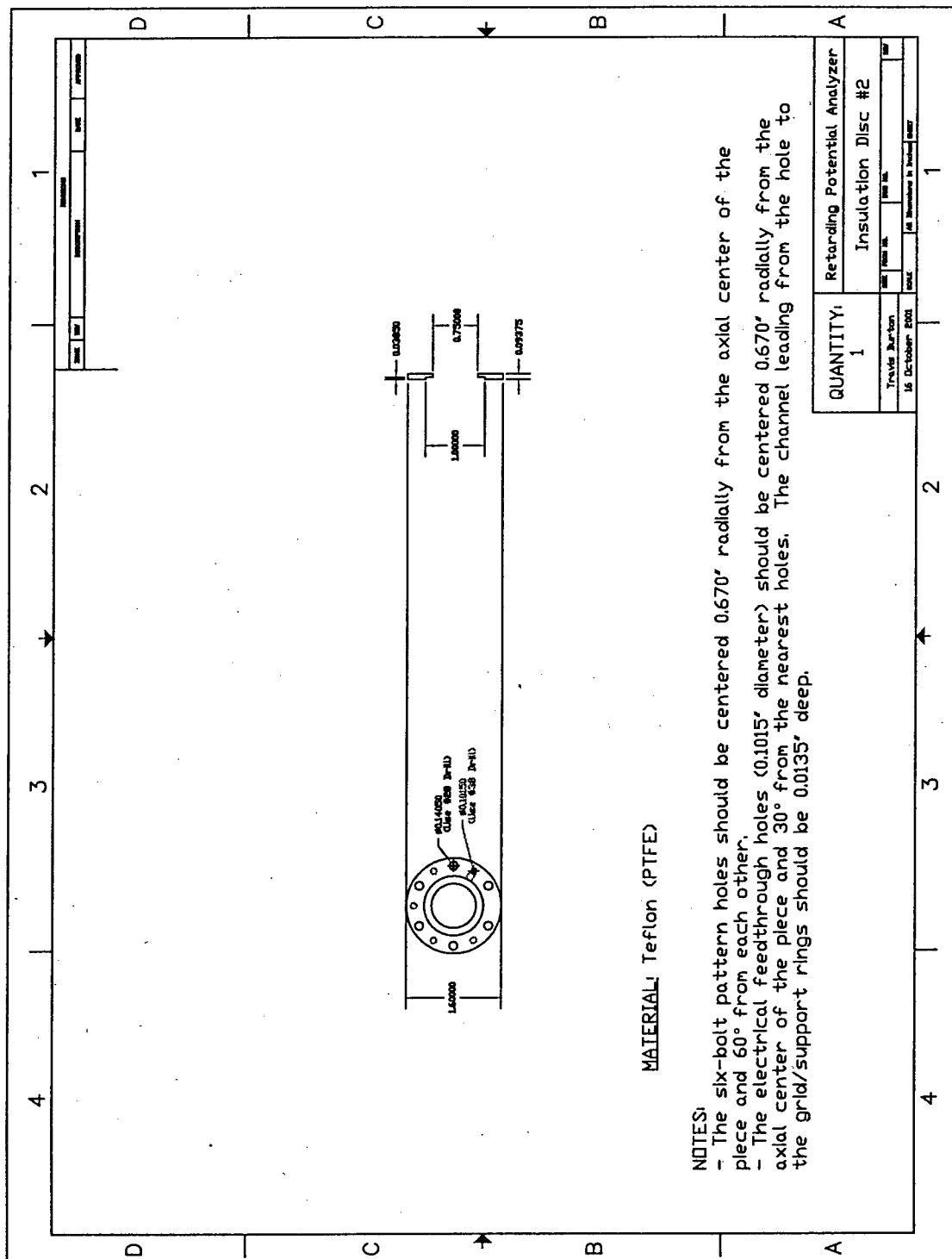


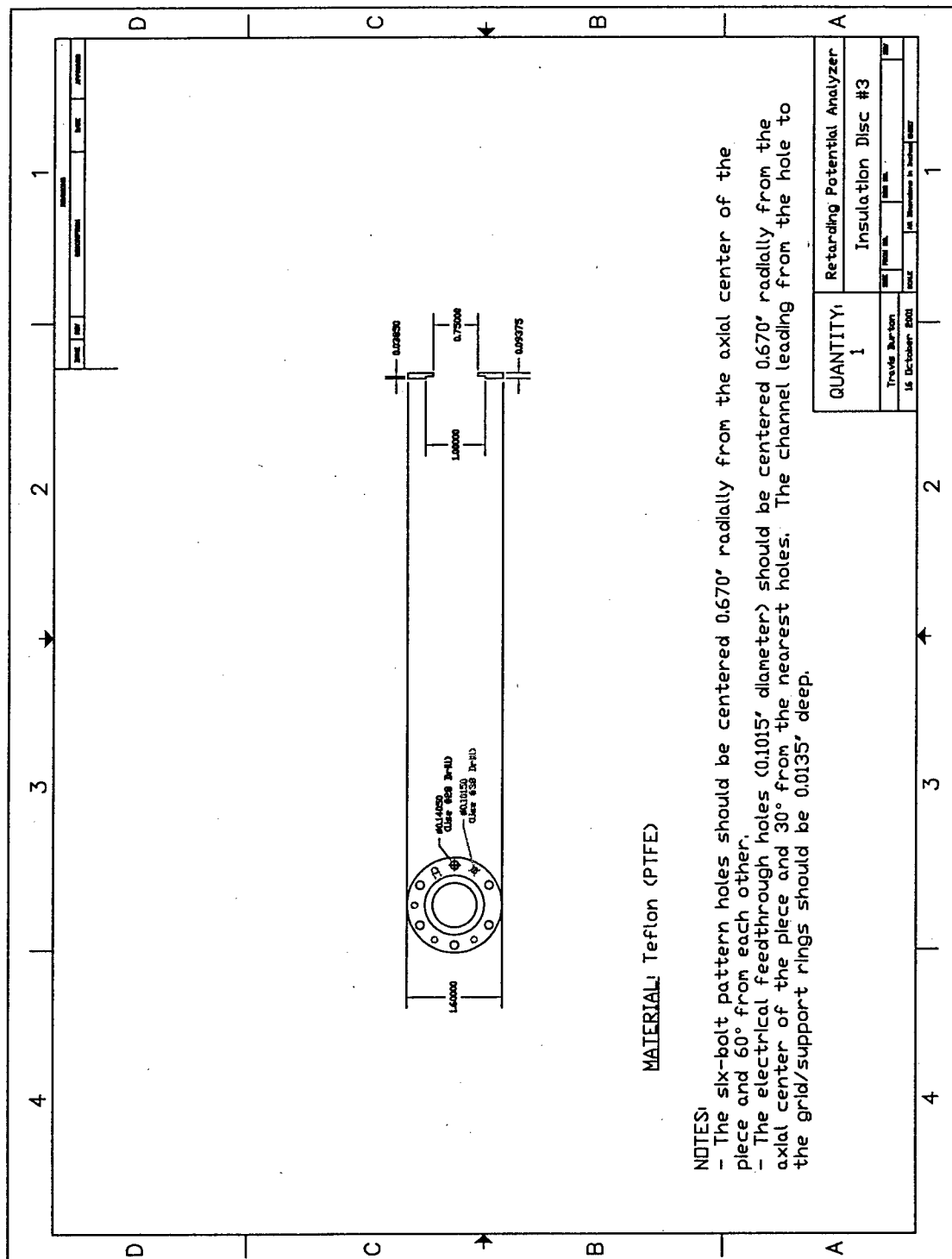


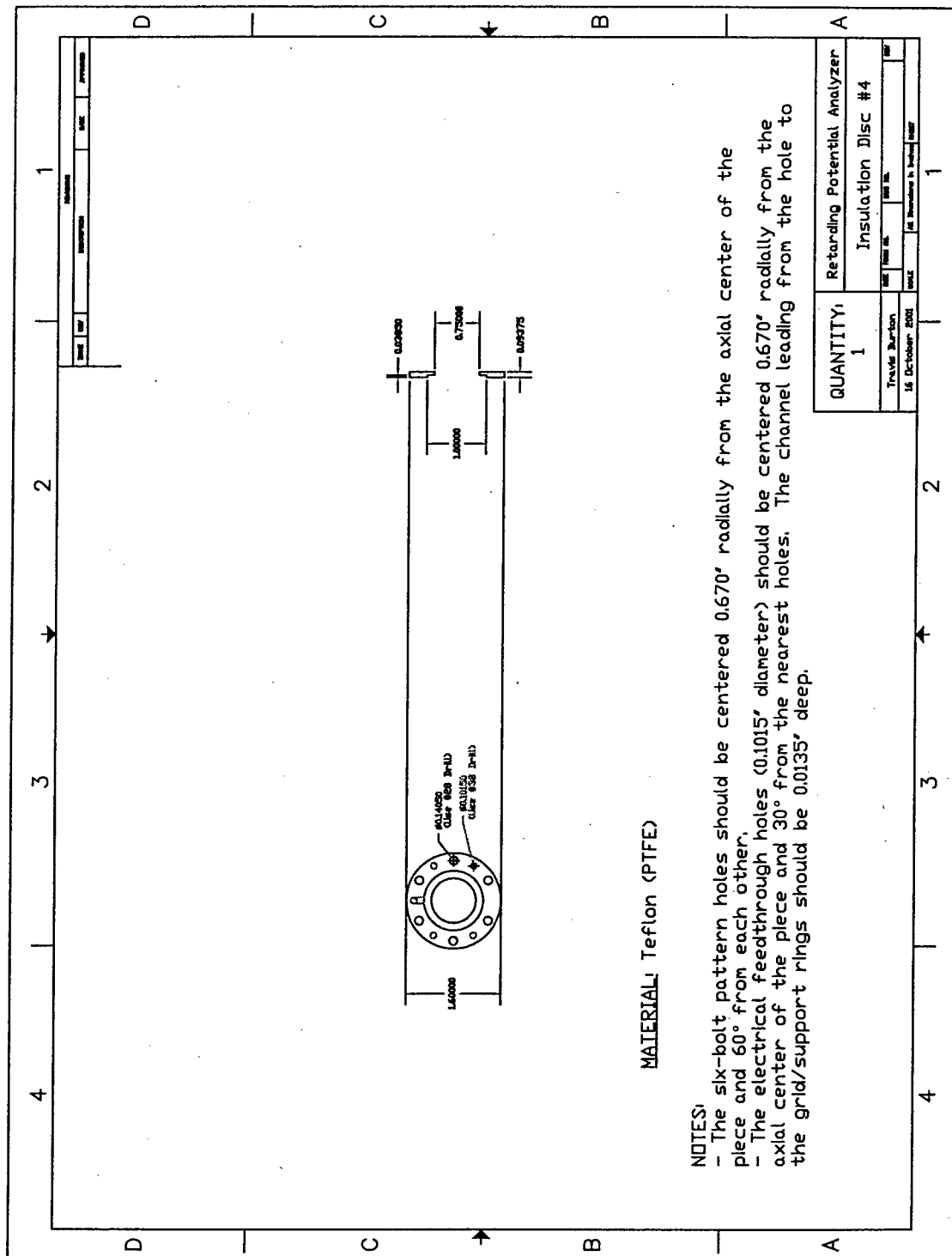


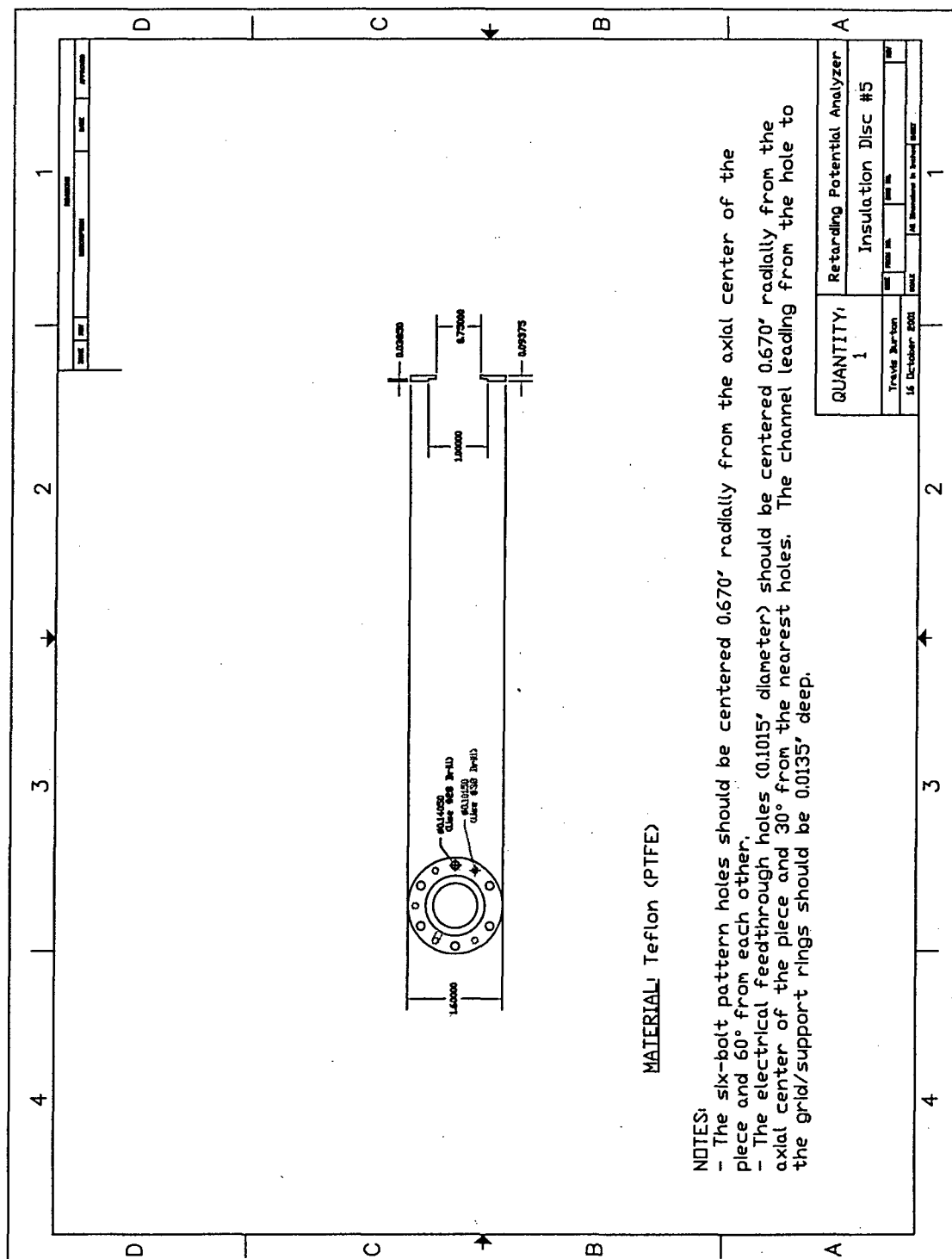


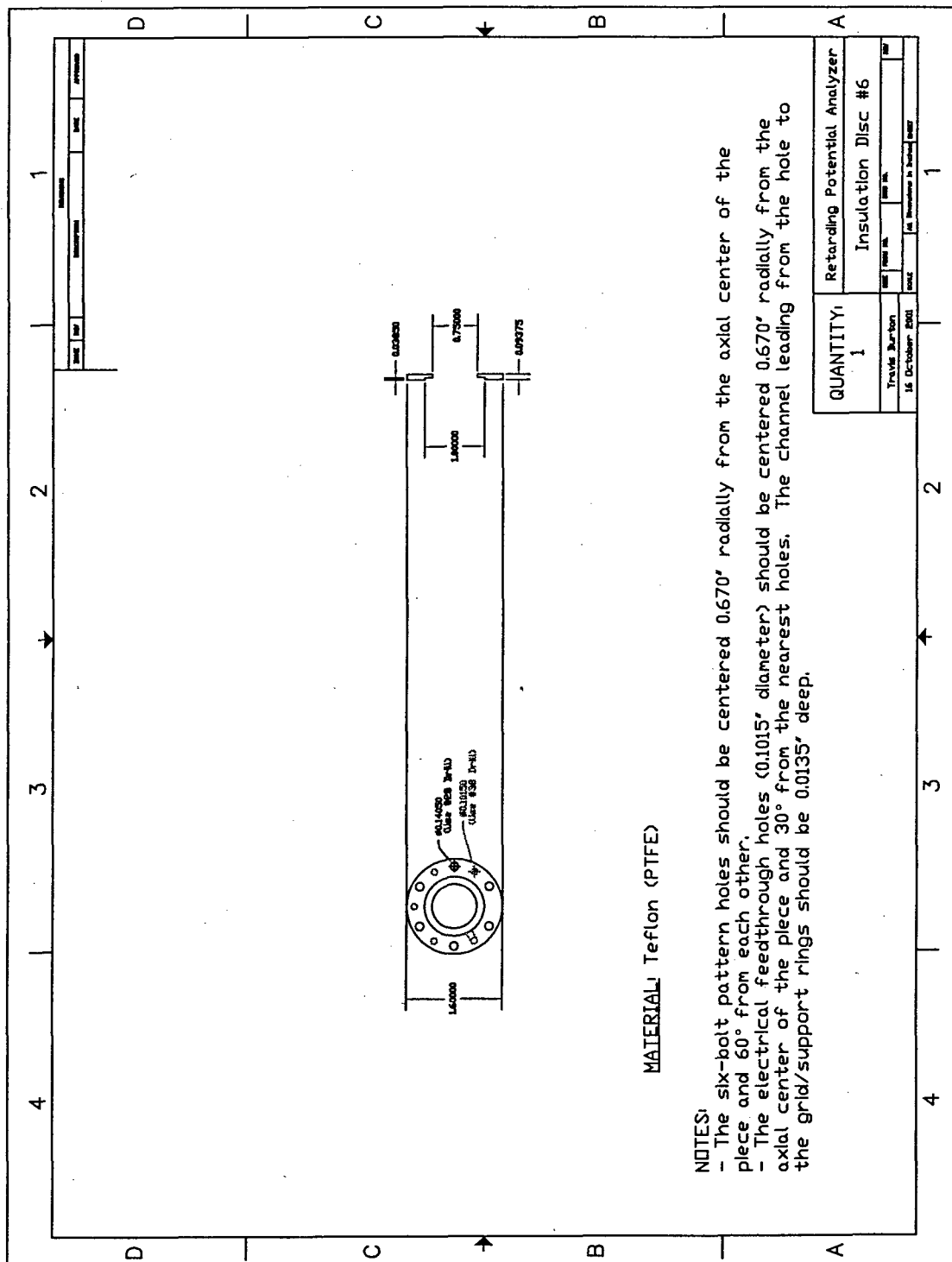


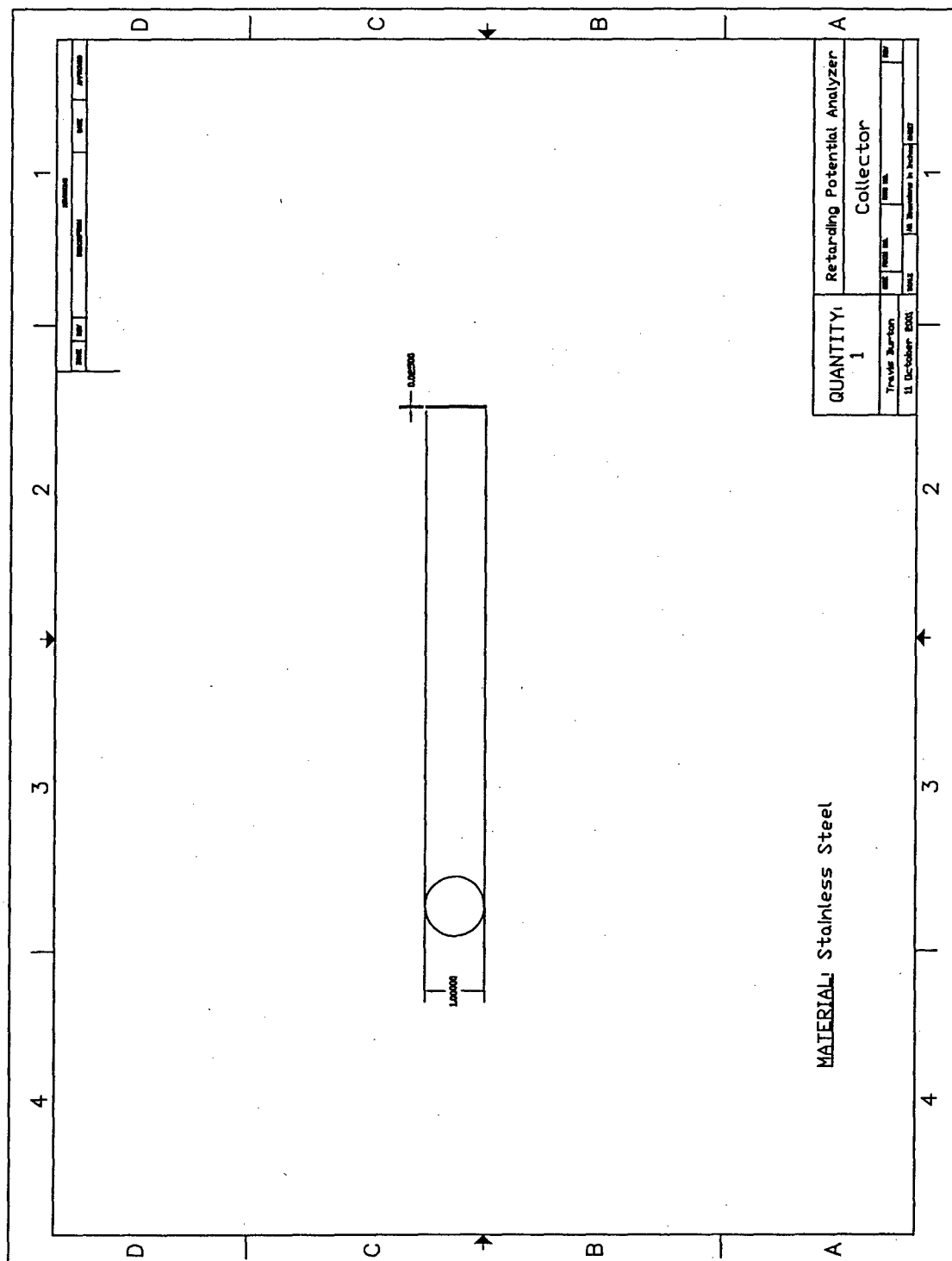


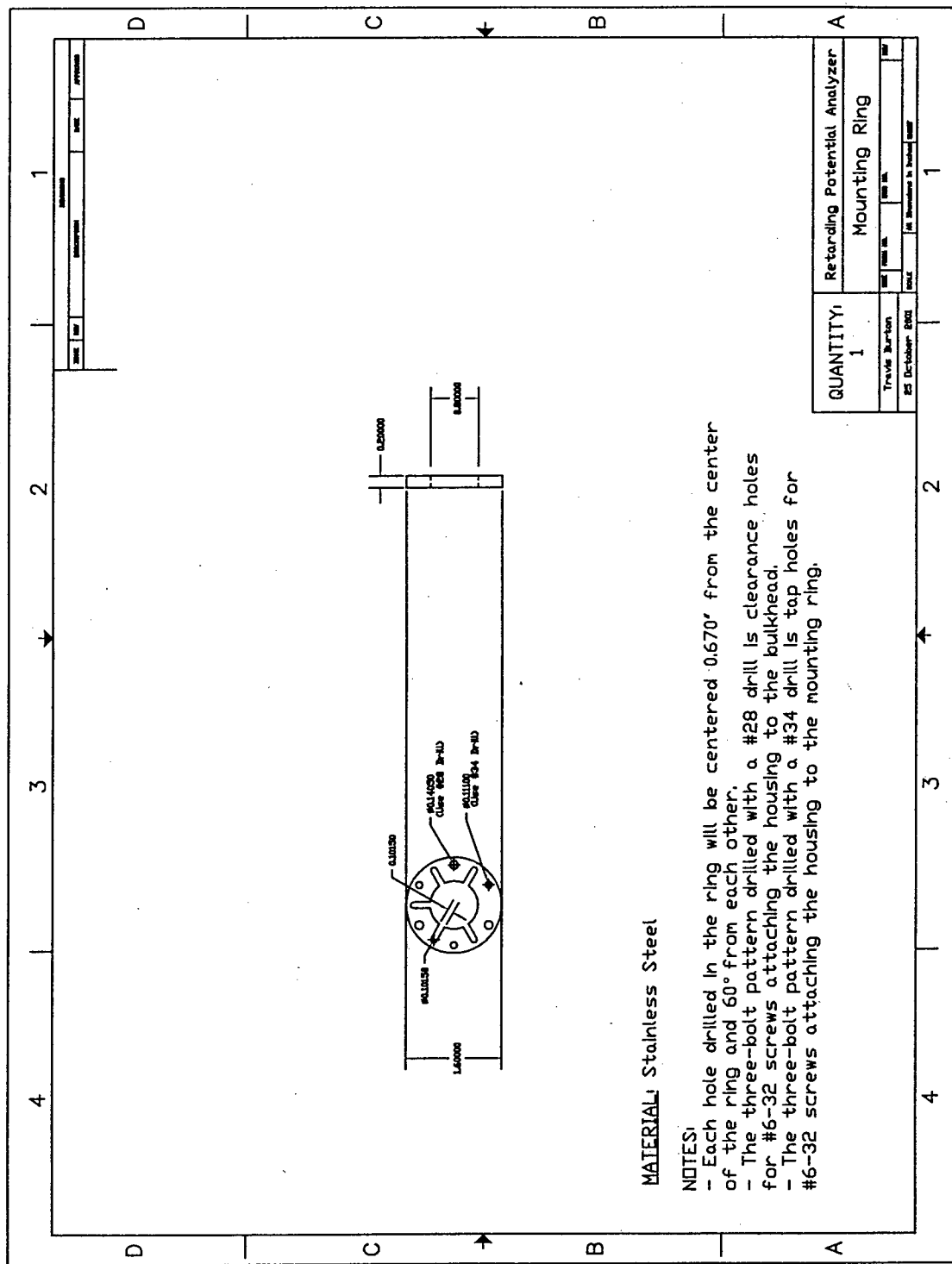


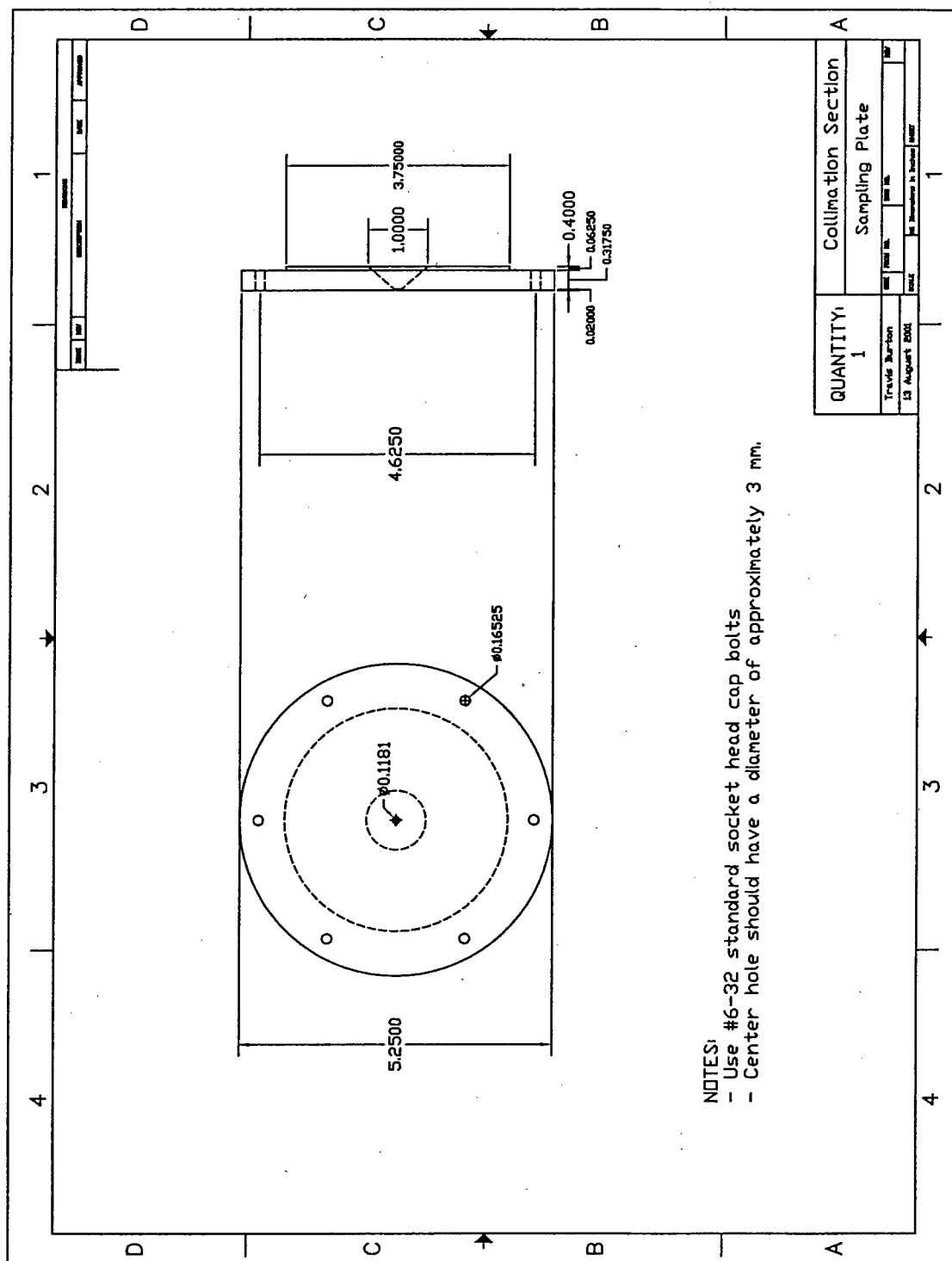




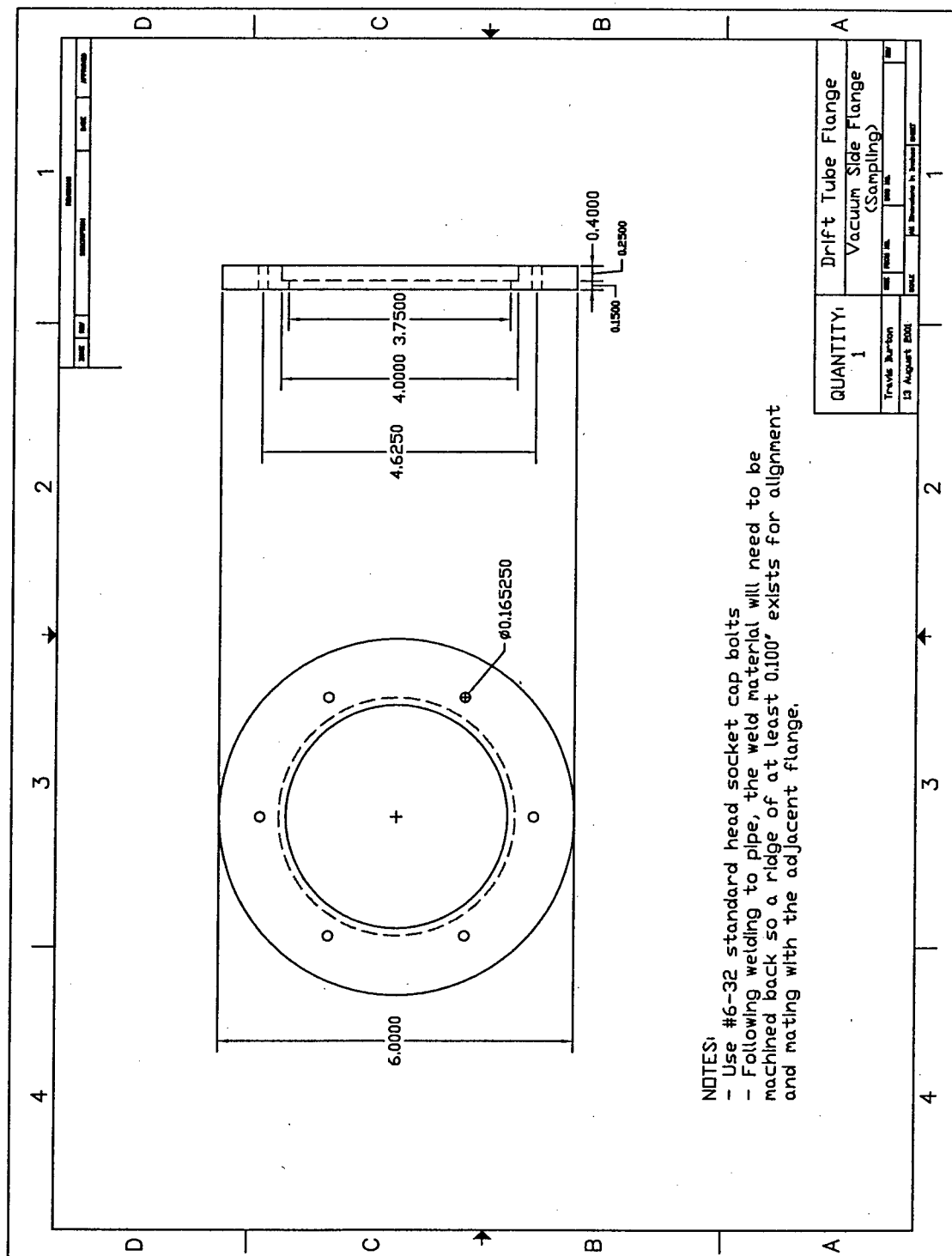


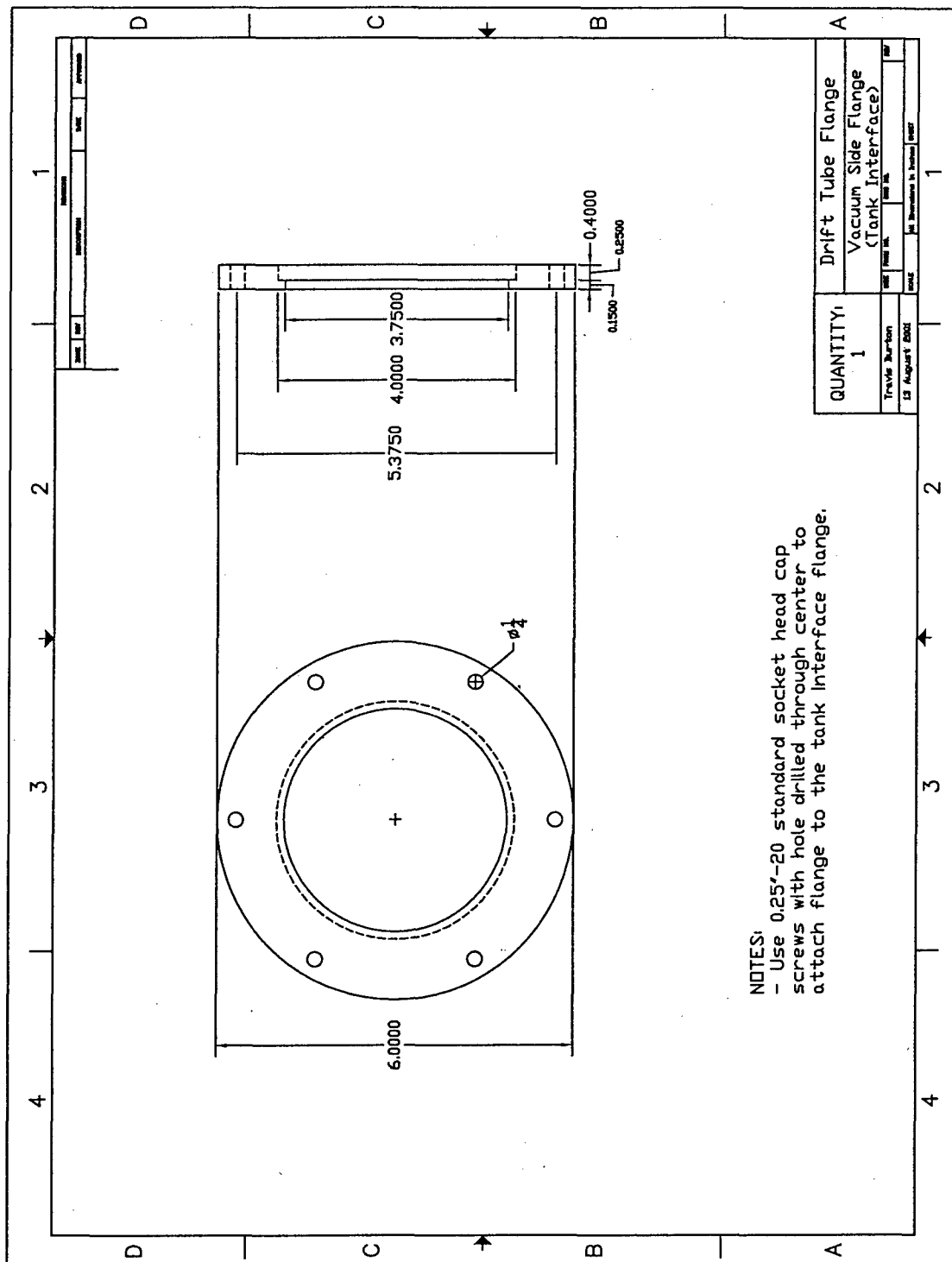


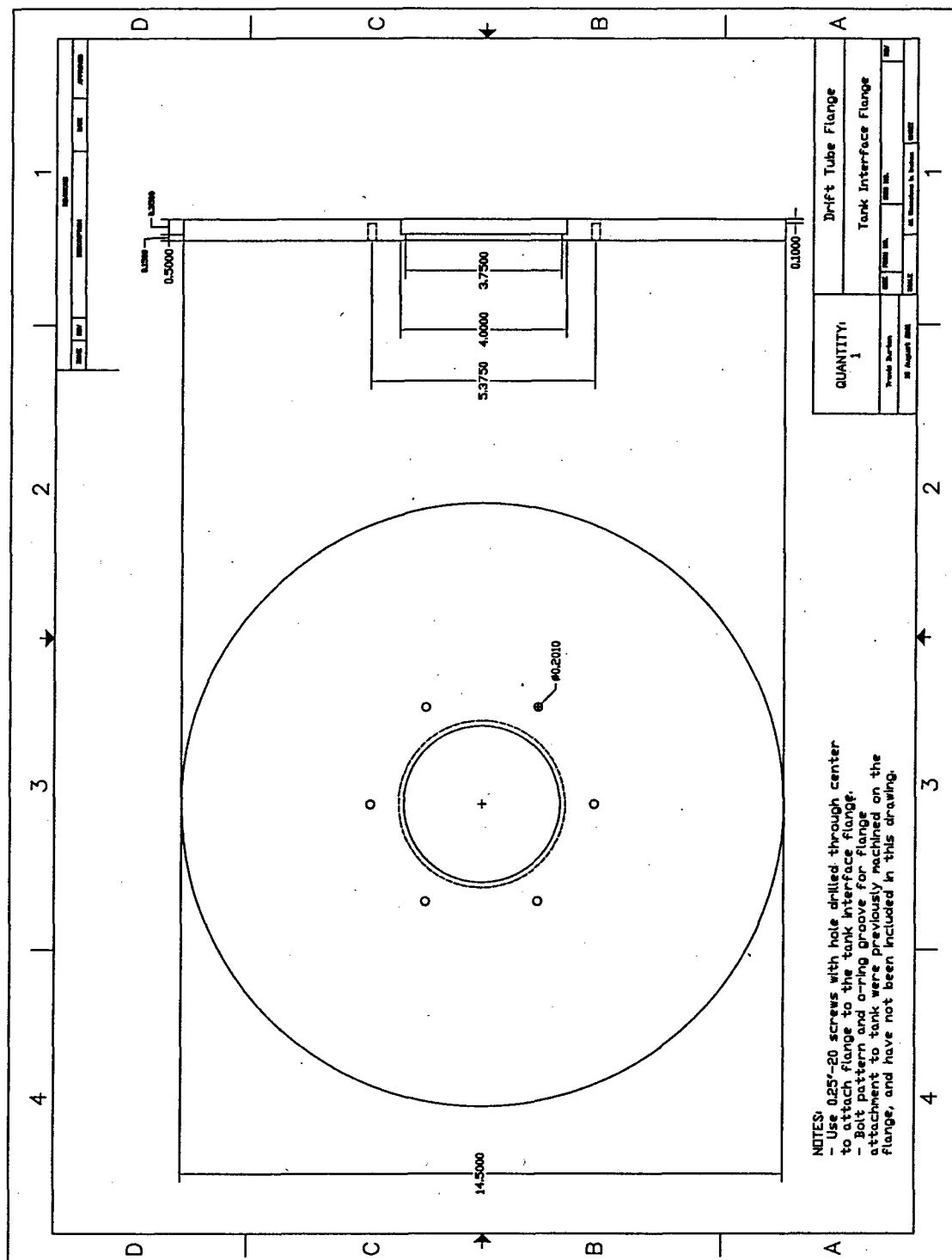


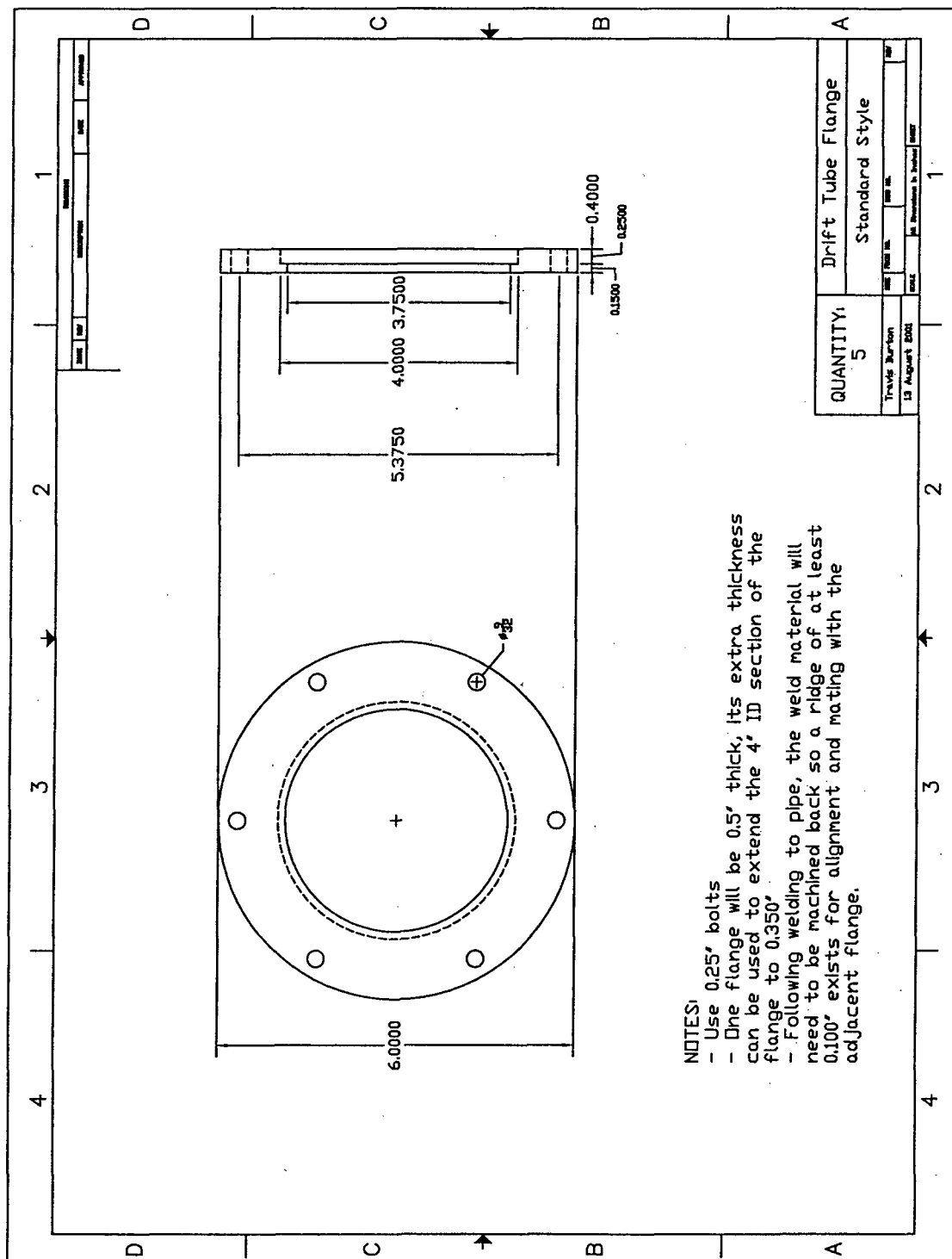


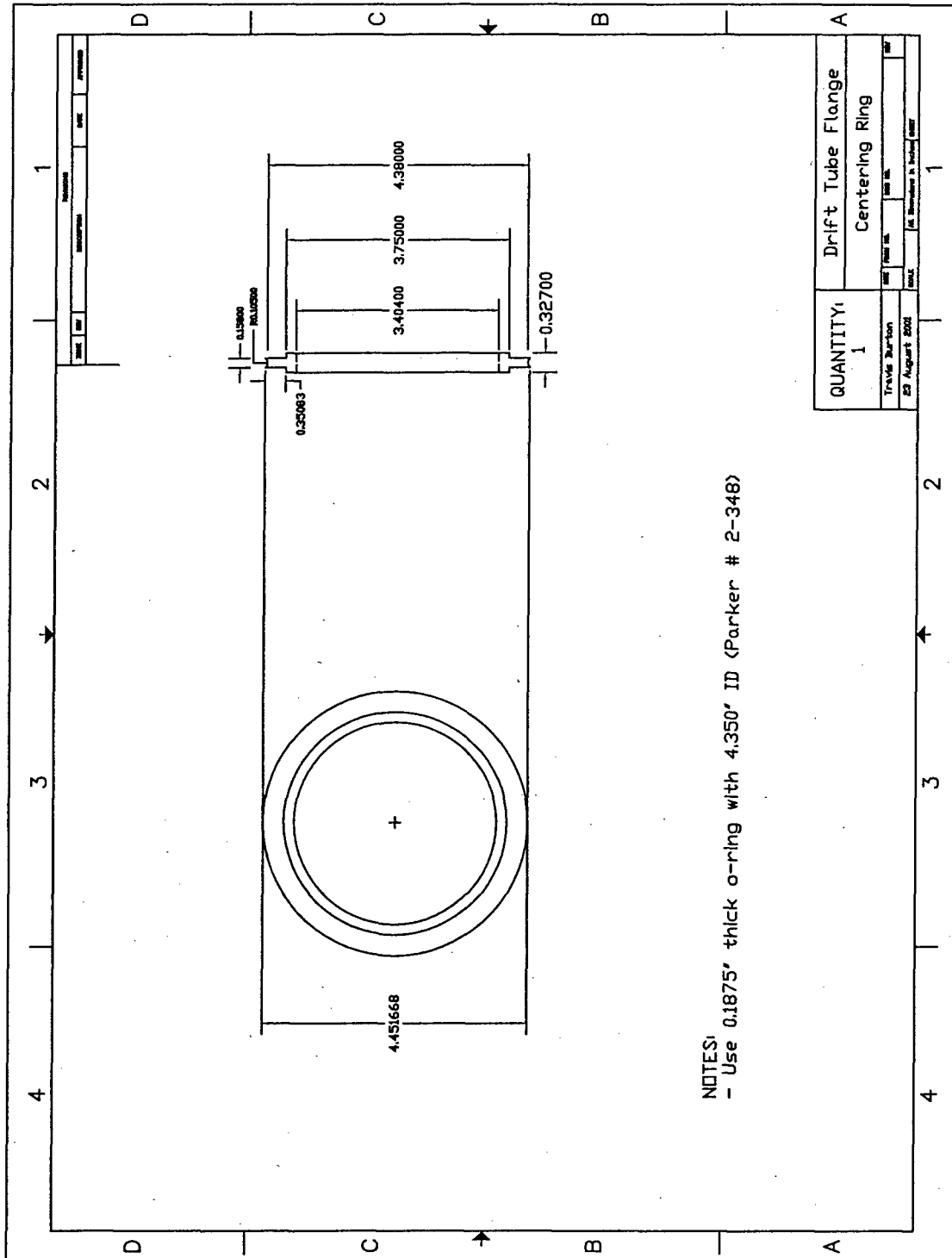
NOTES:
 - Use #6-32 standard socket head cap bolts
 - Center hole should have a diameter of approximately 3 mm.











NOTES:
 - Use 0.1875" thick o-ring with 4.350" ID (Parker # 2-348)

